The Gustaf Werner Institute
University of Uppsala
Uppsala, Sweden

thesis

COHERENT SCATTERING OF PI MESONS FROM HELIUM AT HIGH ENERGIES

ford ekelof

UPPSALA 1972

The Gustaf Werner Institute
University of Uppsala
Uppsala, Sweden

hesis

OHERENT SCATTERING OF PI MESONS

ROM HELIUM AT HIGH ENERGIES

ord ekelöf

UPPSALA 1972

COHERENT SCATTERING OF PI MESONS FROM HELIUM AT HIGH ENERGIES.

INAUGURAL DISSERTATION

BY

TORD EKELÖF
Fil.kand.,civ.ing., Sthlm

By due permission of the Faculty of Science of the University of Uppsala, to be publicly discussed in the lecture hall at the Institute of Physics, Uppsala University, on May 31, 1972 at 10 a.m. for the examination of Doctor of Philosophy (according to Royal proclamation No. 327, 1969).

UPPSALA 1972

To Monique Gapany

This thesis consists of the following four papers

I. 'A measurement of the differential cross section for elastic pion-helium scattering at 7.76 GeV/c'
by T. Ekelöf, B. Höistad, A. Åsberg; C. Busi, S. Dahlgren, A.J. Herz, S. Kullander, G. Lee, D. Websdale; G. Landaud and J. Yonnet.
CERN preprint. Published in Nuclear Physics vol. B35, p. 493 (1971).

II. 'A helium-recoil spectrometer'
by S. Dahlgren, A.J. Herz, S. Kullander, R. Lorenzi; T. Ekelöf, B. Höistad and A. Åsberg.
CERN preprint. To appear in Nuclear Instruments and Methods (1972).

III. 'The data analysis in a counter experiment at the CERN PS, using a helium recoil spectrometer'
by T. Ekelöf.
Gustaf Werner Institute internal report 1/72 (1972).

IV. 'On the ρ meson production in π^{4}He interactions'
by T. Ekelöf.
Gustaf Werner Institute internal report 2/72 (1972).

General background

This thesis concerns a field of physics that has been given several names: elementary particle physics, high energy physics and subnuclear physics. The aim of this field is to describe the microstructure of matter at the lower limit of observable dimensions. In the study of this microstructure use is made of elementary particle beams of very high energies and the limit is set by the maximum energy available. The pi meson particles from the CERN Proton Synchrotron used in the experiment described in paper I had an energy of $8 \cdot 10^{9}$ electron volts corresponding to a lower limit of around $2.5 \cdot 10^{-17}$ metres.

The size of a proton is around 10^{-15} metres and it is thus possible to study the structure of the proton with a particle beam of the above mentioned energy. This can be done by letting the beam hit a hydrogen target and observing the particles that emerge from the interaction between the beam particles and the one-proton nuclei of the target material. It has been shown that more and valuable information on elementary particle interactions can be obtained if targets with nuclei composed of several protons and neutrons are used as well.

In our case helium was used as target material. To detect the helium nuclei that recoil after being hit by particles in the incident beam, a helium-recoil spectrometer was constructed. With this device it is possible to ascertain if the helium nucleus remains intact after the collision. If so the beam particle interacted 'coherently' with all protons and neutrons in the nucleus as if the nucleus had been an entity and the rules for how new elementary particles are produced in such a reaction are then more restrictive than in the case of a hydrogen target. In this way specific particle reactions can be isolated and studied without interference from other reactions.

Summary of thesis

Paper I gives an account of the first experiment with the helium-recoil spectrometer. This experiment measured the angular dependence of the coherent elastic scattering of pi mesons from helium nuclei. The measurements could hardly have been performed with any other technique in use today. The main objects of the experiment was to test the helium-recoil spectrometer, to verify the Glauber multiple scattering theory for coherent interactions at a very high energy and to obtain information on the interaction between pi mesons and nucleons.

Paper II describes the helium-recoil spectrometer. The various components of the device and their operation in the experiment are treated in

detail. The way in which the apparatus can be used in studying processes of elementary particle production is also described and the precision with which the masses of the produced particles can be determined is discussed.

Paper III describes the analysis of the data collected in the experiment. The electronic signals from the various detectors in the experiment were recorded on magnetic tape and fast computers were used to interpret these signals and to extract the useful information from the data. It is stated that the computer programs worked out for this analysis can be used with few changes in new experiments with the recoil spectrometer.

Paper IV presents some theoretical calculations of the process in which rho mesons are coherently produced from high energy pi mesons hitting helium nuclei. The conclusion is that valuable information about the rho and omega mesons could be obtained from measurements of this reaction and that the helium-recoil spectrometer seems to be well suited for such measurements.

Acknowledgements

A common idea about scientists is that their occupation is to sit in a room solving their problems, far away from this world and other people.

Moments of work in isolation are necessary in most occupations but to me the greatest satisfaction in working with science has been given in the many and necessary discussions with teachers, colleagues and collaborators. I have found that it is more often in the exchange of thoughts with other people that new ideas are born than when working alone. To me doing research is to a great extent a social activity where the satisfaction of having achieved a result, as well as any honor from it, is shared between many people.

Therefore I thank all those who have participated in the work described in this thesis for the enjoyment I have had in working with them and for the discussions we have had. Any credit for the results of the work is shared between all these people. They are found in the lists of authors and the acknowledgements of the papers in the thesis. If any of these persons should be given prominence here I wish this to be Sven Kullander, my good friend, collaborator and teacher for the help and encouragement he has given me in the work described in this thesis.

EUROPEAN ORGANIZATION FOR NUCLEAR RESEARCH

A MEASUREMENT OF THE DIFFERENTIAL CROSS-SECTION FOR ELASTIC PION-HELIUM SCATTERING AT 7.76 GeV/c

T. Ekelöf, B. Höistad and A. Åsberg,
The Gustaf Werner Institute, University of Uppsala, Sweden

C. Busi, S. Dahlgren*), A.J. Herz, S. Kullander, G. Lee**),
and D. Websdale,
CERN, Geneva, Switzerland

G. Landaud and J. Yonnet,
University of Caen, Caen, France

ABSTRACT

Results are presented for the region of squared four-momentum transfers between -0.05 and -0.5 $(GeV/c)^2$. The directions of the scattered pions and alpha particles were measured with spark chambers and the momentum of the alphas was obtained from pulse-height and time-of-flight measurements. The results are compared with calculations from the Glauber theory, showing good agreement over the whole momentum-transfer range including the interference-dip region.

Geneva, September 1971

To be submitted to Nuclear Physics

---

*) Now at the Gustaf Werner Institute, University of Uppsala, Sweden.

**) Imperial College, London, England.

1. INTRODUCTION

Over the last few years there has been a growing interest in high-energy hadron-nucleus (A > 1) scattering at high incident momenta. This is partly due to the successes of the Glauber multiple-scattering theory[1] in describing the diffraction-like structure in the differential cross-section[2]. The analysis of measurements[3] of p-^{4}He elastic scattering at 1.7 GeV/c has shown[2,4] that this theory gives better agreement with experimental data for light nuclei than the conventional optical model. The theory contains parameters referring directly to the nuclear wave function and the hadron-nucleon scattering amplitude , making it possible to check or derive these quantities from experimental data[5]. This is especially true for the phase of the hadron-nucleon scattering amplitude at non-zero momentum transfer of which the depth of the interference dip between single and double scattering is a sensitive measure.

The deuteron differential cross-section has been shown[6-9] not to contain an interference dip -- merely a shoulder -- between the single and double scattering regions and this has been explained by Harrington[10] as being due to the d-state admixture in the deuteron ground-state wave function. No such effects are to be expected in the case of scattering of hadrons by ^{4}He which has a symmetric ground-state wave function. It is thus more suitable than deuterium as a target in experiments in which one wishes to obtain information on hadron-nucleon interactions.

Measurements of the p-^{4}He elastic differential cross-section in the interference-dip region have been performed up to 1.7 GeV/c incident momentum[3,11], detecting only the angle and the energy of the scattered proton. The energy resolution was better than 20 MeV so that it was possible to discriminate against inelastic reactions since 20 MeV is the threshold for break-up and excitation of ^{4}He. At incident momenta in the multi-GeV region discrimination against inelastic events is extremely difficult if one measures only the scattered hadron. It is therefore desirable to obtain additional constraints by measuring the momentum and direction of the recoiling ^{4}He nucleus. Such a measurement brings with it some experimental problems as the recoiling ^{4}He acquires a very low kinetic energy and has a high specific energy loss.

An emulsion experiment[12] detecting only the ^{4}He recoil has been performed using incident negative pions of 1.12 GeV/c. The minimum squared four-momentum

transfer $|t|$ was 0.2 $(GeV/c)^2$ and the emulsions were insensitive to singly charged particles. This was the first measurement of the diffraction-dip region in π^--^{4}He scattering above 1 GeV/c.

We have determined the elastic π^--^{4}He differential cross-section at 7.76 GeV/c incident momentum in the $|t|$ range 0.05 to 0.5 $(GeV/c)^2$. The angles of the scattered and the recoiling particles were obtained with spark chambers, and the time of flight and pulse height of the recoil with scintillation counters. The chosen incident momentum lies above the pion-nucleon resonance region which simplifies the theoretical analysis.

2. THE EXPERIMENT

In Fig. 1 the layout of the experiment is shown. The beam was produced on an internal target, at the CERN Proton Synchrotron, momentum analysed and focused onto the helium target 80 m downstream. The mean beam momentum was (7.76 ± 0.40) GeV/c with a momentum bite of 1%. The bursts were 400 ms long and contained of the order of 10^5 negative pions as well as 0.8% $\bar{p}$, 0.8% K^- and at most 4% e^- and μ^-.

The trajectories of the incident pions were determined with a telescope of seven multiwire proportional chambers[13] (MP_{1-7}) divided into two groups separated by 4.5 metres. Each chamber gave a vertical or horizontal position.

The track of the scattered pion was determined by four wire spark chambers[14] (C_{1-4}), each chamber giving both the vertical and the horizontal coordinate of the track. Two of the chambers were read out by means of the magnetostriction method, the other two with the delay-line method[15].

The angle of the recoiling ^{4}He was measured in two cylindrical spark chambers, operating at low gas pressure[16], surrounding a gaseous helium target. The latter consisted of a thin-walled mylar cylinder, 20 mm in diameter, supported by a steel-wire spiral and suitable for pressures up to 20 atm. The recoils were stopped in three circumferential plastic scintillators outside the large spark chamber each covering an azimuthal angle of 42°. The pulse heights produced in the scintillators were recorded and the signals

were also used to measure the time of flight of the ^{4}He; the start pulses being given by the incoming pions in a scintillator just in front of the target.

A detailed account of the instrumentation used for measurements on the recoiling alpha particles is found in ref. 17.

The incident pion was defined by the trigger signature $T_i = S_1 S_2 S_3 S_4 \bar{A}_1 \bar{A}_2 \bar{A}_3 \bar{A}_4$. The signals S_1 to S_4 were obtained from scintillators in the beam and the signals A_1 to A_4 from hole scintillators surrounding it. With this trigger a circular pion channel 15 mm in diameter was centered onto the target.

The outgoing-pion trigger had the signature $T_o = (S_{51}S_{61} + S_{52}S_{62})\, \bar{A}_6 \bar{A}_7 \bar{A}_8 (\overline{S_{51}S_{52}})$. The signal A_6 came from a thick lead-scintillator sandwich counter with a hole letting through the beam and particles scattered through angles up to 6°. Its efficiency for gammas (from decaying π^o) was greater than 99%. The signals S for the outgoing pion came from scintillators divided into upper and lower sections. The scattered pion had to hit either the two upper sections or the two lower ones, no other combination being accepted by the trigger. Only one of the two sections was allowed to be hit -- a double hit indicating at least two outgoing charged particles.

Signals $S_{\alpha 1}$ to $S_{\alpha 3}$ from three circumferential scintillators were used for time-of-flight and pulse-height measurements of the recoil and two others, $A_{\alpha 1}$ and $A_{\alpha 2}$, were used only in the trigger logic. The trigger signature for the recoil was

$$T_\alpha = (\overline{A_{\alpha 1} + A_{\alpha 2}}) \times (S_{\alpha 1} + S_{\alpha 2} + S_{\alpha 3}) \times (\overline{S_{\alpha 1}S_{\alpha 2} + S_{\alpha 2}S_{\alpha 3} + S_{\alpha 1}S_{\alpha 3}}).$$

The event signature came from the coincidence $T_i \times T_o$ followed by a signal T_α between 6 and 56 ns later. The delay of 6 ns eliminated events in which fast particles were scattered out to one of the recoil scintillators. Relative counting rates using various trigger combinations are given in Table 1. The effect of the delayed time window for the recoil is clearly seen.

The trigger background was checked by measuring trigger rates with and without helium gas in the target. The signal-to-background ratio determined in this way varied between two and ten in the pressure range 5 to 20 atm used in the experiment.

3. ERRORS

The standard error in the position determination from the multiwire proportional chambers used in the incident-pion telescope was 0.7 mm, giving a standard error for the angle of the incident pion track of less than 0.3 mr. The standard error of the wire spark chambers in the scattered-pion telescope was 0.6 mm. The corresponding angular error depends on which of the chambers gave the coordinates to each event. The least favourable case was that only two adjacent chambers of C_2, C_3 and C_4 could be used, giving 1 mr as a conservative estimate of the standard error in the determination of the pion scattering angle.

As to the precision of the measurement on the recoils a detailed description is given in Ref. 17. The angular resolution was limited by multiple Coulomb scattering in the target and by the intrinsic error of the cylindrical spark chambers. The Coulomb scattering is energy-dependent and the standard error in the determination of the angle of the track of the recoil ranges from 30 to 20 mr between the low-energy cut-off at a kinetic energy of 6 MeV and the maximum at about 70 MeV

For $|t|$ below 0.1 $(GeV/c)^2$ the standard error is 0.005 $(GeV/c)^2$ and the precision is given by the time-of-flight measurement. In the high-$|t|$ region the error is given by the uncertainty in the pion scattering angle and the spread in the beam momentum. The standard error in this region is 0.01 $(GeV/c)^2$ and the systematic error for the whole $|t|$ range is 0.01 $(GeV/c)^2$.

4. RESULTS AND DISCUSSION

A χ^2 fitting program[18] was used to fit the measured angles and the momentum of the recoil to the hypothesis of elastic $\pi^- - {}^4He$ scattering. The momentum was obtained from the time-of-flight measurement. The pulse height, which was not used in the fit, served to check the hypothesis that the recoils were alpha particles. In addition, the constraint was applied that all the three measured tracks must pass through a vertex inside the target, so that the χ^2 fit had six degrees of freedom. In Fig. 2 we show the distribution of $d\sigma/dt$ for events having $\chi^2 \leq 16$. The shape of the distribution did not change when choosing smaller limits than 16 for χ^2, which showed that most of the "non-elastic" background had been eliminated. The curves in

Fig. 2 were calculated using a program developed by Kofoed-Hansen[19] based on the coherent multiple-scattering theory[1] for various ratios α of the real part to the imaginary part of the πN scattering amplitude. The $\pi^- p$ and $\pi^+ p$ amplitudes $f(t)$ were assumed to be equal and Gaussian and α to be independent of momentum transfer.

In the parametrization

$$f(t) = \frac{ik}{4\pi} \sigma_{\pi N}(1-i\alpha) e^{bt/2} \qquad (1)$$

the values $\sigma_{\pi N} = 26.6$ mb [20] and $b = 7.15$ (GeV/c)$^{-2}$ [21] were used. The nuclear density ρ of the helium was described by a superposition of two Gaussians with a delta function taking the centre-of-mass correlation into account. All other correlations were neglected[19]:

$$\rho(\vec{r}) = N \prod_{i=1}^{4} [e^{-a\vec{r}_i^2} (1-ce^{-d\vec{r}_i^2})] \, \delta(\tfrac{1}{4} \sum_{i=1}^{4} \vec{r}_i) \qquad (2)$$

The parameters in this density function were chosen to fit electron-helium elastic scattering data[22]. Effects due to spin flip and charge exchange were neglected.

The absolute scale on the $d\sigma/dt$ axis was adjusted so that the experimental points extrapolate to the optical point. This was necessary because of uncertainties in the apparatus efficiencies.

The identification of the selected events as $\pi^- - {}^4$He elastic-scattering events was confirmed by the convergence of the $d\sigma/dt$ distribution when choosing different cuts in χ^2. We should like, however, to discuss in some detail the possible sources of background in the region of the diffraction minimum.

Background not originating from interactions with helium was investigated by applying our χ^2 selection criteria to a sample of target-empty events and to a comparable sample of target-full events. In the selected target-empty sample there were no events with $|t| > 0.25$ (GeV/c)^2, whilst an equal incident flux produced 30 good events in the same region of momentum transfer when there was 20 atm of helium in the target. The background of this kind can thus be estimated to be $(0^{+6}_{-0})\%$ for $|t| > 0.25$ (GeV/c)^2.

Non-elastic reactions can be divided into two categories: coherent particle production from helium on the one hand and nuclear excitation and nucleon knock-out by the pion on the other. The coherent production reactions were eliminated to a great extent in the trigger by the signals from A_6, S_5 and A_7.

As the polar angle of the recoil is smaller in particle production than in elastic scattering the recoil-angle distribution will give information on such a background. Without any constraints and for $|t|$'s below 0.15 this distribution was peaked at the mean angle given by the kinematics for elastic scattering and was superimposed on a symmetric background which disappeared after the constraints had been applied[17]. Thus the differential cross-section for coherent particle production would have to drop much less rapidly than the elastic cross-section above $|t| = 0.15$ if it were to lead to an appreciable number of pseudo-elastic background events not being eliminated by the constraints. We consider this extremely improbable, especially as theoretical estimates[5] do not indicate such a great difference between the differential cross-sections of these two reactions.

In a nucleon-knock-out reaction the momentum of the recoiling ^3H or ^3He nucleus is (in the impulse approximation) equal to the momentum of the ejected nucleon prior to the collision. Due to the small amount of high-momentum components in the nuclear wave function one would expect to detect few such events in the dip region. Using data from a $^4He(p,2p)^3H$ experiment[23] for the momentum distribution of ^3He or ^3H nuclei and applying the three kinematical constraints the contamination due to knock-out reactions was calculated to be negligible at all momentum transfers including those of the dip region.

Reactions leading to nuclear excitation constitute the most dangerous background although ^4He, according to all available evidence, always decays via particle emission[27]. At low Q values (Q = Excitation energy - separation energy) the charged decay particles in the reaction

$$\pi^- + {}^4He \rightarrow \pi^- + {}^4He^* \begin{cases} \rightarrow {}^3H + p \\ \rightarrow d + d \end{cases}$$

do not acquire sufficiently high relative velocity to separate appreciably before they reach the scintillator. There is thus a high probability that they will hit the same scintillator section and be accepted in the trigger.

Two such particles will give a larger pulse height than an alpha particle with the same velocity[24].

In the decay mode $^4He^* \rightarrow {}^3He + n$ the relation between pulse height and velocity for the ^3He particle will be very close to the one for an alpha particle, making it impossible to use the pulse height to distinguish such reactions from elastic scattering. For any decay particle the angles measured will, of course, be somewhat different from those expected for elastic scattering, increasingly so as Q increases. The contribution to the background of excited states will therefore be depressed by a factor depending on Q and on the resolution of the measurement of the anglesof the recoils[17].

Reliable data or theoretical estimates of the cross-sections as function of momentum transfer for the excitation of ^4He do not appear to exist, but an approximate calculation based on the work of Maris and Tyrén[25] suggests that this type of background may be significant in the region near the minimum. Experimentally, however, we have evidence that the background due to excited states is likely to be small at all momentum transfers. The lowest state of ^4He, the 0^+ level at 20.2 MeV[26] which is excited very strongly with electrons can decay only into $p + {}^3H$ for kinematical reasons. The presence of an appreciable background from this level, would therefore give rise to events with larger pulse heights than found in elastic reactions. In Fig.3 we show a plot of recoil energies derived from pulse height against recoil energies computed from the pion scattering angle for events selected with $\chi^2 < 16$. As is seen there are no events which fit the predicted ($^3H + p$) curve, their absence indicates that the background from other low-lying levels with the decay $^4He^* \rightarrow n + {}^3He$ is small also.

We conclude that our results are in very good agreement with calculations based on the theory of coherent multiple scattering using some rather crude approximations (Gaussian pion-nucleon amplitudes, constant phase). The measured position of the minimum is at $-t = 0.3$ and from comparison of the curves in Fig. 2 the ratio of the real part to the imaginary part of the πN scattering amplitude lies in the region 0.3 to 0.4 if it is independent of momentum transfer and the background is indeed as small as we believe it to be.

ACKNOWLEDGEMENTS

We thank Professors P. Preiswerk, H. Schopper and H. Tyrén for their support and interest in this work. Many useful discussions with Professor O. Kofoed-Hansen are gratefully acknowledged and we are particularly indebted to him for putting his unpublished results on ^{4}He at our disposal. We thank Dr W. Beusch for his advice and help during the experimental runs, Dr V. Chabaud for providing us with the kinematic fitting program used in the analysis, and Professors L.Bertocchi and J. Trefil for their advice and encouragement during the planning of this experiment.

The work was carried out at CERN with additional financial support from the Statens Råd för Atomforskning, Sweden, and the Centre National pour la Recherche Scientifique, France.

REFERENCES

1) R.J. Glauber, "Lectures in Theoretical Physics", Ed. W.E. Brittin et al. (Interscience Publishers Inc. N.Y. 1959).

2) W. Czyz and L. Lesniak, Phys. Letters 24B, 227 (1967).

3) H. Palevsky, J.L. Friedes, R.J. Sutter, G.W. Bennett, G.J. Igo, W.D. Simpson, G.C. Phillips, D.M. Corley, N.S. Wall, R.L. Stearns and B. Gottschalk, Phys. Rev. Letters 18, 1200 (1967).

4) R.H. Bassel and C. Wilkin, Phys. Rev. Letters 18, 871 (1967).

5) L. Formanek and J. Trefil, Nucl. Phys. B4, 165 (1967).

6) F. Bradamante, G. Fidecaro, M. Fidecaro, M. Giorgi, P. Palazzi, A. Penzo, L. Piemontese, F. Sauli, P. Schiavon and A. Vascotto, Phys. Letters 31B, 87 (1970).

7) J.L. Friedes, S.T. Emerson, H. Palevsky, W.D. Simpson, R.J. Sutter, R.L. Stearns and W. von Witsch, Phys. Rev. Letters 24, 677 (1970).

8) M. Fellinger, E. Gutman, R.C. Lamb, F.C. Peterson, L.S. Schroeder, R.C. Chase, E. Coleman and T.G. Rhoades, Phys. Rev. Letters 22, 1265 (1969).

9) G.W. Bennett, J.L. Friedes, H. Palevsky, R.J. Sutter, G.J. Igo, W.D. Simpson, G.C. Phillips, R.L. Stearns and D.M. Corley, Phys. Rev. Letters 19, 387 (1967).

10) D.R. Harrington, Phys. Rev. Letters 21, 1496 (1968).

11) E.T. Boschitz, W.K. Roberts, J.S. Vincent, K. Gotow, P.C. Gugelot, C.F. Perdrisat and L.W. Swenson, Phys. Rev. Letters 20, 1116 (1968).

12) J. Combe, J. Gardès, M. Querrou, N. Doble and E. Dahl-Jensen, Il Nuovo Cimento, to appear.

13) C. Bemporad, W. Beusch, A.C. Melissinos, E. Schuller, P. Astbury and J.G. Lee, Nucl. Instr. Methods 80, 205 (1970).

14) G. Landaud, F. Lemeilleur, J.P. Patry, H. Saur, H. Yonnet, A. Johansson, G. Tibell, S. Kullander, P.U. Renberg and A. Cordaillat, Nucl. Instr. Meth. 83, 309 (1970).

15) S. Kullander, G. Landaud, R. Lorenzi and J. Yonnet, Nucl. Instr. Meth. 92, 141 (1971).

16) S. Dahlgren, S. Kullander and R. Lorenzi, Nucl. Instr. Meth. 89, 29 (1970).

17) S. Dahlgren, A.J. Herz, S. Kullander, R. Lorenzi, T. Ekelöf, B. Höistad and A. Åsberg, Nucl. Instr. Meth. (to be published).

18) V. Chabaud, Private communication.

19) O. Kofoed-Hansen, private communication.

20) K.J. Foley, R.S. Jones, S.J. Lindenbaum, W.A. Love, S. Ozaki, E.D. Platner, L.A. Quarles and E.H. Willer, Phys. Rev. Letters 19, 330 (1967).

21) T. Lesniak et al., Session U(a), Paper 30, Kiev 1970.

22) R.F. Frosch, J.S. McCarthy, R.E. Rand and M.R. Yearian, Phys. Rev. 160, 874 (1967).

23) C.F. Perdrisat, L.W. Swenson, P.C. Gugelot, E.T. Boschitz, W.K. Roberts, J.S. Vincent and J.R. Priest, Phys. Rev. 187, 1201 (1969).

24) J.B. Birks, Theory and Practive of Scintillation Counting (London: Pergamon Press, 1964).

25) Th.A.J. Maris and H. Tyrén, Nucl. Phys. 3, 35 (1958).

26) R.F. Frosch, R.E. Rand, Hallcrannell, J.S. McCarthy, L.R. Suelzle and M.R. Yearian, Nucl. Phys. A110, 657 (1968).

27) W.E. Meyerhof and T.A. Tombrello, Nucl. Phys. A109, 1 (1968).

FIGURE CAPTIONS

1) Experimental lay-out showing scintillators used for coincidence, S and anticoincidence, A, purposes. The multiwire proportional chambers, MP, give the incident track, the cylindrical wire spark chambers surrounding the target give the α track and the ordinary spark chambers, C, give the outgoing pion track.

2) Differential cross-sections as function of the square of the four-momentum transfer. The curves were calculated by means of the Glauber theory [19] and the formulae listed in the text.

3) Alpha energy determined from pulse height plotted against alpha energy from pion scattering angle for events with $\chi^2 < 16$ according to the hypothesis of elastic scattering. The two trajectories have been calculated from the plots of light response vs energy given in ref. 24.

Total beam	T_i	$T_i T_o$	$T_i T_\alpha$	$T_i^{delay} \times T_\alpha$	$(T_i T_o)^{delay} \times T_\alpha$
1	0,4	2.10^{-4}	$2.4.10^{-4}$	4.10^{-5}	6.10^{-6}

Influence of various trigger combinations on counting rate with 5 atm He in target

TABLE 1

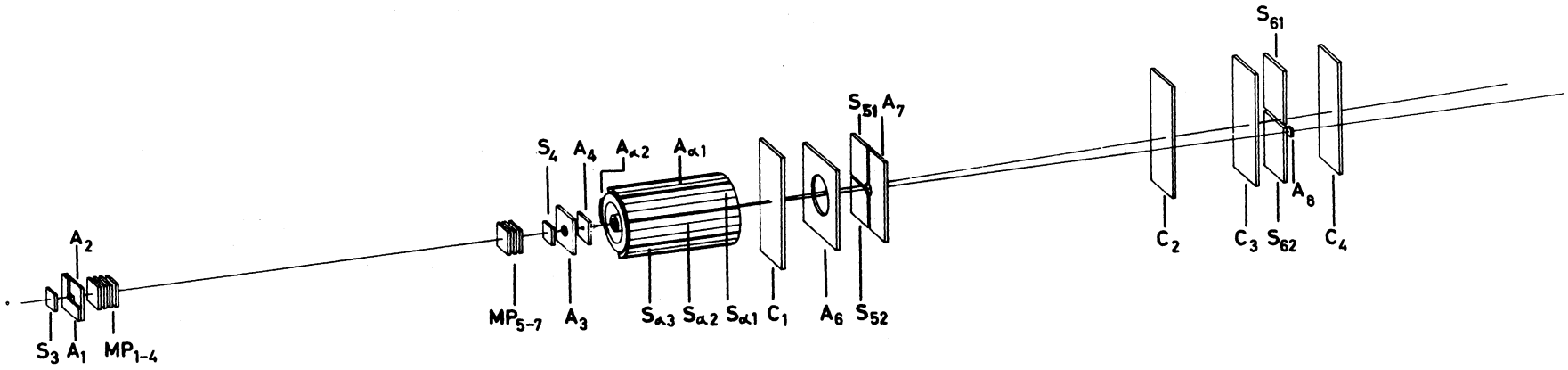

Fig. 1: Experimental lay-out showing scintillators used for coincidence, S and anticoincidence, A, purposes. The multiwire proportional chambers, MP, give the incident track, the cylindrical wire spark chambers surrounding the target give the α track and the ordinary spark chambers, C, give the outgoing pion track.

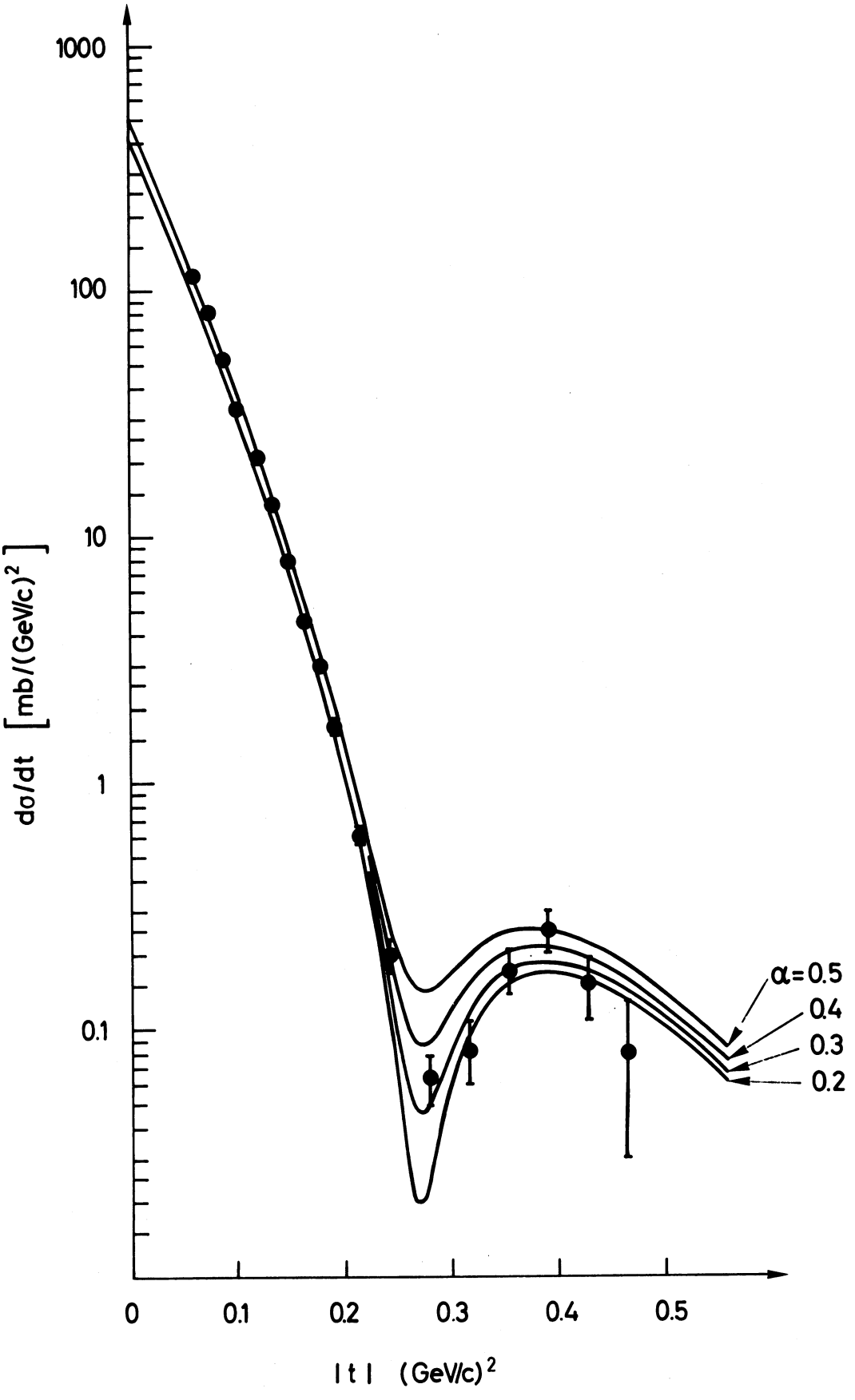

Fig. 2: Differential cross-sections as function of the square of the four-momentum transfer. The curves were calculated by means of the Glauber theory[19] and the formulae listed in the text.

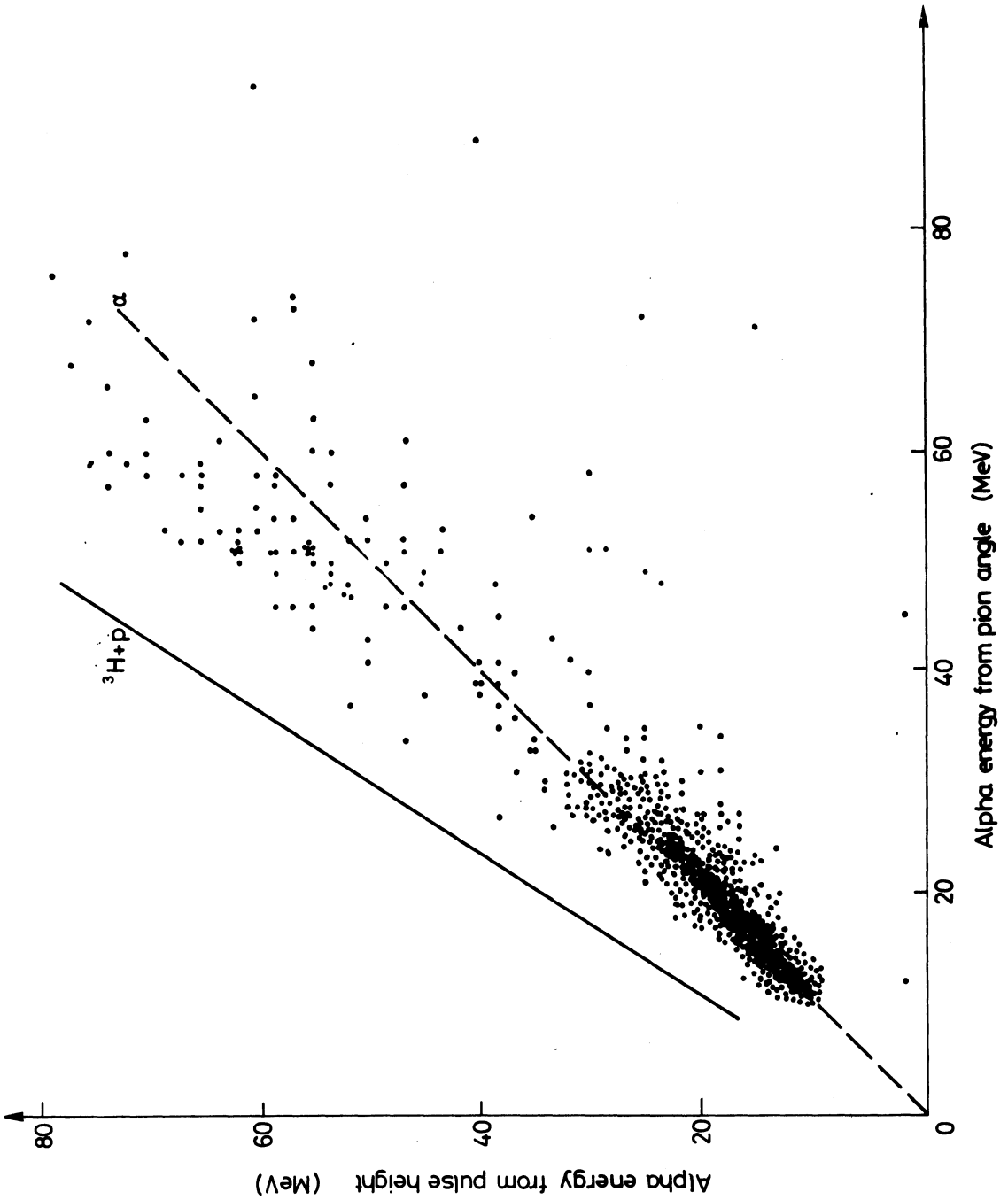

Fig. 3: Alpha energy determined from pulse height plotted against alpha energy from pion scattering angle for events with $\chi^2 < 16$ according to the hypothesis of elastic scattering. The two trajectories have been calculated from the plots of light response vs energy given in ref. 24.

EUROPEAN ORGANIZATION FOR NUCLEAR RESEARCH

A HELIUM-RECOIL SPECTROMETER

S. Dahlgren*), A.J. Herz, S. Kullander and R. Lorenzi
CERN, Geneva, Switzerland

T. Ekelöf, B. Höistad and A. Åsberg
Gustaf Werner Institute, Uppsala, Sweden

SUMMARY

The instrument described is intended for the detection and measurement of α particles from coherent interactions of high-energy particles with ^{4}He nuclei. It allows the determination of the magnitude and the direction of the momenta of the helium recoils from interactions in a pressurized gas target. The measurements are carried out with spark chambers and scintillation counters. Recoils emitted at angles greater than 65° with respect to the beam direction are accepted and the range of azimuth angles covered is 294°.

Geneva - March 1972

(Submitted to Nuclear Instruments and Methods)

---

*) Now at the Gustaf Werner Institute, Uppsala, Sweden.

1. INTRODUCTION

In this paper we describe a device in which one can measure the energy and direction of emission of very slow recoiling nuclei from interactions of high-energy particles in a pressurized gas target. The apparatus was designed for work with helium, but it is possible to modify it to permit operation with hydrogen or deuterium.

There are several justifications for developing such an instrument. The most general one is that the momentum transfer to the target nucleus is one of the variables of greatest physical interest in the investigation of elastic and inelastic collision processes, and that this quantity becomes more and more difficult to determine from measurements on fast secondaries as the momenta of these rise into the multi-GeV/c region. Due to the high rates of energy loss of the recoiling nuclei (which normally have momenta of the order of hundreds of MeV/c) observing them directly is also beset by problems, but once these have been solved the equipment does not have to be scaled up as primary energies increase for the interesting range of momentum transfers remains the same. Furthermore, these measurements provide additional constraints in the kinematic fitting procedures and they allow one to apply very important trigger conditions.

If the identity and the momentum vector of the recoiling nucleus and of the incident particle are known, the mass of the outgoing fast system of secondary particles can be calculated. In Section 3.2 it is shown that with this instrument the dominant contribution to the error in the outgoing mass comes from the error in the determination of the angle at which the recoil is emitted. The uncertainties in the magnitude of the momenta of the incoming and outgoing fast particles are relatively unimportant which is an additional reason why this type of device is suitable for experiments at very high incident momenta.

In the present case, the apparatus was intended primarily for the study of coherent production in interactions of high-energy particles with ^{4}He nuclei[1]. Coherent interactions are defined as collision processes in which the target remains in its ground state, in contrast to semicoherent ones in which there is excitation, and incoherent ones in which the target nucleus breaks up. The study of coherent interactions

is of considerable physical interest because selection rules restrict the variety of secondary systems, thus facilitating the analysis of their properties, and because information on resonance-nucleon scattering inside nuclei can be extracted from the momentum-transfer distribution by application of the Glauber multiple-scattering formalism[2].

From the experimental point of view, ^{4}He is a particularly suitable nucleus for work on such reactions because its lowest excited state has a very high excitation energy, about 20 MeV [3], and because all its excited states decay by particle emission, so that the identification of a recoil α particle guarantees that the event was coherent.

The basic features of the instrument described in this paper are shown diagramatically in Fig. 1. A target containing gas at high pressure (to obtain an adequate event rate) is combined with low-pressure spark chambers to provide measurements on low-momentum recoils. The target is operated at pressures up to 20 atm, and the recoiling alpha particles pass through its thin walls into a surrounding low-pressure region, filled with a helium-alcohol mixture at around 0.05 atm pressure, in which two cylindrical spark chambers are operated. They then come to rest in one of seven plastic scintillators arranged in a cylindrical geometry. The azimuthal acceptance is 294°. The line of flight of the recoils is thus determined by means of spark chambers, and information about their energy comes from their time of flight and the amount of light they produce in the scintillators. In the momentum range of interest it takes the ^{4}He recoil between 6 ns and 60 ns to get to the scintillator from the target. Requiring a pulse from the recoil scintillator within this time interval provides a valuable trigger criterion.

A general view of the apparatus, opened and with the spark chambers extracted, is shown in Fig. 2. The instrument is fully described in Section 2, the performance of its component parts in Section 3, and some relevant experimental results are described in Section 4. A comparison between our recoil-detection technique and some others will be found in Section 5.

2. DESCRIPTION OF THE INSTRUMENT

2.1 Basic design considerations

The apparatus was designed for the investigation of reactions of the type

$$(\text{fast primary particle}) + {}^4\text{He} \rightarrow X + {}^4\text{He} \ , \qquad (1)$$

in which "X" may be any particle or system of particles allowed by kinematics and selection rules. Account had to be taken of the fact that many of the processes to be investigated have very low cross-sections, that a wide range of momentum transfers is of interest and that the final experimental set-up had to be such as to allow discrimination against events in which the ^{4}He is broken up. Before going into detail it is useful to discuss the relations between the magnitudes involved.

The most general case of a collision process between an incoming fast particle and a nucleus of mass M is shown in Fig. 3, which also defines the symbols used for the quantities involved. Without making any approximations other than the excitation energy $E_x^2 \ll M^2$ and that the recoil moves with non-relativistic velocity ($q = 2M^*T$, T being the kinetic energy and $M^* = M + E_x$), one obtains the following relation

$$q_{\parallel}\left[1 - \frac{E_0 + M}{2p_0M^*}\, q_{\parallel}\right] = \frac{m^{*2} - m_0^2}{2p_0} + \frac{E_0 + M}{2p_0M^*}\, q_{\perp}^2 + \frac{E_0}{p_0}\, E_x \ . \qquad (2)$$

At higher incident momentum p_0 a useful approximation relating the longitudinal momentum transfer to the excitations is

$$q_{\parallel} \simeq \frac{m^{*2} - m_0^2}{2p_0} + E_x \ . \qquad (2a)$$

If the interaction is coherent, the excitation energy, $E_x = M^* - M$ of the target nucleus is zero.

Note that the effect on $q_{\parallel}$ of raising the outgoing fast system to a higher invariant mass ($m_0 \rightarrow m^*$) is of the same kind as that of exciting the target nucleus. However, in the case of ^{4}He the lowest excited state has $E_x \approx 20$ MeV, so that the increase in $q_{\parallel}$ (and, hence, the change in

the angle of emission of the recoiling system) is large, as is discussed below in Section 3.2. This facilitates considerably the separation of true coherent coherent processes (for which $E_x = 0$) from semicoherent ones.

In Fig. 4 we show a plot of Eq. (2) for incident protons of 20 GeV/c Ideally one would wish to cover the whole domain of momentum transfer shown in such diagrams. However, in the mass range of primary interest a system in which only recoils emitted at large angles are detected is suitable. This choice lowers the upper limit to the mass of the secondary system X [Eq. (1)], but allows one to accept a wide range of recoil momenta. It has the important practical advantage that it can be arranged that neither the beam nor the fast secondary particles traverse the spark chambers. Using the relation[4)]

$$\sum m_i \sin \theta_i < q_{\parallel} \tag{3}$$

(where the m_i and θ_i are the masses and angles of emission of the fast secondaries), we estimated that the angles at which fast secondaries are emitted will usually be less than about 15° in the range of interest, and the inner radius of the assembly as well as the size of the exit window were chosen accordingly (see Fig. 1).

The range of momentum transfers to the target nucleus accepted by the apparatus should include as much as possible of the forward diffraction peak and the upper limit should be at least high enough to allow observation of the first minimum in the hadron-nucleus differential cross-section. The requirement that the upper limit to the momentum transfer should be high is easily met: a range of 4 mm in plastic scintillator corresponds to T = 70 MeV, q = 720 MeV/c and a four-momentum transfer $t = -0.52$ (GeV/c)^2. Because of the high rate of energy loss of the recoils, the most difficult problem is how to obtain the smallest possible lower limit to the momentum transfer. Our aim has been to reduce it by reducing the wall thickness of the gas target, by operating the windowless cylindrical spark chambers with a helium-alcohol mixture at the lowest possible pressure, and by having good light collection from the scintillators. In this way a lower limit T = 5 MeV corresponding to q = 190 MeV/c, $t = -0.04$ (GeV/c)^2, could be obtained.

When the energy of the recoil is low, its energy loss in the target can be up to 60% of the total energy loss, so that the pressure of the target gas has to be known and kept constant.

2.2 The gas target

To obtain adequate event rates from a helium gas target at pressures of the order of several atmospheres it has to be fairly long: we chose a length of 50 cm. Tests showed that the diameter of the cylinder had to be 2 cm in order to be larger than that of the effective envelope of the available beam. In such a target, there will be 1.4×10^{-6} events per millibarn, atmosphere and incident particle.

The thin walls of the target, in the mg/cm^2 region, must be supported to resist the pressure. The construction used is shown in Fig. 5; it is essentially a spiral of 0.4-mm stainless-steel wire with 2-mm pitch, with a short length of flanged tubing at each end to which the windows and gas connections are attached. The tube of thin foil is inserted into this supporting cage.

The toughest material readily available in the form of thin film is polyethylene terephthalate, sold commercially under a variety of trade names*). We chose it after some testing as the most suitable for the walls of target, although it is somewhat porous, and in spite of the fact that we did not find any foils of thickness less than 25 μm which were completely free of pin holes. Tubes were fabricated from this material by a combination of ultrasonic welding and cementing.

Targets with walls 3.5 μm, 8 μm and 70 μm thick could be used at absolute pressures of 2 atm, 5 atm and 20 atm, respectively. In general, leaks appeared after about 15 hours of operation under pressure. The "thin" targets, 3.5 μm and 8 μm, developed holes, the "thick" ones always failed at the seam: the latter suggests that further improvements in the technique of making joints may lead to longer lifetimes in the case of "thick" targets.

With the dimensions chosen, about 20% of the recoils will be intercepted by the supporting wire spiral. A proportion of these, increasing with recoil momentum, will emerge again having lost energy and undergone

---

*) Trade names frequently encountered are Hostaphan, Melinex and Mylar.

multiple scattering. However, given sufficient information on the momenta and energies of the fast secondaries, most of the events concerned will be rejected in a kinematic fit; the few which pass will, on the average, have been fitted with a low value of the momentum transfer.

2.3 The low-pressure helium spark chambers

The cylindrical wire spark chambers and their read-out system are described in detail in a separate paper[5]; they are shown on the left of Fig. 2. In this section we summarize their principal characteristics and give some data on their performance.

The external dimensions (370 mm diameter × 600 mm long and 700 mm diameter × 800 mm long) are a compromise between the requirements of adequate angular resolution, of low stopping power and Coulomb scattering, and of keeping materials and the sensitive volume out of the beam, its halo and secondary particles. Apart from a region at the bottom, 45° wide in azimuth, used for mechanical supports and electrical connections, the target is completely surrounded by the chambers. They can be operated at pressures as low as 40 Torr with helium gas containing 14% by volume C_2H_5OH. The four conducting planes are made up of wires 50 μm and 70 μm in diameter, giving an over-all transparency of 88%. There are no walls and the effective thickness of gas between the target and the circumferential scintillators is equivalent to 0.7 mg/cm^2 at that pressure.

Both the longitudinal and the azimuthal coordinates of the sparks in both chambers are read out by the current-distribution method. This method has the advantage of simplicity; the fact that only single sparks can be handled by it does not matter in the case of good events as there is only one recoil track.

Reliable performance was obtained as long as the tracks were not inclined more than 25° away from the normal. An important feature of these chambers is that particles of minimum ionization do not produce sparks. This eliminates spurious sparks due to fast particles associated with the beam.

To calibrate the read-out system and test the chambers we used a set of collimated ^{241}Am α-particle sources (5.48 MeV) mounted on a rod in the position of the gas target. With the aid of these sources the

longitudinal angular distributions obtained with mono-directional α particles coming from the chamber axis were found to have standard deviations of 0.51° when the chamber was filled to a pressure of 45 Torr. In experiments there is the additional error due to scattering in the gas and walls of the target. In Fig. 6 we show the calculated standard deviations of the longitudinal angles for two types of targets. The total standard deviations of the azimuthal angles were rather larger, about 1.6° increasing to 2.3° at the lowest recoil energies.

2.4 Scintillators

In Fig. 7 we show one of the circumferential scintillators. Each of these has a sensitive area 50 cm × 27 cm and covers 42° in azimuth. Light guides at each end pass through a cover plate of the vacuum chamber and the photomultipliers are mounted on the outside of this plate (see Fig. 2). Thus each set of scintillator, light guide, photomultiplier and cover plate forms a convenient plug-in unit which can be calibrated separately, away from the main chamber.

To minimize loss of light, constant-cross-section light guides were used. The cross-sectional areas of the scintillator sheets thus could not be more than those of the cathodes of the photomultipliers. This led us to choose 4 mm for the scintillator thickness, matching the cathodes of 42 mm diameter of the photomultipliers used. As mentioned before, 4 mm thickness is also sufficient to stop all alpha particles with energies in the region of interest.

The time of flight of the recoil and the height of the pulse it produces in the scintillator are used both as trigger criteria and as data in the analysis of the experiment. In the trigger system the dependence of the timing on the position at which the recoil hits the scintillator cannot be taken into account so that there is a smearing of what might otherwise be a rather sharp high-energy threshold. For the final analysis, however, detailed calibrations were used.

The response of the plastic scintillator material (Pilot B) to α particles in the energy range 2 to 40 MeV was determined with α-particle sources and at the cyclotrons of the Institute for Atomic Physics in Stockholm[6]. The result is shown in Fig. 8. The output increases linearly

with energy above 20 MeV and we assume that the dependence remains linear above 40 MeV. Note that the range of light outputs to be measured is 70 : 1 between 40 MeV and 3 MeV, 140 : 1 between 70 MeV and 3 MeV. As the response of the photomultipliers was not linear over the entire range they had to be calibrated.

Apart from the attenuation which the light emitted from a point in the scintillator undergoes in passing through the light guide and through two interfaces (Pilot B/Perspex and Perspex/glass), one has to expect variations in transmission due to imperfections in joints, surface finish and the materials used. It is necessary, therefore, to establish the attenuation as function of position for each scintillator assembly separately. This was done by exploring the scintillators with a 5.48-MeV α source (^{241}Am), and Fig. 9 shows a representative set of curves obtained by displacing the source along the long axis of one of the scintillators.

In the data analysis the kinetic energy of the recoil at the surface of the scintillator is calculated using these calibrations, the measured pulse height and the position as determined from the spark chambers. The energy at the scattering point is then obtained by adding the energy losses which vary with energy and with path length in the various media. In Fig. 10 these losses are given for a recoil having the shortest possible track through the mylar (70 μm) and the spark-chamber gas and the longest possible track through the target gas. As can be seen it is necessary to know the interaction point in the target with good precision.

The scintillator pulse is also used as a stop signal -- the start signal comes from a scintillator in front of the target (Fig. 1) -- to obtain the time of flight of the recoil. In the calculation of the recoil energy from its time of flight it is necessary to take the successive energy losses during the flight into account. In Fig. 11 we show the relation between the energy at the scattering point and the time of flight computed with these losses. For comparison, the relation without energy losses is also given.

2.5 Magnetic shielding

In most experiments in which the apparatus may be used, it will be close to a large spectrometer magnet, so that the downstream end of the instrument may be in a strong magnetic field. We have tested cylindrical shields of soft iron having a wall thickness of 3 cm and found that they will provide adequate additional protection for a photomultiplier in a normal shielded housing at least up to fields of about 2 kG. In order not to apply excessive loads to the photomultiplier housings these shields were attached to an independent support.

2.6 The gas-handling system

The density of the helium gas in the target must be known for the calculation of cross-sections, and this density also determines the amount of energy lost by the recoil before it reaches the target wall. In our case the temperature varied only slowly so that it was sufficient to keep the pressure in the target constant; this was done manually. Helium gas at a pressure controlled by an ordinary regulator was passed through a needle valve into one end of the target and escaped to the atmosphere through a second needle valve. The pressure in the target was read on a high-quality manometer. We found that small adjustments of the needle valves every half hour or so were sufficient to keep the pressure within a few per cent. of the nominal value.

The behaviour of the low-pressure spark chambers depends on the density and composition of the helium-alcohol mixture, so that it must be possible to adjust these quantities to predetermined values. In addition they are needed to calculate the energy losses suffered by the recoils. The control system is shown, simplified for clarity, in Fig. 12. The chamber was flushed continuously with helium-alcohol mixture entering via the regulating valve R4 and extracted by the pump P1 via valve R1, and the pressure was maintained constant by means of the contact manometer M1 operating the valve V1. The concentration of alcohol in the chamber gas was monitored continuously by means of a non-dispersive infra-red gas analyser. The output of the controller associated with the analyser operated the valve V2, thus changing the pressure of the gas mixture in the alcohol bubbler and hence the relative concentration of alcohol vapour in it. The regulating valves R2, R3 and R4, in conjunction with the manometer M3, served to adjust the pressures to the desired values.

3. PRECISION AND BACKGROUNDS

3.1 Momentum-transfer resolution

The momentum of the recoil is computed from the measurements of pulse height and time of flight, account being taken of the reconstructed path of the particle and of the energy losses it suffers on the way. The procedure was described in Section 2.4, and as it is rather complex the resolution is best obtained from the experimental results. Figure 15 in Section 4.2 below shows what was achieved in the first full-scale experiment in which the apparatus was used.

3.2 Missing-mass resolution

The contribution made by the recoil spectrometer to the identification of the event depends essentially on the missing-mass resolution obtained from measurements on the recoil and information on the incoming beam. In a complete experiment, measurements on the fast secondaries will always be used to remove background and improve precision by means of kinematic fitting, but here we discuss the resolution obtainable from the recoil spectrometer alone, it being understood that the particle detected is a ^{4}He nucleus. The problems concerning identification of the recoil are taken up in Section 3.3.

The missing-mass resolution can be obtained from Eqs (2). Assuming $E_x = 0$ one finds, with definitions as in Fig. 3,

$$(\Delta m^*)^2 = \left(\frac{q \cos \theta_\alpha}{m^*}\right)^2 (\Delta p_0)^2 + \left(\frac{p_0 \cos \theta_\alpha - q(1 + E_0/M)}{m^*}\right)^2 (\Delta q)^2 + \left(\frac{p_0 q \sin \theta_\alpha}{m^*}\right)^2 (\Delta \theta_\alpha)^2 \qquad (4)$$

which is valid as long as $\Delta m^* \ll m^*$. As will now be shown, and as can be seen from inspection of Fig. 4, the most important term is that in $\Delta\theta_\alpha$, so that a good approximation is

$$\Delta m^* \simeq \frac{p_0 q \sin \theta_\alpha}{m^*} \Delta\theta_\alpha \quad . \qquad (4a)$$

We now describe the effects of errors in θ_α, recoil momentum q, and beam momentum p_0.

The performance of the spark chambers has been discussed in Section 2.3, and we refer to Fig. 7 for the expected angular resolution. For numerical examples we take the production of mass 1070 MeV/c^2 by 8-GeV/c π^- and that of mass 1688 MeV/c^2 by 20-GeV/c protons. At a momentum transfer q = 346 MeV/c and with a total standard error of 15 mr in θ_α (error in direction of primary included) we find the corresponding contributions to the standard error in m^* to be 39 MeV/c^2 and 62 MeV/c^2, respectively.

In order to obtain realistic estimates of the errors involved in determining the recoil momenta from pulse height and time of flight, use will be made of data obtained in the test experiments described in Section 4. Figure 15 shows the relative standard errors for runs with targets with 70-μm walls. At a recoil momentum of 346 MeV/c the standard error is about 5 MeV/c, and in the case of the same numerical examples as above this gives contributions to the standard error in m^* of 1.8 MeV/c^2 and 5.0 MeV/c^2, respectively, small in comparison with those due to the uncertainty in the angle of the recoil.

In Eq. (4) the term in Δp_0 takes account of the uncertainty in the momentum of the incident beam. If we assume that the distribution of beam momenta has a standard deviation of 1%, we find that the contribution due to Δp_0 to the standard error in m^* is 8.1 MeV/c^2 for both the numerical examples used before.

Thus the total standard errors in m^* are 40 MeV/c^2 for the production of mass 1070 MeV/c^2 by 8-GeV/c pions, and 63 MeV/c^2 for production of 1688 MeV/c^2 by 20-GeV/c protons, in both examples at a momentum transfer q = 346 MeV/c.

3.3 Backgrounds

Background events can be divided into three classes: unwanted types of events in which there is a ^{4}He recoil nucleus in the ground state, events in which the target nucleus is excited or disintegrated and, finally, spurious events due to interactions of the particles in the beam

and its halo with the structure of the apparatus rather than with the target helium. Regardless of the type of experiment, one of the trigger requirements must always be that a particle is detected in one, and only one, of the circumferential scintillators during the time interval within which ^{4}He recoils are expected: between about 6 ns and 60 ns after the passage of the incident particle. Furthermore, there must not be any prompt coincidences between the arrival of a beam particle and a pulse in any of the circumferential scintillators. These are basic trigger conditions common to all the experiments for which the apparatus was designed, and in what follows we assume that they are met.

3.3.1 Background with a true ^{4}He recoil

By definition, all such events are due to coherent interactions; they form part of the background either because the outgoing fast system is of an unwanted type (but was accepted by the trigger system), or because the recoiling α particle passed through one or more of the wires of the target support cage or the spark chambers, suffering scattering and energy loss. These events can be eliminated by kinematic fitting, using information on the incoming and outgoing fast particles in combination with the data provided by the recoil spectrometer.

3.3.2 Events leading to break-up of the target ^{4}He

These events can be of two types: those in which there is a knock-out reaction leaving behind a residual nucleus, and those in which an intermediate excited state, ^{4}He*, is formed.

In a nucleon-knock-out reaction, the momenta of the recoiling ^{3}H's or ^{3}He's will, in the impulse approximation, be equal and opposite to those of the ejected nucleons prior to the collision: they will have a Fermi distribution and be oriented isotropically. Very few of them will have the momentum and direction that would make them mimic a wanted coherent event in a kinematic fit. A calculation was carried out for the specific case of elastic π^- ^{4}He scattering and it was found that after applying the kinematic constraints the background due to this type of reaction was negligible throughout the range of momentum transfer involved[7].

The possible contribution to background from semicoherent reactions which give rise to the formation of an excited helium nucleus has to be discussed in more detail. According to the evidence available, the lowest excited state of ^{4}He has an excitation energy of 20.2 MeV and there are thought to be eight or more levels with excitations up to 28 MeV [3]. All these states decay by particle emission[3], and as the separation energies are large (19.814 MeV for ^{3}H + p, 20.578 MeV for ^{3}He + n), the Q values are low.

Consider the semicoherent reaction

$$(m) + {}^4\mathrm{He} \rightarrow (m^*) + {}^4\mathrm{He}^* \quad \Big\lfloor \rightarrow {}^3\mathrm{He} + n \tag{5}$$

Equation (2a) shows that the longitudinal component, $q_{\parallel}$, of the momentum of the recoiling ^{4}He*, will be E_x MeV/c greater than the longitudinal momentum of the ^{4}He recoil would have been if the reaction had been coherent. However, the momentum and direction of the ^{3}He are different from those of the parent ^{4}He* because of the non-zero Q value. In some cases such an event will be accepted, the ^{3}He having a direction close to what a ^{4}He recoil would have had in a coherent event and producing a pulse height similar to that in the coherent case. Given that m^* and $q_\perp$ are measured by means of a fast-particle spectrometer, with errors Δm^* and $\Delta q_\perp$, and by means of the recoil detector with errors given by Figs. 7 and 15, one can compute the fraction of events of type (5) in which the information obtained from the recoil agrees within the errors with that coming from the fast particles. This fraction of the events will be accepted as coherent in a fit. In Fig. 13 we show the results of such a calculation for a specific case: that of the production of mass 1070 MeV/c^2 by 15-GeV/c pions, the fast-particle spectrometer measuring with the precision indicated in the figure and the performance of the recoil spectrometer being as discussed above. The χ^2 function contained three terms: in addition to the differences in m^* and $q_\perp$ the difference in azimuthal angles of the scattering planes given by the two devices was included. Events were considered acceptable if their χ^2 corresponded to a probability of 5% or more. Calculations giving acceptances as function of transverse momentum transfer were carried out for various produced

masses and also for incident protons and always gave qualitatively the same result as that shown in Fig. 13. One may therefore conclude that at most a few per cent. of semicoherent reactions of type (5) will be wrongly identified in a fit as being coherent.

Discrimination against the reaction

$$(m) + {}^4He \rightarrow (m^*) + {}^4He^* \quad \Big\lfloor \rightarrow {}^3H + p \qquad (6)$$

is even greater than against reaction (5) when both the triton and the proton stop in the scintillator, for then the pulse height will be about twice that expected for the ^4He recoil from the coherent process. It is of interest to note that since the probability for the decay $^4He^* \rightarrow {}^3H + p$ should be similar to that for $^4He^* \rightarrow {}^3He + n$ and since the former decay is easily identified experimentally one also has a check on the occurence of the latter.

4.3.3 Background not due to collisions with target ^4He

Interactions in the target support, windows, and the rest of the apparatus can produce slow particles that satisfy the trigger requirements. The amount of this kind of background can easily be checked during a run by observing the difference between the trigger rates with and without target gas. It is extremely unlikely for such events to survive the geometric and kinematic acceptance criteria in the final analysis (see also Section 4.2), but it is clearly desirable to keep this background low by careful beam design and by minimizing the amount of material in the beam and its halo.

4. RESULTS FROM TEST EXPERIMENTS

4.1 Elastic p ^4He scattering at 185 MeV

The first tests of the equipment were carried out at the 185-MeV synchro-cyclotron of the Gustaf Werner Institute, Uppsala. These tests were made primarily to investigate the operation of the circumferential scintillators and the low-pressure spark chambers in the presence of a beam of instantaneous intensity around 10^6 particles per second and to

gain experience on backgrounds. The spectrometer was combined with a scintillator for the scattered protons. An absorber was used to stop inelastically scattered protons of energy less than 145 MeV.

In the analysis of these tests it was established that the methods used to compute the energy from the time of flight and from the pulse height gave results which agreed within a standard error of 0.4 MeV.

The elastic peak in the recoil angular distribution from the spark chambers was identified and the angular standard error was found to be around 1.5° for recoil scattering angles between 78° and 73°, consistent with expectation (Fig. 6). It was obtained from the distribution of the differences between the recoil angles as measured directly and the same angles as calculated from the pulse heights and times of flight. This distribution is shown in Fig. 14. For the lower curve the constraint has been applied that the time of flight and pulse height should be consistent with an alpha particle and that the two azimuthal track coordinates from the spark chambers should give a line traversing the target.

The trigger rate without target gas was found to be 25% of the rate with the target gas at 5 atm pressure. The lower cut-off in the square of the four-momentum transfer was found to be $t = -0.04$ $(GeV/c)^2$ with 8-μm target walls and 2.5 atm pressure.

4.2 Elastic scattering at 7.76 GeV/c

Further experience was gained during an experiment carried out at the CERN Proton Synchrotron in a beam of 7.76-GeV/c negative pions. In this experiment a measurement of the differential cross-section for elastic π^- ^{4}He scattering over the -t range 0.05 to 0.5 $(GeV/c)^2$ was made with clear detection of the first diffraction minimum[7]. Here we shall confine ourselves to some remarks relevant to the recoil spectrometer and its performance.

The coordinates of the incident and scattered particles were measured with high precision so that a complete geometrical reconstruction could be made. The vertex reconstruction and the kinematics imposed a total of six constraints in the χ^2 fitting program for elastic scattering. This eliminated nearly all background events.

The errors in the recoil momenta determined from the pulse height and from the time-of-flight measurements were estimated as follows. Every recoil particle produces a pulse in the upstream as well as in the downstream photomultiplier. One can thus obtain distributions of the differences between upstream and downstream values for both pulse height and time of flight. The standard error of an upstream-downstream average can then be estimated from the corresponding distribution of upstream-downstream differences. In Fig. 15 the relative standard errors are shown for runs with targets having 70-μm walls filled to a pressure of 15 atm.

The angular resolution of the spark chambers was checked by comparing the measured recoil angle with that calculated from the pion scattering angle under the hypothesis of elastic scattering (the error in the pion scattering angle was much less than the corresponding relative error in the recoil angle, assuming elastic events). This was done for the sample of χ^2-selected elastic events and the results were in good agreement with the theoretical calculations of Fig. 7.

The event rate during the data taking was one per PS burst (one PS burst every two seconds). The trigger rates without target gas were as low as 10% of the rate with 20 atm and out of the events collected without target gas only a negligible number survived the final χ^2 analysis.

Requiring a recoil signal within a time-of-flight gate between 6 ns and 60 ns after the passage of the fast particle reduced the trigger rate by a factor 30 [7].

In the analysis of the χ^2-selected data, inspection of the two-dimensional distribution of pulse height and time of flight showed that the occurrence of (^{3}H + p) final states was negligible; thus the semicoherent background had been excluded successfully[7].

In Fig. 16 the missing-mass distribution is displayed. The upper curve is an unselected sample of registered events and the lower curve is a sample with $\chi^2 < 12.6$. The total number of events was reduced from

44100 to 7500 by this requirement, whilst the peak value corresponding to elastic events was only reduced from 700 to 500. In the calculation of the missing mass only information from the recoil spectrometer was used, i.e. the length and direction of the recoil momentum vector, and the data represented by the lower curve in Fig. 16 have not been fitted, only selected. This selection, on the other hand, was done with the aid of the χ^2 function which contains also complementary information, coming from the incident and the scattered fast particles. The distribution is centred around the square of the pion mass and the standard deviation is 0.13 GeV/c^2.

For a resonance of mass 1070 MeV/c^2 the standard error in the missing mass would be 60 MeV/c^2 for the same momentum transfer as in elastic scattering if it is assumed that the error in recoil angle is the same. This figure is about 50% larger than the 39 MeV/c^2 estimated in Section 3.1. Bearing in mind the rapid variation of the angular error with momentum (Fig. 7) in the selected momentum interval (300 - 400 MeV/c) the agreement is satisfactory.

5. CONCLUSIONS AND COMPARISONS WITH OTHER TECHNIQUES

The recoil spectrometer we describe satisfies the basic design requirements: it provides measurements of the momenta and directions of recoil alpha particles emitted at large angles from coherent interactions with ^{4}He in a gas target. Furthermore, it allows the inclusion in the trigger criteria of the detection of a recoil having a time of flight within the expected time interval. This reduces by a large factor the number of spurious events. The instrument also has a very wide angle of acceptance so that it is suitable for the investigation of processes with low cross-sections. The experiment on π^- ^{4}He elastic scattering at 7.76 GeV/c could not have been performed with any other technique in current use today.

Several other methods of detection and measurement provide information on recoils in coherent interactions of high-energy particles with nuclei other than ^{1}H and ^{2}H. However, none of them, as far as we know, provides the combination of advantages of the device we have described above. In particular,

i) the helium bubble chamber cannot be triggered selectively;

ii) silicon semiconductor detectors can be used as targets in experiments on coherent interactions with Si nuclei[8], here the pulse height due to the event can be used to discriminate against nuclear break-up, and the energy of the recoil may be measured, but not the angle, another disadvantage is that the detector has to be in the beam;

iii) semiconductor particle identifiers can be used to detect the recoil and measure its energy[9], but for reasons of cost this method can only be used when it is sufficient to cover small solid angles; and, finally,

iv) streamer chambers filled with helium can, in principle, provide good measurements, but they do not, as yet, allow the recoil to be included in the trigger[10].

In its present form, the instrument could already be used for experiments on coherent interactions of particles in the 100 GeV to 300 GeV range, though the missing-mass resolution would not be as good as it is at lower primary energies. However, further developments, leading to improved angular resolution and, hence, higher missing-mass resolution, appear feasible. We feel confident, therefore, that it will be possible to use this type of device successfully, not only now but also at the accelerators of the new 200/300 GeV generation.

Acknowledgements

We are most grateful, for much advice and many ideas, to all those who participated in the design and building of the apparatus. In particular, we should like to express our thanks to Mr R. Benoit, Mr K. Brock, Mr U. Brotschi, Mr R. Grabit, Mr A. Ménétrey and Mr P. Schilly. We very much appreciated the assistance and cooperation extended to us by Mr J. Augsburger and Dr G. Muratori and their staffs. It is a pleasure to acknowledge the help given during the early tests by the Uppsala cyclotron crew and by Mr J. Dorell. We should like to thank also Professor O. Kofoed-Hansen for his assistance during design and initial testing, and for useful discussions and much encouragement thereafter. To the late Professor P. Preiswerk and Professors H. Schopper and H. Tyrén we are much indebted for the support they have given to this work.

REFERENCES

1) T. Bunaciu, D. Evans, A.J. Herz, S. Kullander, A. Manz and Ph. Rosselet, Proposal to CERN Electronics Experiments Committee (CERN, Geneva, 19 July 1967).

2) J. Formanek and J. Trefil, Nuclear Phys. B3, 155 (1967); K.S. Kölbig and B. Margolis, Nuclear Phys. B6, 85 (1968).

3) W.E. Meyerhof and T.A. Tombrello, Nuclear Phys. A109, 39 (1968).

4) C.M. Fisher, W.M. Gibson, A. Mason, W.A. Venus and D. Evans, Nuovo Cimento 27, 761 (1963).

5) S. Dahlgren, S. Kullander and R. Lorenzi, Nuclear Instrum. Methods 89, 29 (1970).

6) B. Höistad, J. Dorell and A. Åsberg, Gustaf Werner Institute, Univ. Uppsala, Internal Report GWI-PH 4/69, March 1969.

7) T. Ekelöf, B. Höistad, A. Åsberg, C. Busi, S. Dahlgren, A.J. Herz, S. Kullander, G. Lee, D. Websdale, G. Landaud and J. Yonnet, Nuclear Phys. B35, 493 (1971).

8) G. Bellini, M. di Corato, P.F. Manfredi, G. Vegni, p. 269 and P.F. Manfredi, D. Misler, V. Varoli, p.275 *in* Proc. Topical Seminar on Interactions of Elementary Particles with Nuclei, Trieste, 15-17 Sept. 1970, (INFN, Trieste, 1971).

9) M. Brossard, J. Combe, J. Fain, J. Gardès, L. Méritet, M. Querrou, D. Riss, B. Chambon, D. Drain, N. Madjar and C. Pastor, Nuclear Instrum. Methods 93, 529 (1971).

10) NAL Proposal 86A by Seattle-Orsay Collaboration; see also H.J. Lubatti, Review presented at Argonne Summer Workshop, 28-30 June 1971 (Preprint VTL-PUB-7, University of Washington, Seattle).

Figure captions

Fig. 1 : Diagramatic view of the recoil spectrometer.

Fig. 2 : The recoil spectrometer opened and with the cylindrical spark chambers extracted. Inside the vacuum vessel can be seen the circumferential scintillators and the gas target.

Fig. 3 : Symbols used in the text to describe the general case of a collision between a fast particle (mass m_0) and a heavy target nucleus (mass M). The excitation energy $E_x = M^* - M$ and the kinetic energy $T = E_{M^*} - M^*$.

Fig. 4 : Equation (2) plotted for incident protons of 20 MeV/c with the outgoing mass m^* as parameter.

Fig. 5 : The gas target.

Fig. 6 : The standard error in the measurement of the recoil angle as calculated from Coulomb scattering and the intrinsic resolution of the spark chambers. The pressures were 5 atm and 15 atm respectively.

Fig. 7 : One of the circumferential scintillators.

Fig. 8 : Light output from Pilot B scintillator plastic as a function of the kinetic energy of an absorbed alpha particle.

Fig. 9 : Light outputs from the scintillator in Fig. 7, caused by α particles from a 5.48-MeV source, as a function of the position of the source along the long axis of the scintillator.

Fig. 10 : Diagram showing how kinetic energy is lost by the ^{4}He recoil in different media on its way from the scattering point (0) to the scintillator (3) (see sketch). The curves give the kinetic energy at the scattering point (T_0) as function of the kinetic energy after traversing the target

high-pressure helium (i = 1), after traversing also the target wall (i = 2), and finally when arriving at the scintillator after having also traversed the spark chamber gas (i = 3).

Fig. 11 : Time of flight as function of the kinetic energy T_0 at the interaction point (see Fig. 10) with energy losses taken into account and, for comparison, in vacuum.

Fig. 12 : The gas-handling system for the spark chambers.

Fig. 13 : Fraction of semicoherent events accepted as coherent when information from the recoil spectrometer is combined with values of m^*, $q_\perp$ and azimuthal angle determined by means of a fast-particle spectrometer. Symbols as in Fig. 3.

Fig. 14 : Distribution of the differences between recoil angles as measured by the spark chambers and those computed from the recoil kinetic energies derived from pulse-height/time-of-flight measurements. Upper histogram: raw data. Lower histogram: events remaining after application of the criteria described in the text.

Fig. 15 : Standard error of measurement of recoil momentum as derived from pulse height (PH), from time of flight (TOF) and from combining both (TOT).

Fig. 16 : Distribution of the square of the missing mass. Upper histogram: no selection. Lower histogram: same sample after elimination of events with $\chi^2 > 12.6$ (6 degrees of freedom).

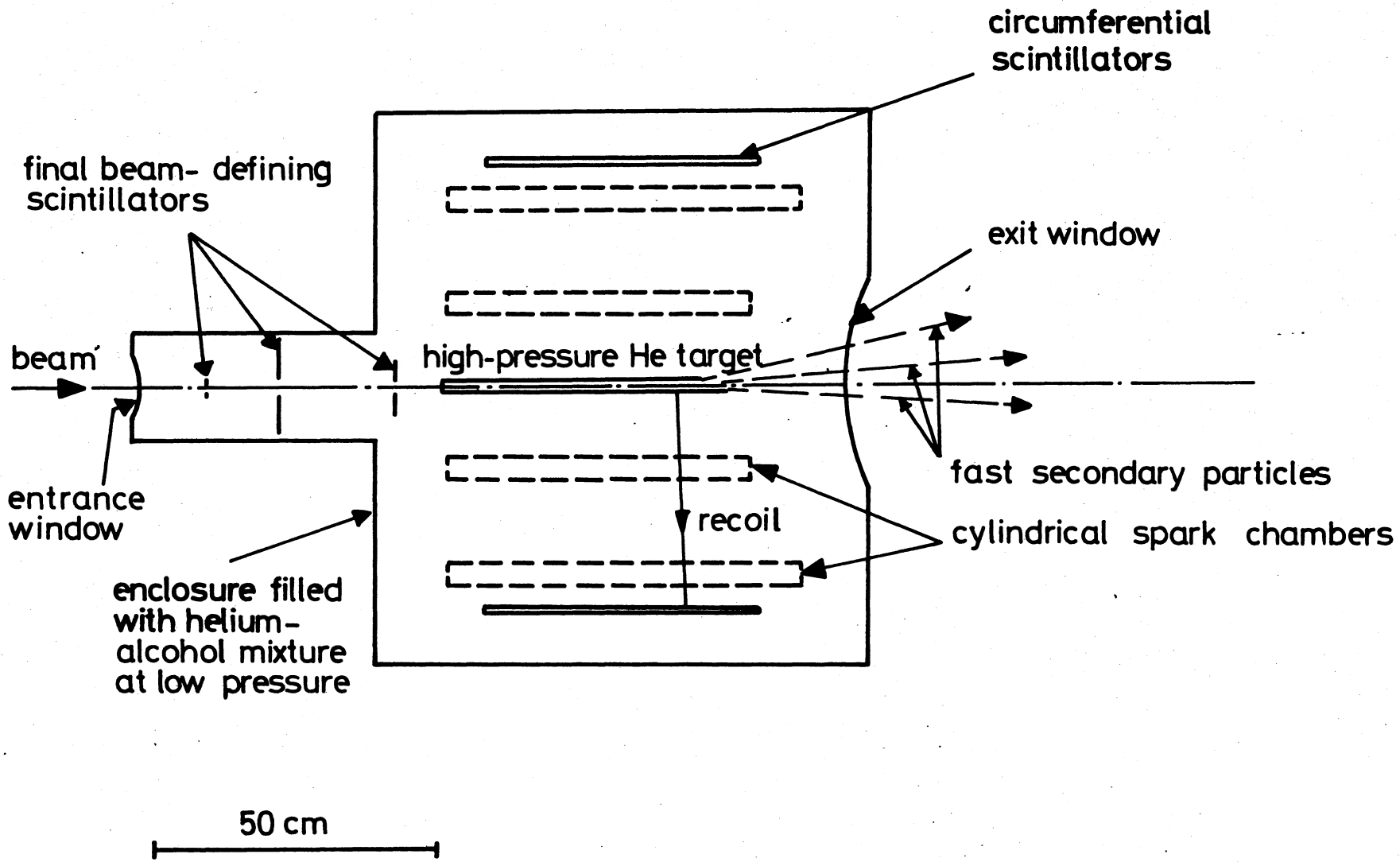
circumferential scintillators
final beam- defining scintillators
exit window
beam
high-pressure He target
entrance window
recoil
fast secondary particles
cylindrical spark chambers
enclosure filled with helium-alcohol mixture at low pressure
50 cm

Fig. 1

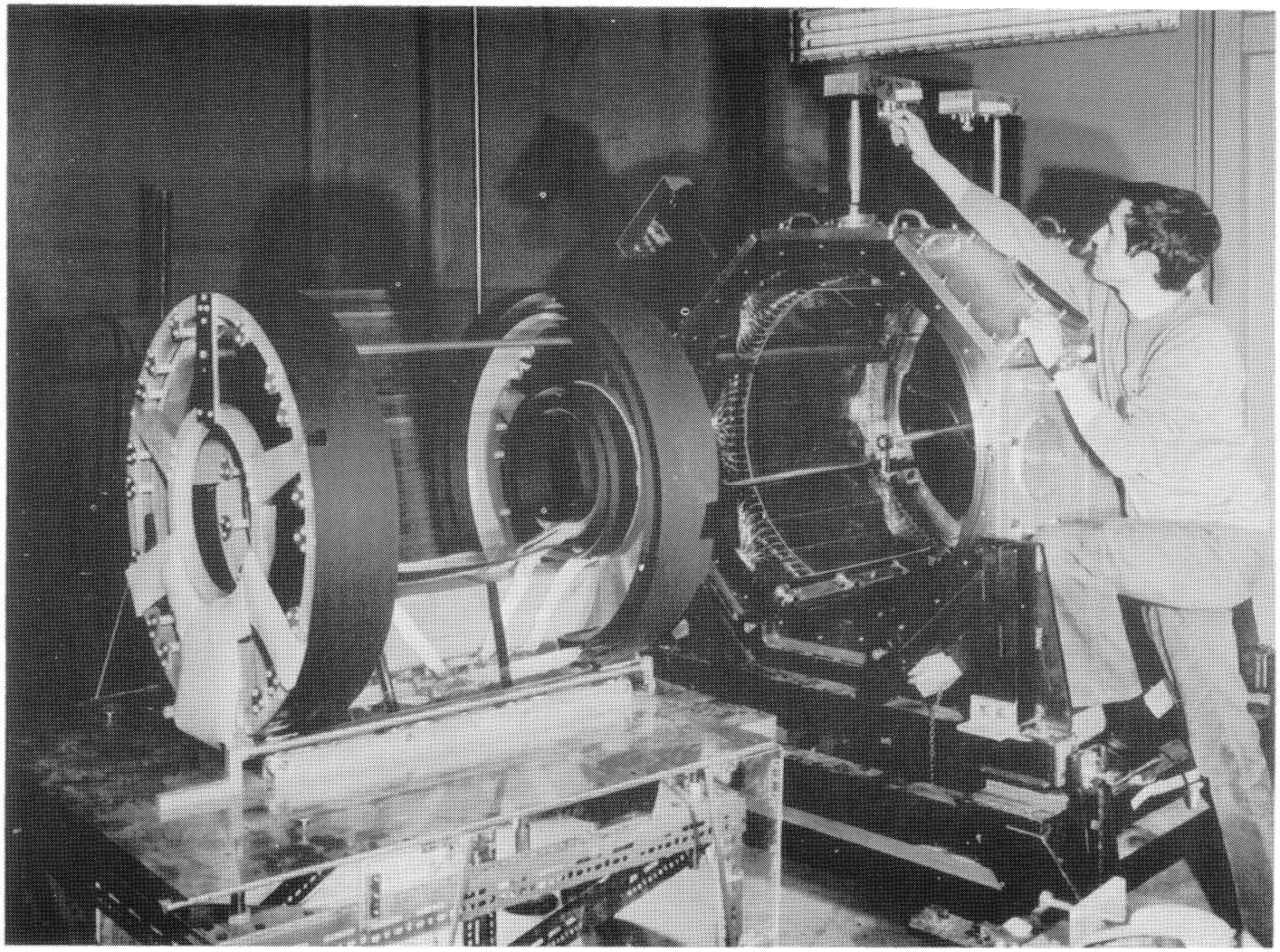

Fig. 2

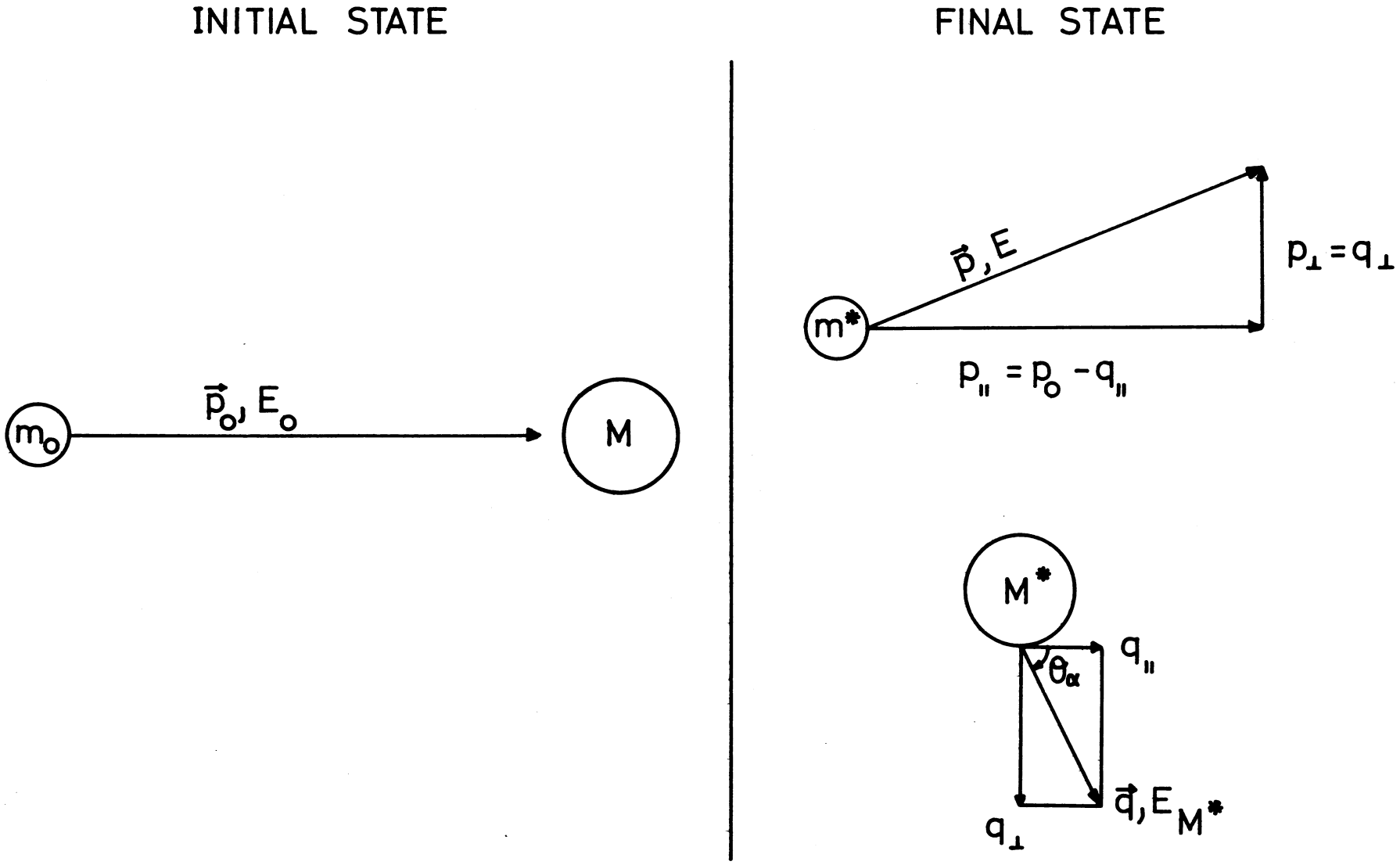
INITIAL STATE
FINAL STATE
m_o
$\vec{p}_o, E_o$
M
$\vec{p}, E$
m^*
$p_\perp = q_\perp$
$p_\parallel = p_o - q_\parallel$
M^*
$q_\parallel$
θ_α
$\vec{q}, E_{M^*}$
$q_\perp$

Fig. 3

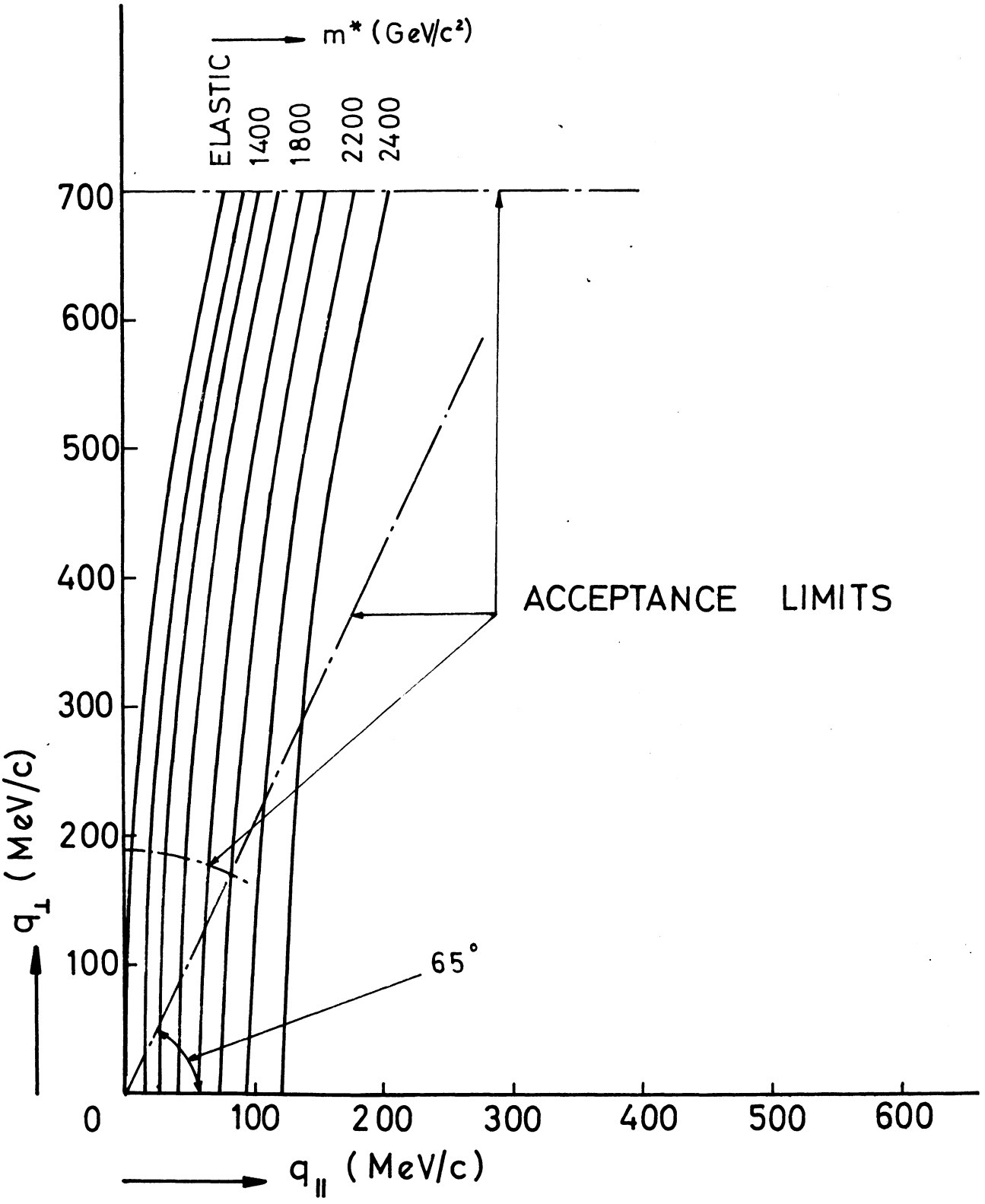
m* (GeV/c²)
ELASTIC
1400
1800
2200
2400
700
600
500
400
300
200
100
0
ACCEPTANCE LIMITS
65°
q⊥ (MeV/c)
100
200
300
400
500
600
q∥ (MeV/c)

Fig. 4

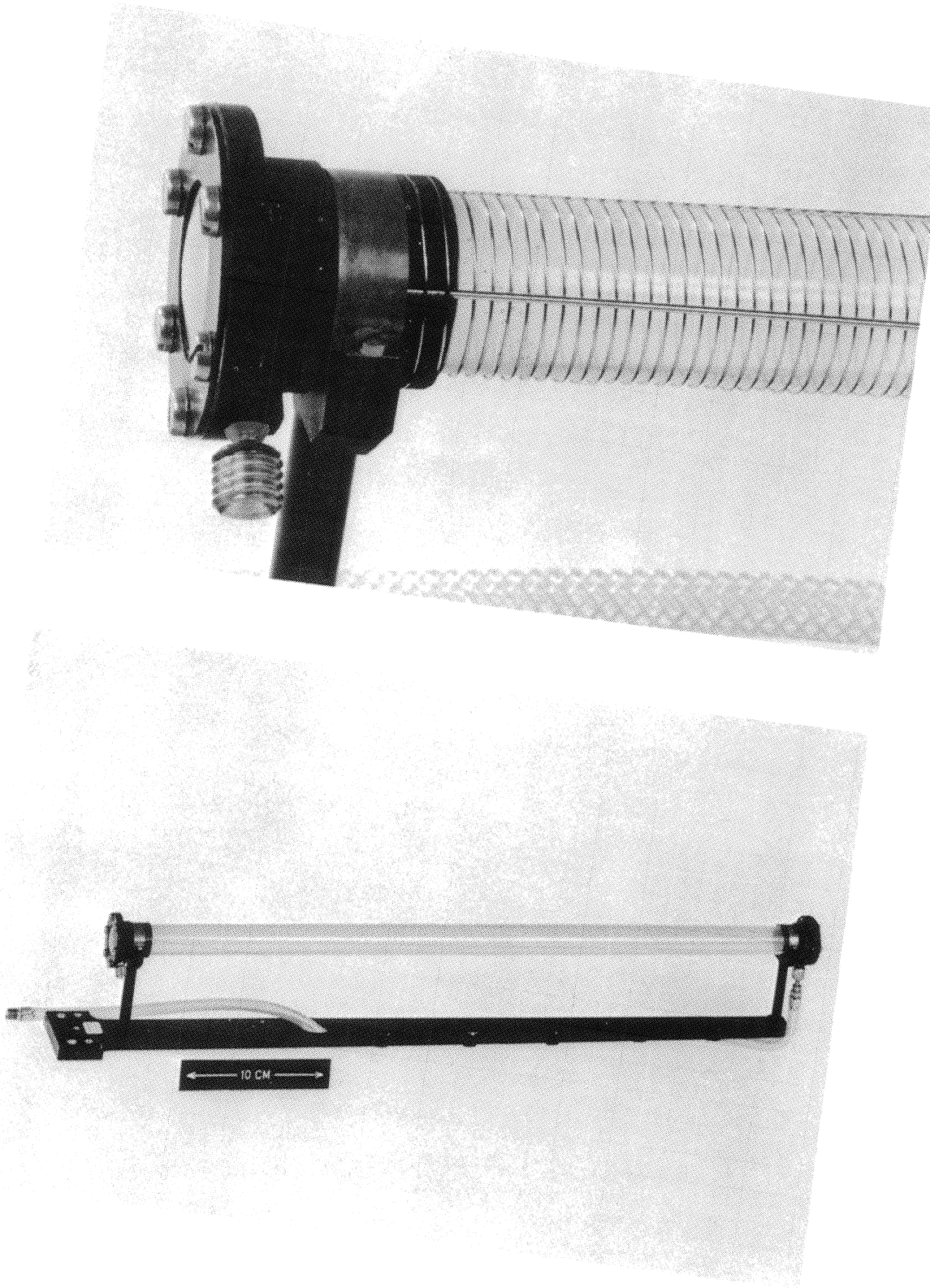

Fig. 5

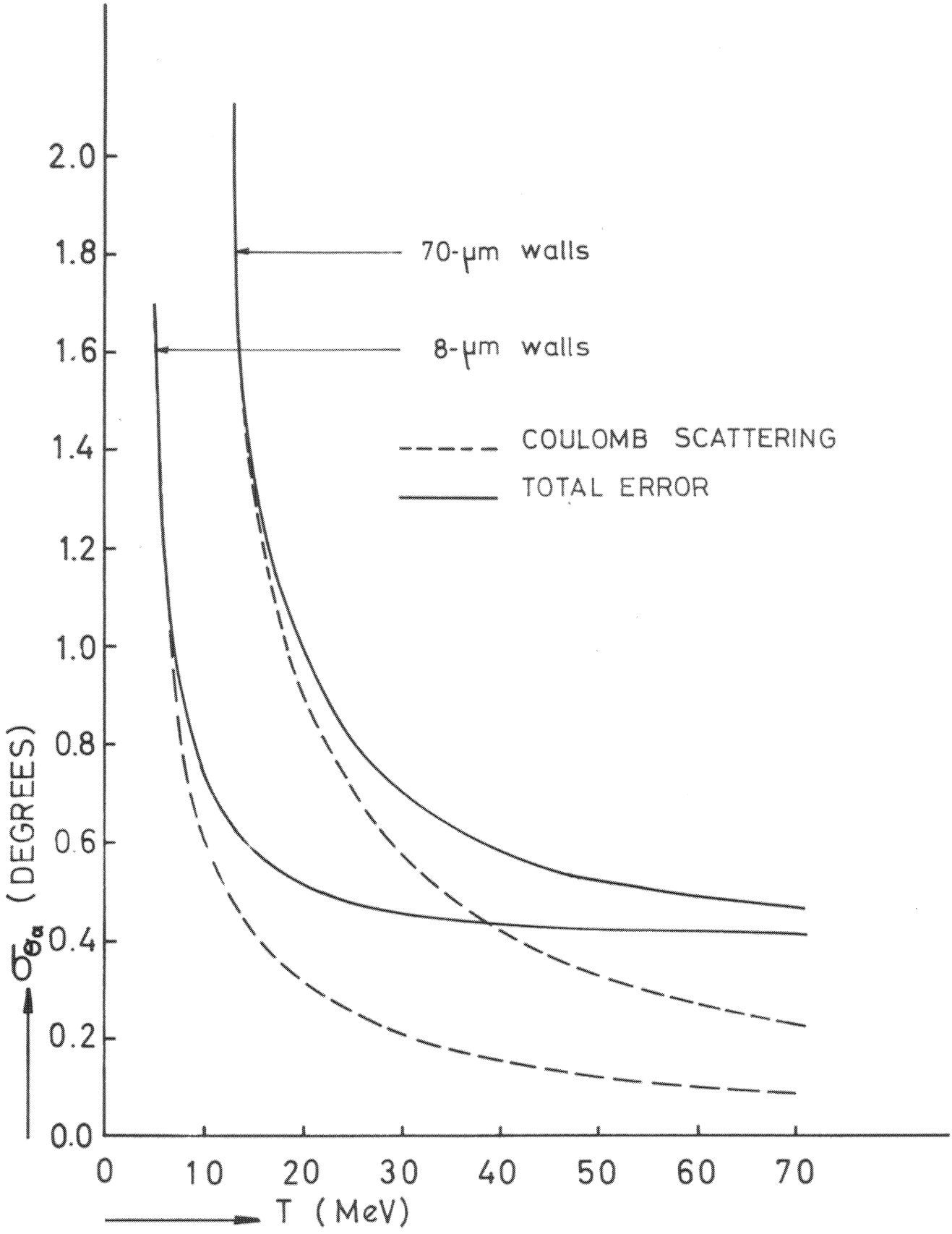
2.0
1.8
1.6
1.4
1.2
1.0
0.8
0.6
0.4
0.2
0.0
70-μm walls
8-μm walls
COULOMB SCATTERING
TOTAL ERROR
σ_{θ_a} (DEGREES)
0
10
20
30
40
50
60
70
T (MeV)

Fig. 6

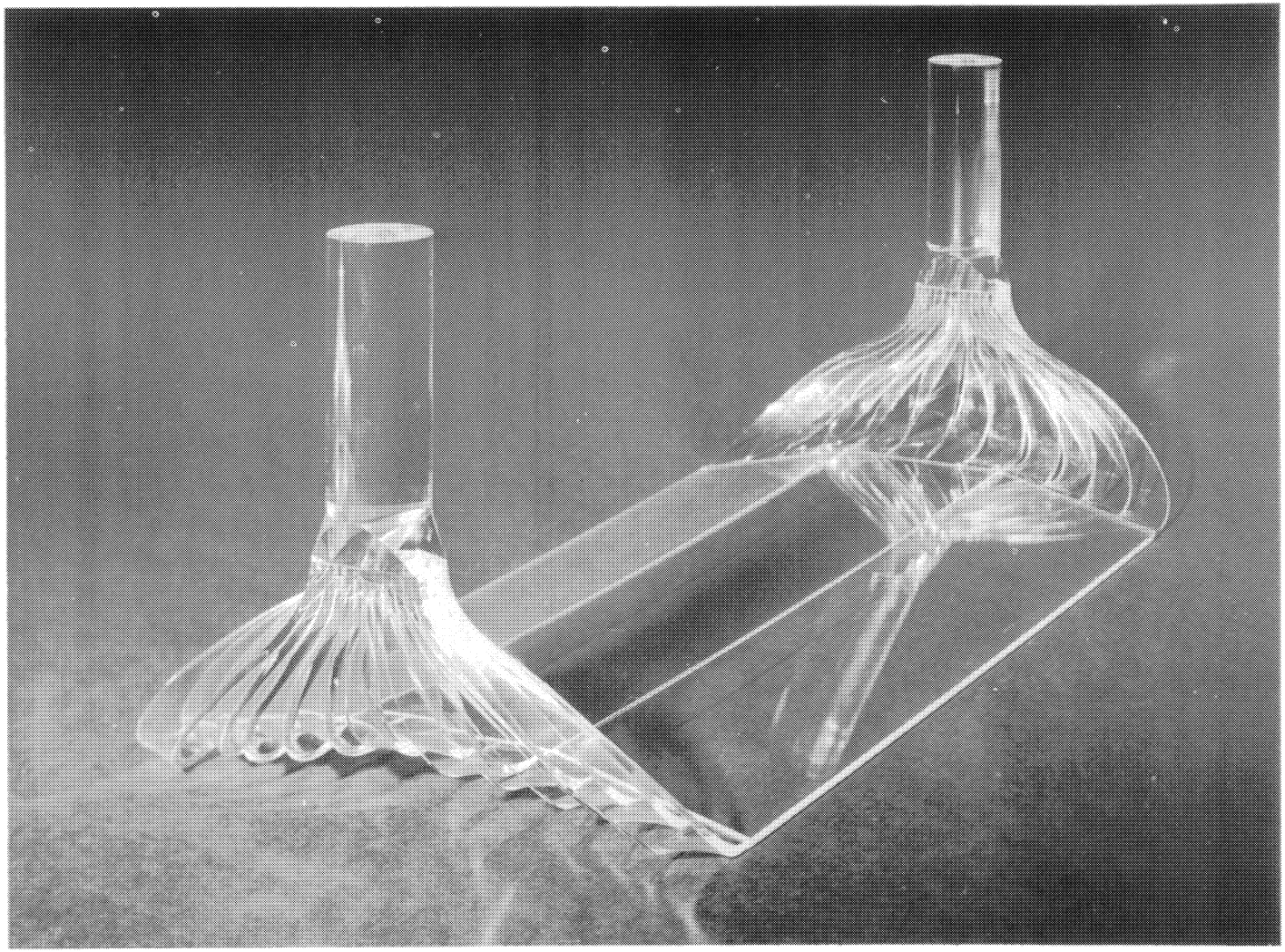

Fig. 7

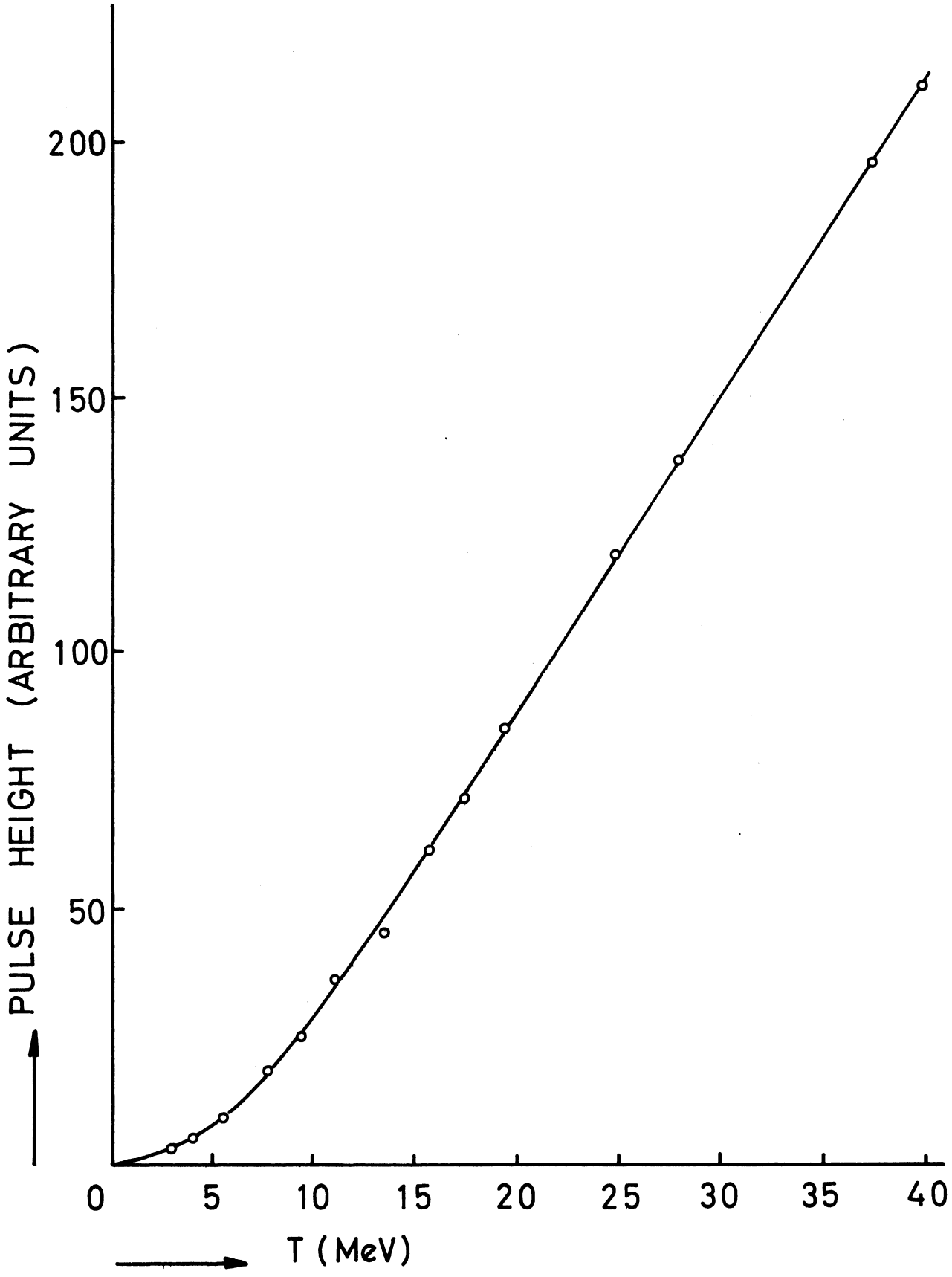
PULSE HEIGHT (ARBITRARY UNITS)
200
150
100
50
0
5
10
15
20
25
30
35
40
T (MeV)

Fig. 8

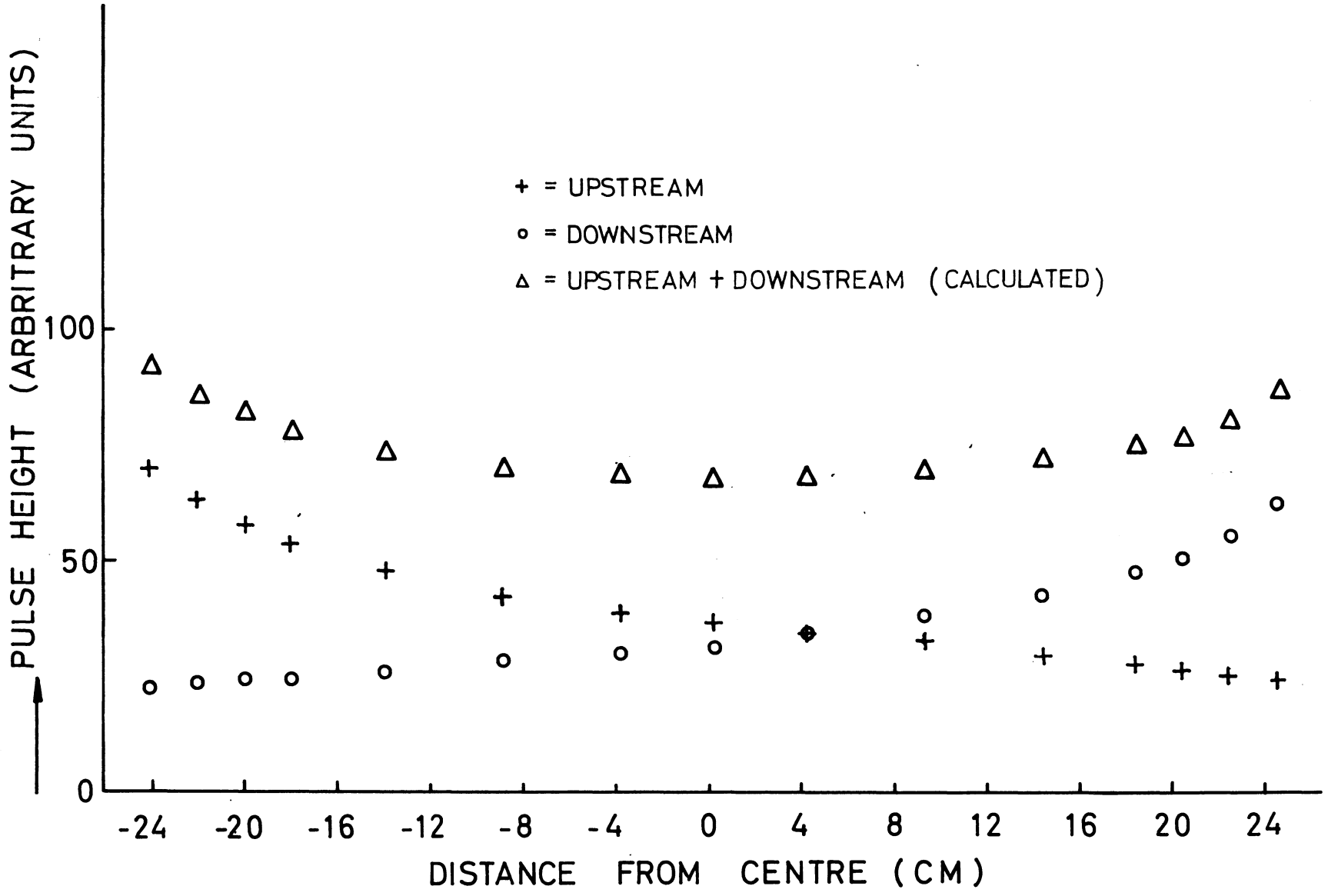
+ = UPSTREAM
o = DOWNSTREAM
Δ = UPSTREAM + DOWNSTREAM (CALCULATED)
PULSE HEIGHT (ARBRITRARY UNITS)
100
50
0
-24
-20
-16
-12
-8
-4
0
4
8
12
16
20
24
DISTANCE FROM CENTRE (CM)

Fig. 9

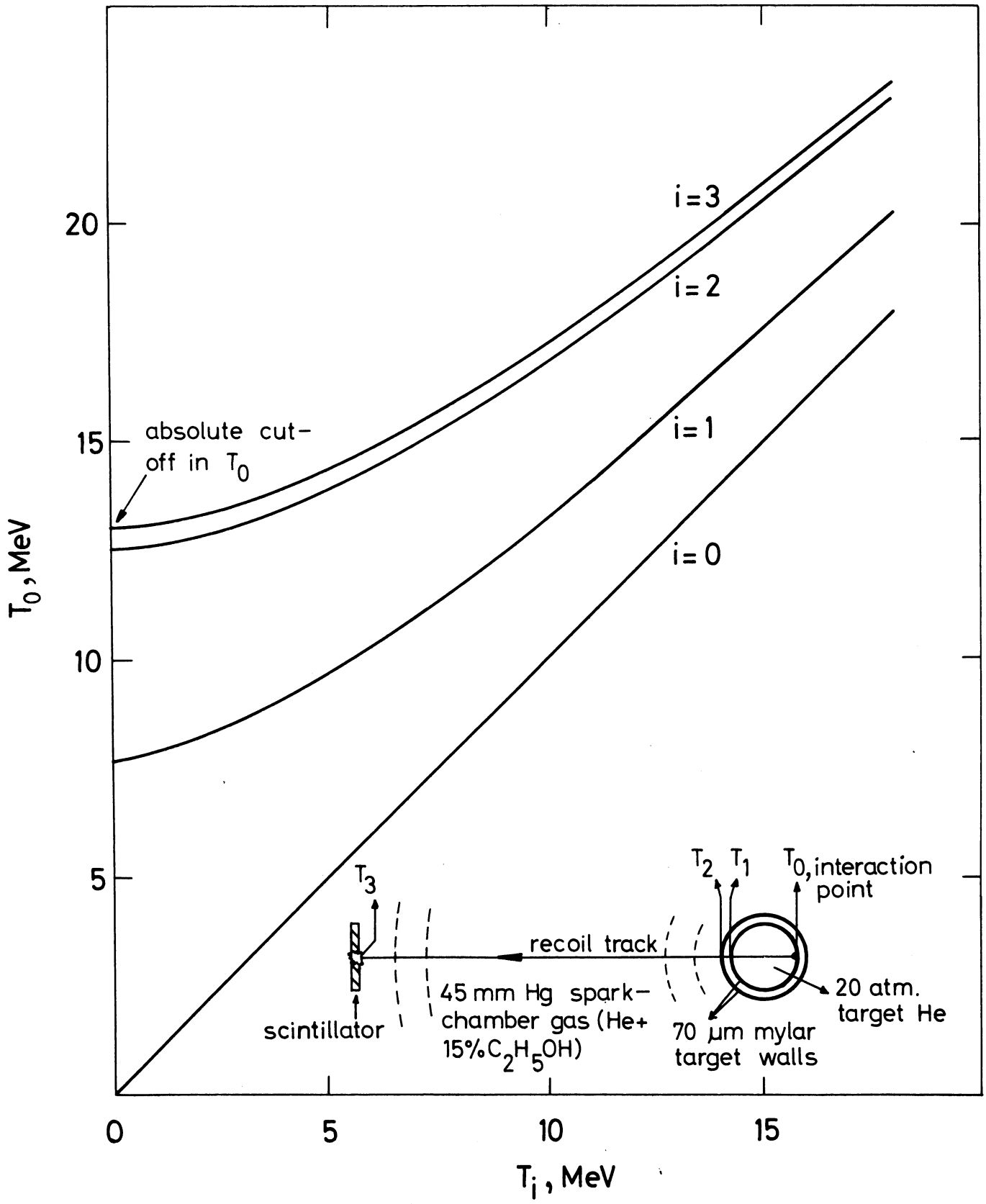
i=3
i=2
i=1
i=0
absolute cut-off in T_0
T_0, MeV
T_i, MeV
0
5
10
15
20
T_3
T_2
T_1
T_0, interaction point
recoil track
scintillator
45 mm Hg spark-chamber gas (He+ 15% C_2H_5OH)
70 μm mylar target walls
20 atm. target He

Fig. 10

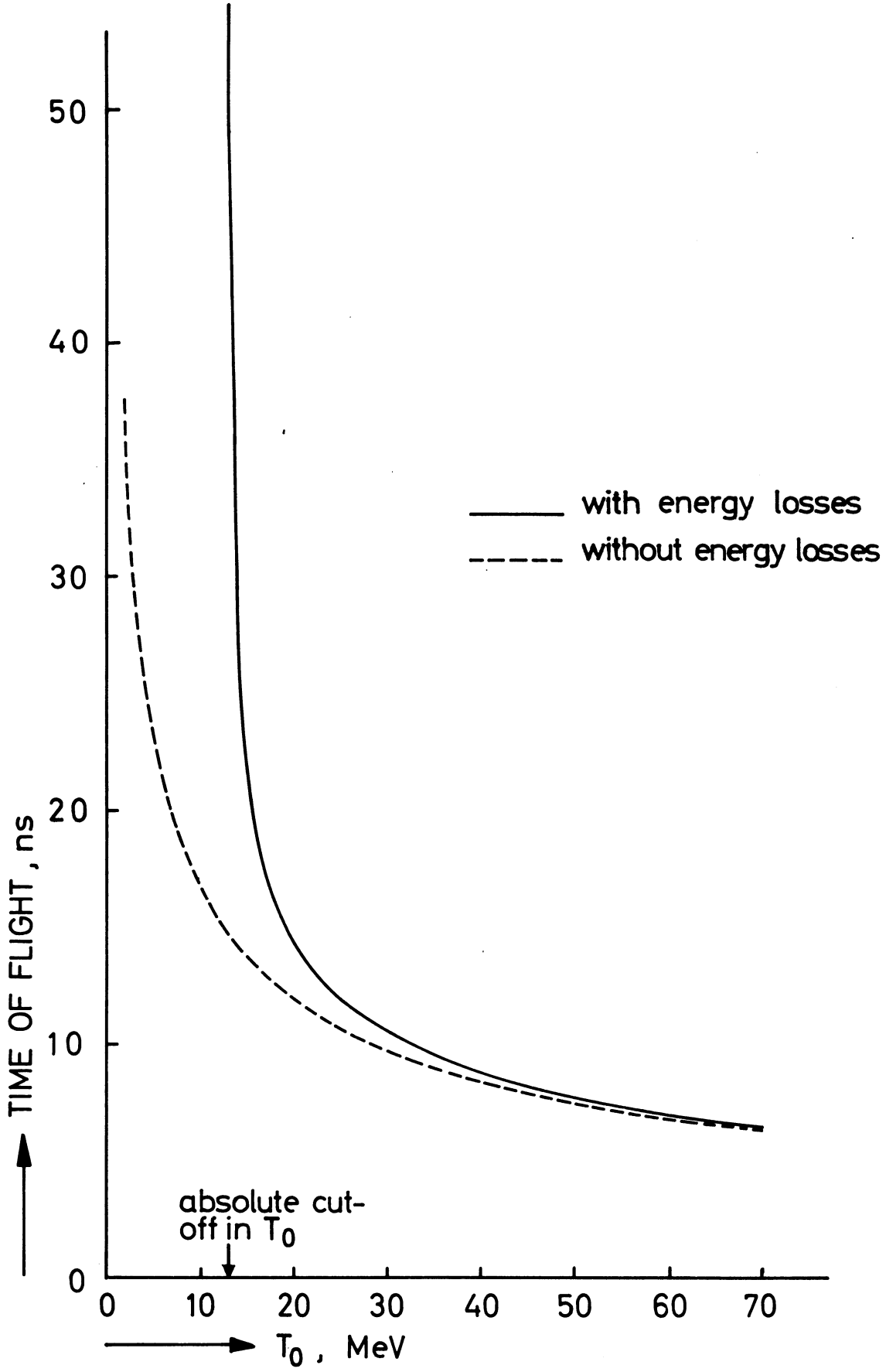
50
40
30
20
10
0
TIME OF FLIGHT, ns
with energy losses
without energy losses
absolute cut-
off in T_0
0
10
20
30
40
50
60
70
T_0, MeV

Fig. 11

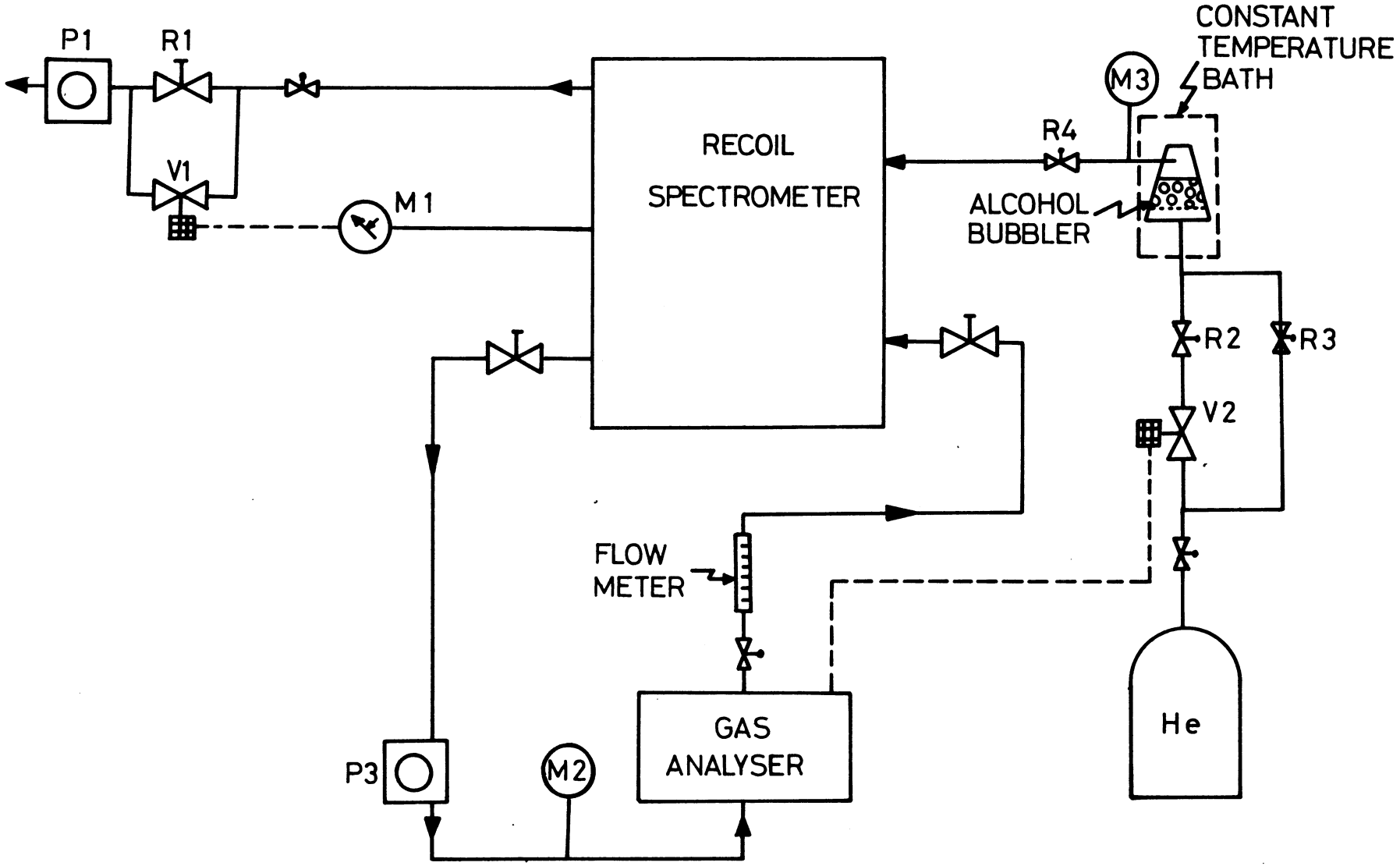
P1
R1
V1
M1
RECOIL
SPECTROMETER
CONSTANT
TEMPERATURE
BATH
M3
R4
ALCOHOL
BUBBLER
R2
R3
V2
FLOW
METER
GAS
ANALYSER
He
P3
M2

Fig. 12

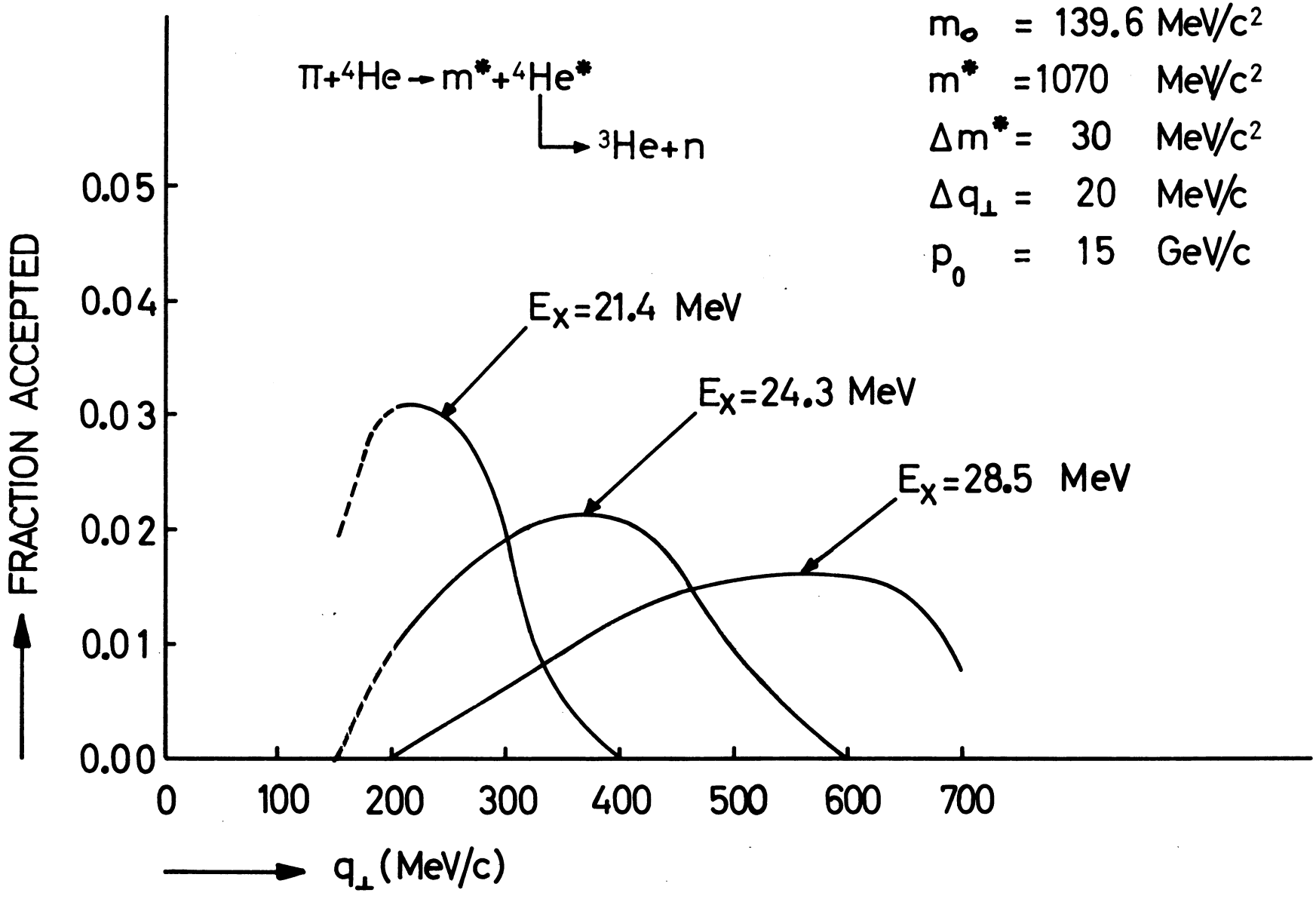
m_o = 139.6 MeV/c²
m^* =1070 MeV/c²
Δm^* = 30 MeV/c²
$\Delta q_\perp$ = 20 MeV/c
p_0 = 15 GeV/c
$\pi + {}^4He \rightarrow m^* + {}^4He^*$
$\hookrightarrow {}^3He + n$
E_X=21.4 MeV
E_X=24.3 MeV
E_X=28.5 MeV
FRACTION ACCEPTED
0.05
0.04
0.03
0.02
0.01
0.00
0
100
200
300
400
500
600
700
$q_\perp$ (MeV/c)

Fig. 13

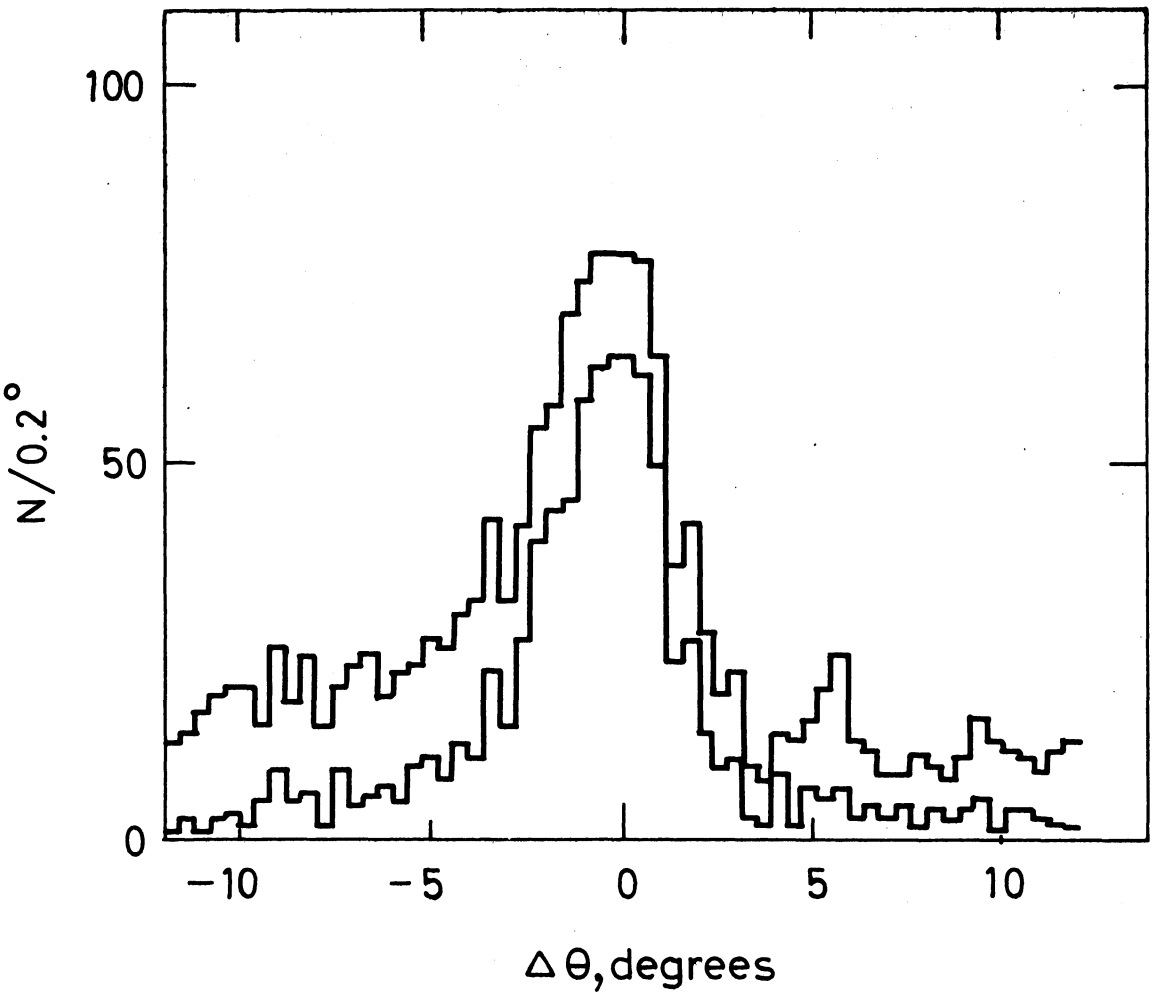

Fig. 14

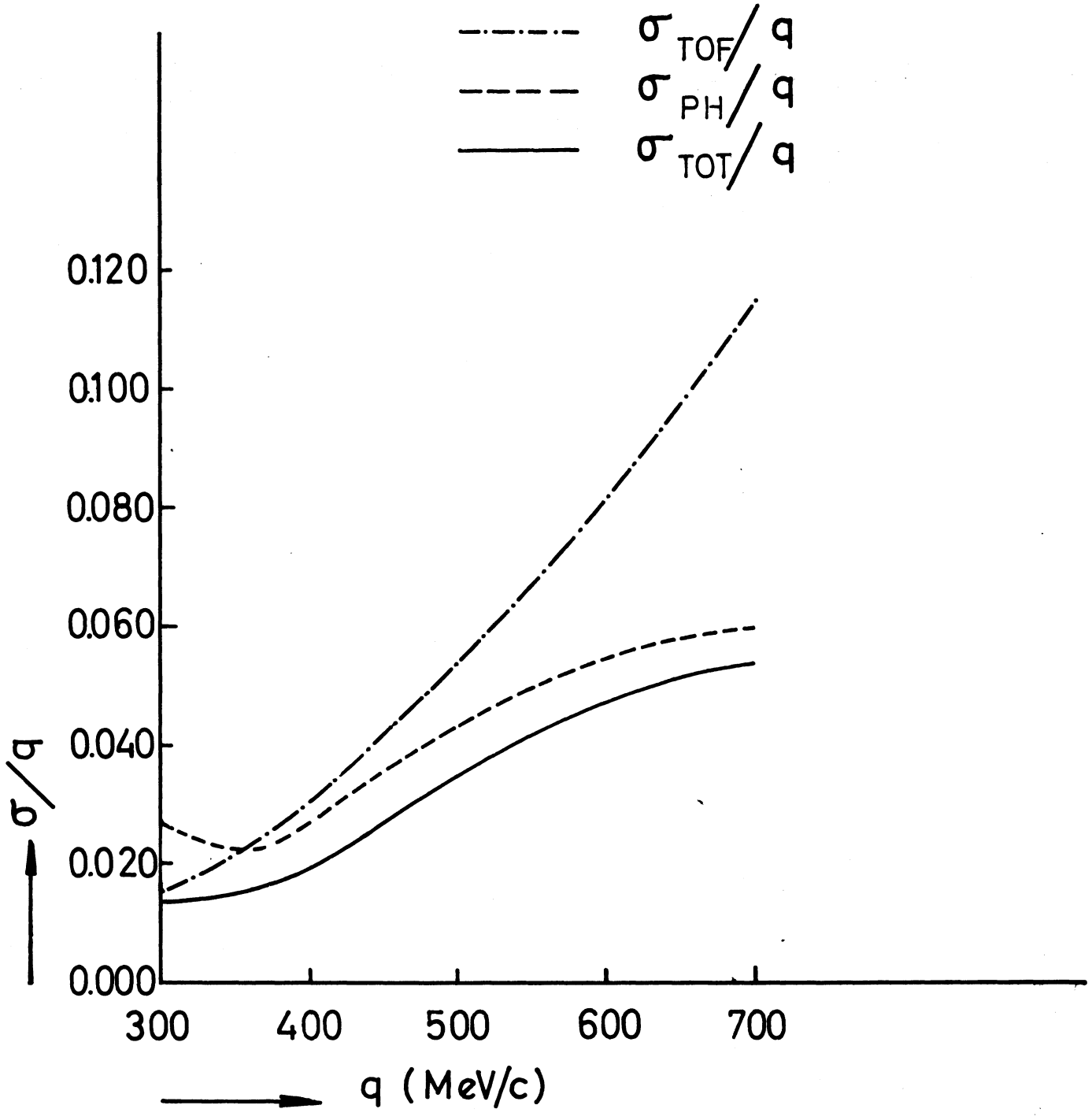
σ TOF / q
σ PH / q
σ TOT / q
0.120
0.100
0.080
0.060
0.040
0.020
0.000
σ/q
300
400
500
600
700
q (MeV/c)

Fig. 15

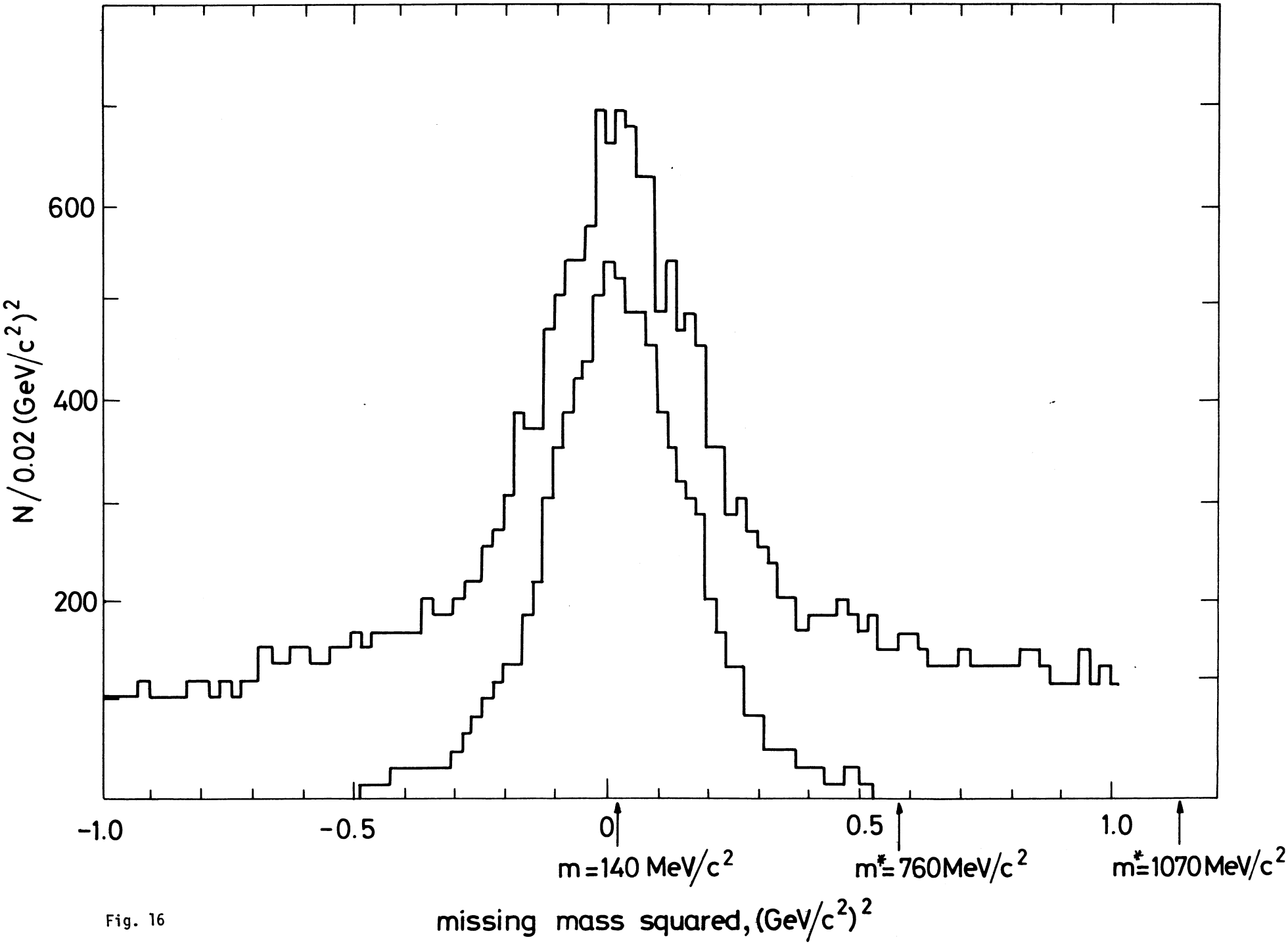
600
400
200
N/0.02 (GeV/c²)²
-1.0
-0.5
0
0.5
1.0
m = 140 MeV/c²
m* = 760 MeV/c²
m* = 1070 MeV/c²
missing mass squared, (GeV/c²)²

Fig. 16

UPPSALA UNIVERSITY, GUSTAF WERNER INSTITUTE

THE DATA ANALYSIS IN A COUNTER EXPERIMENT AT THE CERN PS, USING A HELIUM RECOIL SPECTROMETER

Tord Ekelöf
Gustaf Werner Institute, Uppsala, Sweden

ABSTRACT

A counter experiment to measure the $\pi^{-}{}^{4}$He elastic cross section using a helium recoil spectrometer has been carried out and a description is given of the main lines in the data analysis, including the raw data evaluation, the investigation of systematic and statistical errors, the χ^2 fitting of the data and the comparison of the results with theory.

1. INTRODUCTION

This paper describes the data analysis in an experiment on elastic π^- ^{4}He scattering[1] using a recoil spectrometer[2]. The two main steps in this analysis are the evaluation of the raw data to give particle tracks and momenta, described in chapter two, and the fitting and selection of the evaluated data, described in chapter three. The comparison of the obtained differential cross section with the Glauber theory is commented on in chapter four. Below we will first give a short recapitulation of the relevant physics in the experiment and the experimental set up.

1.1 The purpose of the experiment

The proposal [3] to use a recoil spectrometer to measure coherent interactions between hadrons and ^{4}He nuclei was put forward at CERN in 1967. Since then the recoil spectrometer has been constructed and used to measure the differential cross section of coherent elastic scattering of negative pions from helium at 8 GeV/c and preparations are now in progress to use this instrument for coherent production of I = 1/2 baryon states on ^{4}He using 20 GeV/c protons [4].

The interest in investigating coherent interactions with nuclei has several grounds. One of these has been to test the validity of the Glauber multiple scattering theory [5] in describing this kind of interactions. This question has by now been investigated in several experiments [5] over a large range of incident momenta and momentum transfers and the validity has been shown to be very good. The experiment described here is the first that has been carried out with a helium target at an incident momentum sufficiently high for the basic approximations of the theory to be well satisfied.

Furthermore, admitting the validity of the Glauber theory, information on nuclear structure and on hadron-nucleon scattering amplitudes can be extracted from the experimental data. The prospect of getting information on short range correlations in nuclei from measurements on coherent reactions has been carefully investigated. By now it is rather clear that this is not possible in practice [6]. On the other hand - knowing that details in the nuclear structure will not pertub the data - one can get information on the phase of the hadron-nucleon scattering amplitude at non zero values of the momentum transfer. In the case of coherent production of resonances information on the resonance-nucleon scattering amplitudes can be obtained as well [7].

By definition a hadron-nucleus reaction is coherent if the target nucleus is left in its ground state after the collision. It is thus possible to ascertain the coherency of a reaction if the energy resolution in the measurement of the fast secondaries is better than the smallest excitation energy of the nucleus. Usually this means that a resolution of a few MeV is necessary and for particles of multi-GeV energies this is hardly attainable. The alternative is to observe directly the nucleus and from measurements of it select those events in which the nucleus was not excited or broken up. For this the ^{4}He nucleus is especially suitable since its lowest excitation energy is 20 MeV and since it has no excited levels that do not decay by particle emission. Another advantage of observing the nucleus is that this provides extra kinematical constraints and improves the momentum transfer resolution in the measurement.

The experiment described here was thus performed essentially to test the Glauber theory at high incident momenta, to provide information on the phase of the pion-nucleon scattering amplitude at non-zero momentum transfers and to test a new useful experimental device, the helium recoil spectrometer.

1.2 The experimental set-up

Our set-up is described in detail in section 2 and fig. 1 of ref. 1. Apart from the trigger system it consists mainly of three parts: a telescope of multiwire proportional chambers measuring the track of the incident pion, a helium-recoil spectrometer to measure the direction and momentum of the recoiling nucleus and a set of spark chambers to measure the track of the scattered pion.

The recoil spectrometer is described in detail in sec. 2 of ref. 2 and a diagrammatic view of the device is found in fig. 1. It consists of two cylindrical spark chambers surrounding a high-pressure helium gas target with very thin walls. The spark chambers are operated in a helium-alcohol gas mixture at 0.05 atm pressure and there are no walls between them in order to make possible measurements of very low momentum recoils. Outside and around the spark chambers are placed scintillators in which the recoiling nuclei stop, giving light signals that are used for pulse-height and time-of-flight analysis.

The data from the multiwire proportional chambers were fed via electronic pattern units to a SDS 920 computer for buffering and recording on magnetic tape. The computer also performed a few on-line computations for checking purposes. The data from the set of spark chambers

chambers were fed via digitizing circuits and electronic scalers to a buffer unit and from there written on to magnetic tape by a 7330 IBM tape recorder. The data from the recoil spectrometer was fed via digitizers and scalers to the SDS computer as well as to the IBM tape recorder and was thus recorded on both tapes.

This division of the data on two tapes has its explanation in that the two fast particle track measuring systems existed as tested units together with their data recording devices and these could not easily be merged.

2. THE EVALUATION OF THE RAW DATA

The raw data on the magnetic tapes were converted to track coordinates and momenta of the detected particles and the results of this were written out on new tapes, called the data summary tapes. This evaluation of the raw data is described below with the focus placed on the helium recoil spectrometer. The multiwire proportional chambers and the fast secondary spark chambers and their read-out systems have been used in other experiments [8,9] and the treatment of the raw data from these devices will not be discussed in great detail.

2.1 Preparative calculations for the evaluation of the raw data from the helium recoil spectrometer

From the helium recoil spectrometer information is obtained on the recoil track through the cylindrical spark chambers, on the amount of light produced in the plastic scintillator and on the time of flight of the recoil.

With the current-distribution method used for the read-out of the recoil spark chambers [10] the signals from each side of the spark chamber plane are inversely proportional to the distances from the spark to the spark chamber sides. The parameter used to interpret these signals was the difference between the two signals, divided by their sum to make the parameter independant of the magnitude of the spark current. This parameter is roughly linearly dependant on the position of the spark along the spark chamber. It was used as argument in second degree polynomials that were fitted to the coordinates of the rays from the collimated alpha sources used in the calibration of the chambers. [10] Since the measured angular range in the experiment was small (86° - 83°) and close to 90°, the correction due to the effects of the clearing field mentioned in ref. 10 were neglected.

The evaluation of the recoil kinetic energy from the pulse height and from the time of flight is dependent on the recoil track geometry. This is so even if the recoil energy losses by ionization in the different media in the spectrometer are neglected. Since the lower limit in measurable recoil energies is set by the energy losses, these losses are considerable near the lower cut-off and have to be taken into account. They are dependent on the kinetic energy of the recoil and on the recoil track lengths in different stopping media. It should be noted that the use of the information on the track geometry couples the recoil kinetic energy evaluations to the geometrical evaluation. In this way systematic and stocastic errors in the geometrical reconstruction will give coupled errors in the evaluated recoil momentum.

For the evaluation of the pulse-height and time-of-flight raw data the following relations were worked out beforehand and polynomials were fitted to the results:

1) the relative amplitude of the signal from the photomultiplier as function of alpha particle energy (see fig. 8 ref. 2),

2) the dependence of the photomultiplier output on the position of the stopped recoil (see fig. 9 ref. 1),

3) the time of flight as function of the time digitizer output (linear),

4) range as function of kinetic energy and kinetic energy as function of range for alpha particles in the target helium gas, the mylar of the target walls and the spark chamber helium-alcohol gas mixture (see fig. 2),

5) the recoil starting energy as function of time of flight and path length in the helium-alcohol gas mixture of the recoil spark chambers.

Of these functions the three first were obtained in calibrations and the two last were calculated from published data on the stopping power for protons in different elements [11] and from the dependence of the effective helium charge on kinetic energy of the helium nucleus [12]. The stopping power for protons in mylar and alcohol was obtained by linearly adding together the stopping power in hydrogen, carbon and oxygen according to the relative chemical compositions of mylar (8C + 10H + 5O) and alcohol (2C + 6H + 1O). In the same way the stopping power for protons in the helium-alcohol gas mixture was obtained by adding the stopping powers of each component according to the mixing ratio (in atomic weights).

To obtain the stopping power of a medium for alpha particles from that for protons the following relation was used

$$\left(\frac{dE}{dx}\right)_\alpha / \left(\frac{dE}{dx}\right)_p = Z_\alpha^2 / Z_p^2$$

where dE/dx is the stopping power and Z is the charge of the particle.

The effective charge of the proton will remain close to unity even below kinetic energies of 1 MeV whereas the effective charge of the alpha particle will start to deviate from two at kinetic energies of the order of a few MeV [12]. This deviation was taken into account in the calculations. Finally the range R was obtained by numerical integration

$$R(T) = \int_0^T dE \; 1/\frac{dE}{dx}$$

These range-energy relations could then be readily used to compute the energy of the recoil at the scattering point from the energy at the scintillator derived from the pulse height measurement. For this was needed the path lengths in and the densities of the stopping media.

The method used to compensate for the energy losses could not be as direct in the time-of-flight case as in the pulse-height case. The greater part of the total kinetic energy loss of the recoil occurred in the high pressure helium of the target and the mylar target walls in a path length on average one target radius ($\sim$ 1 cm). Then the recoil spent most of its time of flight moving from the target to the scintillator ($\sim$ 38 cm) in the low pressure spark chamber gas, where it successively lost a rather small but not negligible part of the total energy loss.

For the transformation of the time of flight to kinetic energy in the data evaluation the following calculation was carried out beforehand. For a series of starting energies, E, and flight path lengths, L, the time of flight, TOF, was calculated, taking the successive energy losses by ionization in the helium-alcohol gas mixture into account. In this way points were obtained in a three-dimensional space TOFxExL and in this space a bivariate polynomial was fitted to the points to give E as function of TOF and L (relation 5 in the list above).

2.2 The raw data evaluation code PIALPHA

This section describes the code PIALPHA that contains all the routines which were used for the evaluation of the raw data in the experiment. It was used during the runs for direct checks of the performance of the experimental equipment, indicating failures in the instrumentation and improvements to be done. The system of parameters measured was overdetermined and many cross checks were possible. The same code was also used, after extensive checks, for the final conversion of the raw data to track coordinates and momenta. A schematic flow diagram is shown in fig. 3.

The main program was used only to steer the flow between the subroutines and setting flags for the events indicating whether the different experimental devices had worked properly or not. The first subroutine to be called read all the set-up parameters and polynomial fit coefficients from cards.

Then two subroutines were called reading one event-record from each of the two data tapes. The main program checked that the two records referred to the same event by comparing the recoil spark chamber data (eight four-digit numbers) of the two records.

The binary information from each wire in the multiwire proportional chambers was stored as a bit on the tape written by the SDS computer - each bit corresponding to a coordinate in the chamber plane. These bits were decoded in the SDS-tape reading routine and interpreted with the aid of the measured positions of the chambers.

The information from the set of spark chambers, stored on the tape written by the IBM tape recorder, were given as numbers proportional to the travel time of the mechanical and electromagnetic pulses used in the magnetostrictive and delay-line read out systems [9] of the spark chambers. These numbers were transformed linearly to give position coordinates in the spark chamber planes knowing the positions of the chambers.

From the signals given by the recoil spark chambers the same kind of parameters that were used to calculate the calibration fit polynomials were computed. These parameters were then used with the polynomials to give two azimuthal and two longitudinal coordinates of the recoil track.

At this point of the analysis of an event all the geometrical information supplied had been evaluated. If all of the measuring devices involved had given enough information, the tracks of the incoming and outgoing pion and of the recoil could be reconstructed. This was done

in another subroutine by fitting straight lines to the track coordinates. If, for reasons of apparatus inefficiency, there was not sufficient information for all three tracks to be reconstructed the event was flagged.

The three tracks were treated independently of each other - the vertex constraint was not used in the fitting procedure. Approximate vertex coordinates were calculated from the incident and recoil tracks. The subroutine also calculated the recoil path lengths in the different stopping media in the spectrometer and the coordinates of the track end point in the recoil scintillator for later use in the pulse-height and time-of-flight evaluation.

In the pulse-height subroutine the two photomultiplier signals were treated independently throughout the evaluation, resulting in two different estimates of the recoil kinetic energy. Firstly the subroutine computed the kinetic energy of the recoil at the scintillator using the raw data and the polynomials 1 and 2 mentioned in sec. 2.1. Then the range-energy polynomials 4 were used to get the recoil kinetic energy at the scattering point in the target. This was done as is illustrated in figure 2. The energy losses suffered by the recoil and their variations with kinetic energy are drawn for a special case in fig. 10 of ref. 1.

The two times of flight given by the two separate photomultipliers were treated separately in the time-of-flight routine, giving two estimates of the recoil kinetic energy as in the pulse height case. The time derived from the raw data and the calibration fit polynomial 3 (sec. 2.1) was corrected for the time used by the incident particle to get from the time-defining scintillator 40 cm upstream from the target to the reaction vertex and for the light travel time in the recoil scintillator. This corrected time of flight was then fed together with the calculated track length into the bivariate fit polynomial 5 (sec. 2.1). The resulting kinetic energy was finally compensated for the energy losses in the target gas and the surrounding mylar foil using the range-energy polynomials 4. The measured time of flight as function of the resulting recoil kinetic energy at scattering point is shown for a special case in fig. 11 of ref. 1. This figure demonstrates the importance of taking the energy losses in the spark chamber gas into account at low recoil kinetic energies.

At this stage the geometry of the three tracks and the momenta of the incident particle and the recoil were known. Supposing that the event is an elastic one the kinetic energy of the recoil is uniquely related by the kine-

matics to the recoil angle and to the scattering angle of the pion. Any one of these three quantities determine the two others and the formulae for this interrelation are derived in Appendix I. To make the three measured quantities directly comparable with each other these formulae were used in a kinematics subroutine to calculate from each measured quantity the other two. There is one more condition imposed by the kinematics: the reaction should be coplanar and there were thus three kinematical constraints in the measurement.

After each event had been evaluated by the subroutines the resulting data were written out on the data summary tape. The full information of an event was contained in 156 data words, making up one event-record. When all events on the two tapes in an experimental run had been treated, the main program printed out a 'run identification and summing up'-page. In fig. 4 such a page is shown. From this could be found the total number of successfully evaluated events and the percentage of events that had failed to be fully evaluated for different reasons (apparatus inefficiencies, background etc.).

3. CHECKING AND FITTING OF THE EVALUATED DATA

There were three kinematical and three geometrical constraints in the measurements and in the second step of the analysis the data on the data summary tape was analysed in a χ^2 fitting code. Before this was done the data were thoroughly checked for systematic errors and the appropriate statistical errors, to be used in the fitting procedure, were derived.

To use the χ^2 fitting method there must not be any systematic errors in the data and the statistical errors must be correctly estimated. The checking and adjustment of these quantities can be done with the aid of so called 'pull quantities' in the χ^2-analysis but only to a very limited extent since it is not certain that a systematic or wrongly estimated statistical error will show up clearly in these pull quantities. On the other hand it most probably will cause the resulting fit to be erroneous. Therefore it was important to check the consistency of the data and to estimate carefully the statistical errors before the χ^2-fit was performed. In section 3:1 the checking of systematic errors will be described, in section 2:2 the methods to derive the statistical errors are given and in section 3:3 the χ^2 fitting is treated.

3.1 The checking of systematic errors

A total of 257 000 events were recorded, divided into 64 files on the magnetic tapes. Eliminating those files that could be judged to be of no value from a first inspection (apparatus failures etc.) brought this figure down to 195 000 events. Of these events 120 000 were recorded with 20 atm target gas pressure, 66 000 with 5 atm pressure and 9000 events with no target gas (to check the background).

Of the high target pressure events only 72 000 were flagged by the PIALPHA code as having sufficient parameters measured to be 'full constraint events'. The corresponding figure for low target pressure events was as low as 20 000 events.

In order to check these data on the data summary tapes, extended use was made of the histogram routine SUMX [13] available at CERN. Errors in calibrations and programming faults in the code PIALPHA, causing systematic errors in the data, were checked for in the following ways:

i. The kinematics subroutine in PIALPHA calculated the kinetic energy of the recoil from the measured recoil angle and from the measured pion scattering angle. In this way there were four estimates of the recoil energy - the mean value from the pulse-height measurement, the mean value from the time-of-flight measurement and two values from the angles. With SUMX the differences between the various energy estimates were displayed in series of histograms. For each histogram in such a series the mean of the two energies was confined to a certain interval. The deviation from zero of the mean of these distributions indicated systematic errors and their widths gave an idea of the statistical errors of the various measurements. The variations of these errors with kinetic energy could be studied in the series of histograms. Such variations were also studied in two-dimensional plots of the different energy estimates.

ii. For the pulse-height measurement there were 18 calibration values to be checked, one for the upstream and one for the downstream photomultipliers of all the nine plane sections of the circumferential scintillator (each section covered 14° in azimuth). This could be done by selecting events from the middle part of each of the nine sections using the information given by the recoil spark chambers. For each section a study was then made of the distribution of differences between upstream and downstream values of energy from pulse height. Any deviation from zero of the mean of these distributions could only be explained by

faulty calibration values. Checking the two pulse-height energies for each section against the energy from time of flights or energy from pion scattering angle helped to indicate how the calibrations should be corrected.

The energies from the time-of-flight measurement was checked in much the same way - only that the number of calibrations was six, one for each photomultiplier. It should be noted that the kinetic energy is roughly inversely proportional to the square of the time of flight. Thus if the time-of-flight calibration is adjusted to fit the other energy measurements in the high-energy range (where a small systematic error in time of flight corresponds to a very big systematic error in kinetic energy) it will have a very good precision at small energies (where the conditions are the inversed).

The above mentioned histograms of differences between upstream downstream values were used also to determine the statistical errors and we will return to this point in the next section.

iii. As described above the pulse-height and the time-of-flight measurements both contained the condition that the upstream and downstream values should be equal. Likewise the recoil spark chamber measurement contained a condition of consistancy: the azimuthal coordinates from the two cylindrical spark chamber should give a line traversing the target. If the distribution of the distance of the recoil track from the beam axis was not centered at zero this meant that the azimuthal calibration of the chambers had to be corrected. Each of the azimuthal coordinates was also checked against the measured azimuthal coordinate of the scattered pion, assuming an elastic and thus coplanar event.

The data on dip angle given by the recoil spark chambers did not contain any constraints other than that the reconstructed track should traverse the target between the longitudinal target end points. For kinematical reasons there should be no recoil scattering angles greater than 90°. This limit could be set even smaller since there was a non zero lower cut-off in momentum transfer. In the case of the high pressure target this cut-off was 86°. Due to the multiple Coulomb scattering of the recoil - which had a rather predominant effect near the lower cut-off - the cut-off limit in angle was smeared out.

With a Monte-Carlo program the distribution of measured recoil angles was simulated. This program was based on the theory of multiple Coulomb scattering in Appendix 3 and the hypothesis of a differential cross section exponentially decreasing with the four-momentum trans-

fer squared. The histogram of measured recoil angles could then be compared with the simulated distribution. Any difference of the peak position along the angular scale between these two distributions would indicate a systematic error in the longitudinal coordinates of the recoil spark chambers.

iv. There were seven multiwire proportional chambers in the incident beam - three measuring the vertical and four the horizontal coordinates. Since the reconstructed tracks were rectilinear there were many possibilities for cross-checking the positioning of the chambers. The most sensitive check though was that because of the trigger condition the reconstructed tracks should point into the target. The coordinates of the reaction vertex were estimated from the intersection point between the incident track and a plane perpendicular to the beam at a level given by the recoil track. The distribution of vertices in this plane should then be confined to the circular target area (diameter 2 cm).

v. There were four spark chambers measuring the scattered pion, three with both horizontal and vertical coordinates read out and one with only horizontal coordinate read out. So as for the proportional chambers there were many possibilities of cross checking to verify the positioning of the chambers. Also the distribution of reaction vertices in planes perpendicular to the beam was used to check as above. A further condition used was that the reconstructed track should traverse the target between the longitudinal target end points.

vi. The vertex constraint was also used for checks. The incident and outgoing fast particle tracks gave one vertex point each in the plane perpendicular to the beam. The distribution of the distance between these two points offered a very sensible check of positioning errors, especially for the fast secondary spark chambers. Furthermore the longitudinal coordinates of the vertex given by the recoil track and by the scattered pion track were compared. This constituted a very sensible check of the reconstruction of the scattered pion track.

All these checks were carried out separately for each run and the calibrations were adjusted. To get better statistics in the high momentum transfer region, where the cross section is low, the data from several files were added.

3.2. Estimations of statistical errors

When the recoil scintillator was calibrated, using α particles of different energies, the resolution in the height determination and the timing of the pulses was also investigated [14]. For several reasons these measurements could not be used for the final estimation of statistical errors and instead the distributions of energy differences as described in section 3.1 were used. Supposing that the statistical variations of the two separate measurements are equal and independent, the standard deviation of the energy difference is twice the standard error of one of the measurements. This error estimate does not contain the contributions from the energy straggling of the recoil and the uncertainty in the reconstructed recoil track geometry. These contributions could only be important near the cut-off where the recoil energy loss is considerable. In Appendix 2 it is shown that the energy straggling effect can be neglected. This was also assumed for the influence of the uncertainty in the recoil track geometry. The statistical errors obtained are displayed in fig. 15 of ref. 2 in which the relative standard error of the combined pulse-height and time-of-flight measurements is seen to vary from 1.4% at the lower recoil momentum limit 300 MeV/c to 5% at the upper limit 700 MeV/c.

The statistical errors in the recoil angles were due to the limited intrinsic resolution of the spark chambers and to the Coulomb scattering in the different materials of the spectrometer. The intrinsic resolution was investigated in the calibration of the spark chambers [10]. In these calibrations using alpha sources there was only the helium-alcohol gas mixture that caused multiple Coulomb scattering. To obtain the intrinsic resolution the effect of multiple Coulomb scattering was subtracted from the measured variation. Under actual experimental conditions there was an extra contribution to the multiple Coulomb scattering in the target gas and the mylar target wall. In Appendix 3 it is shown how the effects of multiple Coulomb scattering were calculated and some results are shown in fig. 6 of ref. 2. At high momentum transfers the standard error in the recoil angle was around 0.5° and this error was growing when going towards smaller momentum transfers. The same calculations were used in the Monte-Carlo program described in sec. 3.1. The form of the angular distributions simulated with this program was in very good agreement with the experimentally obtained distribution.

As mentioned earlier the multiwire proportional chambers and the scattered pion spark chambers had been used in earlier experiments and

in these the standard errors in the position determination had been observed to be 0.7 mm [8] and 0.6 mm [9] respectively. These errors were investigated also in this experiment in the fits of tracks with more than two coordinates in the horizontal or vertical plane. A good agreement with the earlier found values was established.

3.3. The test selection and the final χ^2 fitting of the data

Before the 92 000 full constraint events mentioned in the beginning of sec. 3.1 were fed into the χ^2 code, together with their statistical errors described in sec. 3.2, the evaluated data were analyzed in a more simple fashion to gain insight and confidence in the evaluated data. The method employed was to select subclasses of events out of the 92 000 by requiring that the events in each class should fulfill some simple test criteria. Many such test criteria were tried and the effects on different distributions were studied using the SUMX code.

The aim with these tests was to cut out background events and the tests were constructed accordingly. At high energies the cross section for inelastic $\pi^- {}^4\mathrm{He}$ reactions is 3 to 4 times greater than that for the elastic reaction [19] and the occurrence of different kinds of background in the collected data was dependent on the trigger used and the high energy physics involved. A discussion of these problems is carried out in sec. 4 of ref. 1 and sec. 3.3 of ref. 2 and will not be taken up here. Below are given the different selection criteria used and their effects. The figures are valid for a representative part of the high pressure target runs.

Test 1 - The two azimuthal coordinates of the recoil track given by the two cylindrical spark chambers should not differ from each other more than the FWHM of the distribution of their difference. This test cut out 50% of the events.

Test 2 - The difference between the azimuthal angles of the recoil and the scattered pion should not deviate from 180° more than one FWHM of the distribution of their difference. This test cut out 60% of the events.

Test 3 - The difference between the recoil angle measured with the recoil spark chambers and the same angle as computed from the measured pion scattering angle (under the hypothesis of elastic scattering) should not be greater than one FWHM of their difference. This test cut out 45% of the events.

Use was not made of the conditions that could be imposed by comparing the two scattering angles with the pulse-height and time-of-flight

measurements of the recoil momentum. This wad due to the strong variations with recoil momentum of the statistical errors in the latter quantities. A simple test condition could thus not be imposed without introducing a bias in the cross-section distribution.

Requiring all the conditions 1 - 3 to be fullfilled cut out as much as 80% of the events. In the distribution of recoil kinetic energies of the remaining 20% sample the diffraction minimum and secondary maximum could be clearly observed. Fig. 5 shows how the diffraction structure was 'filtered out' of the background by successive application of the tests mentioned above.

This was the method employed to analyze the data in a more qualitative way and the diffraction structure was first found using this kind of selection by simple tests. However, it should be noted that this method has several weak points. It was not feasible to use certain constraints to select events since the corresponding test limits varied with momentum transfer. Also, there certainly were variations in the statistical errors of the quantities in the tests employed (for example the Coulomb multiple scattering error is dependent on the recoil kinetic energy). Furthermore the different statistical errors were not correlated with this method.

The employed χ^2 code [15] fitted all the coordinates to the elastic scattering hypothesis and the vertex constraint in a unified manner taking all correlations into account. In the fit the measured parameters were weighted according to their statistical errors which were calculated for each event separately and the resulting χ^2 sum was thus a much more representative and bias free test variable than the test variables described above.

To investigate the results of the χ^2 analysis the difference between the fitted quantity and the measured quantity, divided by the standard error of the measured quantity was studied for all parameters supplied to the χ^2 code. In the ideal case these pull quantities should have normal Gaussian distributions with mean value zero. A deviation of the mean from zero was taken as an indication of a systematic error somewhere and if the standard deviation of the distribution was not equal to unity, one or several of the statistical errors had to be adjusted. The difficult point in this work was to find out which of the parameters that should be changed and by how much. This difficulty was due to the coupling of all parameters in the χ^2 fit and usually a systematic error or wrongly estimated statistical error had more or less

pronounced effects on all pull-quantity distributions. Naturally though there was a tendency for the pull quantity that contained the parameters to be corrected also to be the most influenced. The situation would have been very difficult if there had been several parameters with systematic errors and faulty statistical errors. These errors would have interfered with each other and all the pull quantity distributions would have been distorted in a way which would have been very difficult to disentangle. This is the reason why the systematic and statistical errors had to be well investigated before using the χ^2 code.

One more distribution - the distribution of χ^2:s - could be used to check the overall performance of the χ^2 fit. There were six degrees of freedom in the fit and the distribution in fig. 6 is the χ^2-distribution obtained, which checks rather well with what should be expected.

When the χ^2 analysis was carried out a new data summary tape was produced, containing all the information of the previous tape plus the fitted quantities from the χ^2 analysis together with the χ^2 value. With this second tape new cross-checks were possible. The influence on different kinds of distributions when varying the χ^2 level of confidence was observed. Among the distributions studied were those previously used to select events.

The most interesting histogram to investigate was the recoil kinetic energy histogram, since it was directly proportional to the differential cross section curve looked for. In fig. 7 is shown how the diffraction minimum-maximum structure was 'filtered out' of the background by choosing successively higher levels of confidence of the data. The curves refer to the same sample of events as in fig. 5 and 6. As is seen in fig. 7 the distribution does not change its shape above 1% confidence level. This was the finally chosen level of confidence and the resulting differential cross section is shown in fig. 8 together with some curves calculated from theory.

In a separate investigation the data from the recoil spectrometer were used to calculate the missing mass squared of the fast secondary system. The formula for this is given in Appendix 4. The missing mass squared distribution of the χ^2 selected elastic events should obviously be centered around the pion mass. This condition offered a check of the analysed and selected data and it is further discussed in sec. 2.1 and 4.2 of ref. 2. The distribution is found in fig. 16 of the same reference and from this the missing mass resolution of the recoil spectrometer can be found.

Although that the trigger system had been constructed to cut out as much inelastic background as possible and that the ρ- and A_1-mesons production cross sections are known to be rather small, some effort was made to investigate the missing mass squared distribution in the mass range of these resonances. For this samples of events were selected that were non-coplanar and had recoil momenta that did not fit the measured fast secondary scattering angle under the elastic hypothesis. No evidence of any structure around 1 $(GeV/c)^2$ in the missing mass squared distribution of these samples could be found though. This was most probably due to the severe trigger used [1].

4. THE COMPARISON WITH THEORY

The differential crosssection curves that are shown in fig. 8 together with the result of the measurements are calculated with a code [17] based on the Glauber multiple scattering theory. The basic approximations of this theory can be expressed in several ways - one is to say that the individual phase shifts caused by each nucleon in the nucleus during the collision should be additive. This is a valid approximation if the incident momentum is sufficiently high for the incident particle to see the nuclear nucleons as stationary objects and have a de Broglie wave length much shorter than the range of the interaction potential. These conditions are fulfilled for incident momenta of the order of several GeV/c and more and at these momenta the nucleons can be thought to cast sharp shadows in the nucleus. For lower momenta one cannot neglect the de Broglie wave length of the beam particle and Fresnel diffraction will become important.

It has been shown that by cancellation effects many of the results of the Glauber theory remain approximately the same even when Fresnel diffraction appears [16]. This explains why the Glauber theory has been able to describe phenomena at incident momenta below the limits set by its basic approximations. In our case though the incident momentum was 7.76 GeV/c and the basic approximations are well satisfied, so the original Glauber theory can be used with good confidence.

In the very simplest Glauber description of the elastic coherent scattering process the nuclear form factor is a Gaussian, with a delta function to take the center-of-mass motion into account, and the incident particle-nucleon scattering amplitude is exponential and imaginary. In this case the analytic expression for the differential cross section is very simple [18] and there are only three input parameters to

the formula: the nuclear radius, the incident particle-nucleon total cross section and the slope of the differential cross section of the incident particle-nucleon elastic scattering. These are parameters that are well established from other experiments, [19,20] so in this case there are no free parameters at all.

There are many refinements possible to this simple description like including effects of Fermi motion, spin flip, charge exchange and intermediate states and using a more precise nuclear form factor including correlation effects and a complex scattering amplitude with varying phase. At the incident momentum of our experiment and with the statistical uncertainty of the data indicated in fig. 8, only two refinements of the theory would have an effect of importance.

The first is to introduce a real part in the incident particle-nucleon scattering amplitude - see formula (1) of ref. 1. The real part was taken to be a constant fraction of the imaginary part, independent of momentum transfer.

The second refinement is to choose a form factor parametrization which can be better fitted to the experimentally measured ^{4}He nucleus form factor than the simple Gaussian. The parametrization chosen is given by formula (2) in ref. 1 as a superposition of Gaussians. With such a form factor the analytical expression of the differential cross section is no longer trivial to derive because it is no longer possible to apply in a simple way the method of Gartenhaus and Schwarz [21] to get rid of the centre-of-mass delta function. It is never the less possible to arrive at a analytical expression. This expression is given in ref. 22 and is described as a number of multiple integrals by the authors in ref. 6.

Since the nuclear wave function had been determined in earlier experiments [20] there was really only the phase to vary when comparing the data points to the theory. As a consequence, since the Glauber approximations are well satisfied at the given incident momentum, the prediction about the phase from the comparison of the data with the theory can be well justified.

Concluding remarks

This paper has given an account of the methods used in the analysis of the data from a helium-recoil spectrometer and the experience gained in the analysis of a first experiment with this apparatus. The codes and routines used to analyse the recoil spectrometer data were extensively tested and used in the course of the experiment and many of them can be used in new experiments with the apparatus. Such experiments will include large magnetic spectrometers for the fast secondary particles and new beam measuring systems, demanding new routines for the analysis of the data from the incident and outgoing fast particles. The routines concerning the recoil measurements will much remain the same though. Also some of the experience gained in combining the recoil spectrometer data with the data from a fast particle measuring system will certainly be of use, also when this system will be more complex than the one used in this experiment.

Acknowledgements

Sven Kullander and Staffan Dahlgren have read the drafts of this paper and given many valuable suggestions for which I am indebted. Lotten Borgman typed the manuscript.

Appendix 1

Relativistic kinematics formulae for an elastic two-body collision

Symbols

before

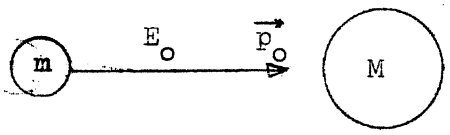

after

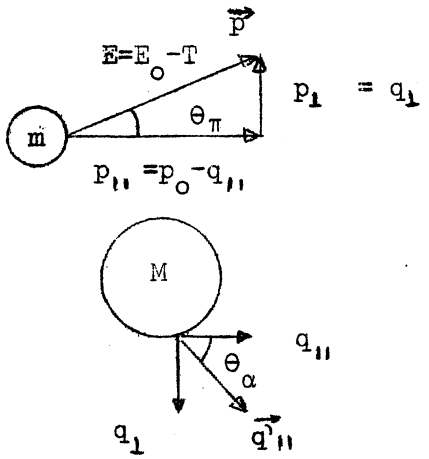

kinetic energy $T = E - M$

In the experiment the fast secondary scattering angle θ_π, the recoil scattering angle θ_α and the recoil kinetic energy T were measured. Any two of these parameters are completely determined by the third in an elastic coherent reaction. The relativistically correct formulae that interrelate these parameters are:

1. Fast secondary scattering angle from

a. recoil kinetic energy: $$\theta_\pi = \arccos \frac{p_o^2 - T \cdot (E_o+M)}{p_o\sqrt{(E_o-T)^2 - m^2}}$$

b. recoil scattering angle: $$\theta_\pi = \operatorname{arccot}\left[\left(\frac{E_o+M}{2M} \cdot \frac{1}{\cos^2\theta_\alpha} - \frac{p_o^2}{2M(E_o+M)} - 1\right)\cot\theta_\alpha\right]$$

2. Recoil scattering angle from

a. fast secondary scattering angle:

$$\theta_\alpha = \operatorname{arccot}\left[\frac{\cot\theta_\pi - \sqrt{\cot^2\theta_\pi - 4\left(\frac{E_o+M}{2M} - \frac{p_o^2}{2M(E_o+M)} - 1\right)\frac{E_o+M}{2M}}}{2\left(\frac{E_o+M}{2M} - \frac{p_o^2}{2M(E_o+M)} - 1\right)}\right]$$

b. recoil kinetic energy: $\theta_\alpha = \arccos\left(\frac{E_o+M}{p_o}\sqrt{\frac{T}{2M+T}}\right)$

3. Recoil kinetic energy from

a. recoil scattering angle: $T = \frac{2M(p_o\cos\theta_\alpha)^2}{(E_o+M)^2-(p_o\cos\theta_\alpha)^2}$

b. fast secondary scattering angle:

$$T = \frac{M+E_o\sin^2\theta_\pi - \sqrt{(M+E_o\sin^2\theta_\pi)^2 - \left[\left(\frac{E_o+M}{p_o}\right)^2 - \cos^2\theta_\pi\right] p_o^2 \sin^2\theta_\pi}}{\left(\frac{E_o+M}{p_o}\right)^2 - \cos^2\theta_\pi}$$

Derivation of the formulae

The invariant m^2 is $m^2 = E^2-p^2 = (E_o-T)^2-(p_o-q_{\parallel})^2-q_\perp^2$

$$\Longrightarrow q^2 = q_{\parallel}^2 + q_\perp^2 = E_o^2 + T^2 - 2E_oT - p_o^2 + 2p_oq_{\parallel} - m^2 =$$

$$= 2p_oq_{\parallel} + T^2 - 2E_oT \qquad (1)$$

The invariant M^2 is $M^2 = E_M^2 - q^2 = (M+T)^2 - q^2$

$$\Longrightarrow q^2 = -M^2 + M^2 + T^2 + 2MT = T^2+2MT = q_\perp^2 + q_{\parallel}^2 \qquad (2)$$

$$(1) \text{ and } (2) \Longrightarrow \quad q_{\parallel} = \frac{T(E_o+M)}{p_o} \qquad (3)$$

We now have the parallell component of the momentum transfer as function of recoil kinetic energy. This is sufficient to get the two scattering angles since:

$$\cos\theta_\alpha = \frac{q_{\parallel}}{q} = \frac{T(E_o+M)}{p_o}\cdot\frac{1}{\sqrt{T^2+2MT}} = \frac{E_o+M}{p_o}\sqrt{\frac{T}{2M+T}} \Longrightarrow 2b$$

$$\cos\theta_\pi = \frac{p_{\parallel}}{p} = \frac{p_o-q_{\parallel}}{p} = \frac{p_o^2 - T(E_o+M)}{p_o\sqrt{(E-T)^2 - m_o^2}} \Longrightarrow \quad 1a$$

The inverse relations 3a and 3b are given by simple (but in the case of 1a laborious) quadratic inversions. The relations between the scattering angles can be derived observing that

$$\frac{\cot \theta_\pi}{\operatorname{cct} \theta_\alpha} = \frac{p_o - q_{ii}}{q_{ii}} = \frac{p_o}{q_{ii}} - 1$$

Using (3) we obtain

$$\cot \theta_\pi = \left(\frac{p_o^2}{T(E_o+M)} - 1\right) \cot\theta_\alpha$$

Inserting the expression 3a for T as function of θ_α we obtain 1b. By a simple (but laborious) quadratic inversion of 1b we obtain 2a.

Appendix 2

The straggling of the recoil nuclei in the helium recoil spectrometer

In the helium recoil spectrometer the recoil energy loss by ionization in matter is considerable near the cut off and here is commented on the influence of energy straggling on the kinetic energy resolution. In ref. 22 results are given of measurements of energy straggling at considerable energy losses, using protons and alpha particles. The experimental results are compared with the predictions of the original Bohr theory - which does not include energy dependence - and more recent theories including energy dependence. Disagreements with the Bohr theory predictions are found at energy losses greater than 20% and the Bohr formula is found to give an underestimate by a factor growing with energy loss. This factor is around 2.2 for the example of 80 MeV alpha particles losing 90% of their energy.

The Bohr formula is

$$\sigma_E = 4\pi e^4 z^2 ZNX \quad \text{where}$$

σ_E is the standard deviation in a Gaussian energy distribution
z is the charge of the penetrating particle
Z is the number of electrons per atom (molecule)
N is the number of atoms (molecules) per unit volume
X is the particle path length

Inserting values corresponding to the three media which the recoil traverses one obtains:

one cm in 20 atm helium gas gives $\sigma_1 = 17$ keV
70 μm in solid mylar gives $\sigma_2 = 45$ keV
38 cm in the sparkchamber gas gives $\sigma_3 = 5$ keV

Sum $\sigma_E = 67$ keV

This is about 4 times less than the energy resolution of the recoil spectrometer at the lower cut off in energy. The conclusion is that the contribution to the measurement error from the recoil energy straggling can only be of any importance in a very small range of kinetic energies just around cut-off (see ref. 16) where anyhow - for other reasons - reliable data cannot be obtained with the recoil spectrometer.

Appendix 3

The multiple Coulomb scattering in the helium recoil spectrometer

In the Fermi model of multiple Coulomb scattering - outlined in a paper by Rossi and Greisen [23] - the lateral and angular distributions of charged particles that pass through matter are derived from a diffusion differential equation. Eyges [23] has worked out solutions to this equation taking in account the energy lost by the particles in the matter. In the helium recoil spectrometer the energy loss is considerable near the lower cut off in momentum transfer and to calculate the effects of multiple Coulomb scattering the Eyges formulae were used.

The often used Fermi formulae for the angular and lateral deviations of charged particles passing in matter are

$$\sigma_\theta^2 = \frac{z^2}{2} \cdot \frac{E_s^2}{(p\beta)^2} \cdot t \; ; \quad \sigma_y^2 = \frac{z^2}{6} \cdot \frac{E_s^2}{(p\beta)^2} \cdot t^3 = \frac{1}{3} \cdot \sigma_\theta^2 \cdot t^2$$

where σ_θ = standard deviation of angular-distribution

σ_y = standard deviation of lateral distribution

$E_s = m_e c^2 \sqrt{4\pi/\alpha} = 21$ MeV

p = momentum of the particles

β = velocity of the particles

z = charge of particles

t = particle path length in the matter measured in scattering lengths

The factor 1/3 in the relation between σ_y^2 and σ_θ^2 comes from the integration of the angular deviations along the particle path in the matter.

The corresponding generalized Eyges formulae in which energy losses are taken into account are

$$\sigma_\theta^2 = \frac{1}{2} E_s^2 \int_0^t \frac{z(t')}{(p(t') \cdot \beta(t'))^2} \, dt' \; ; \quad \sigma_y^2 = \frac{1}{2} E_s^2 \int_0^t \frac{(t-t')^2 \cdot z^2(t')}{(p(t') \cdot \beta(t'))^2} \, dt'$$

Here p and β are seen to be functions of the position coordinate t' along the track in the matter and in our case also the variation in z was accounted for. If p,β and z are constants the Eyges formulae re-

duce to Fermi formulae. The factor $(t-t')^2$ gives a high weight to large values of $t-t'$ in the integration. This is explained by the fact that small angular deviations are more important for the lateral deviation at $t'= t$ the farther from t they occurs. (A factor t'^2 instead of $(t-t')^2$ would give the same Fermi formula in the energy-independent case but the weighting would be wrong!)

In our case the particles were nonrelativistic and the formula used in the numerical calculation of the multiple Coulomb scattering was

$$\sigma_y^2 = \frac{E_s^2}{8} \sum_{i=1}^{3} \frac{\rho_i}{L_i} \int_{t_i}^{t_{i+1}} \frac{(t-t')^2 \cdot z_i^2 (T(t'))}{T_i^2 (t')} \, dt'$$

where i = 1 refers to the target helium

i = 2 refers to the target wall mylar

i = 3 refers to the spark chamber gas mixture

$T_i(t')$ = recoil kinetic energy as function of range in medium i (see sec. 2.1)

$t_{i+1}-t_i$ = path length in medium i

$z_i(T)$ = alpha particle effective charge as function of energy in medium i (see sec. 2.1)

ρ_i = density of medium i

L_i = scattering length of medium i

The scattering length L for composite media was calculated from tabulated values for elements using the formula

$$\frac{1}{L} = \sum_j \frac{p_j}{L_j}$$

where L_j = scattering length of element j

p_j = atomic fraction of element j in the composite medium.

The values used were

L = 38 g/cm^2 for alcohol, 39.5 g/cm^2 for mylar and 85.4 g/cm^2 for helium. Results from these calculations for a special case are shown in fig. 6 of ref. 2.

Appendix 4

The missing mass formula

Symbols:

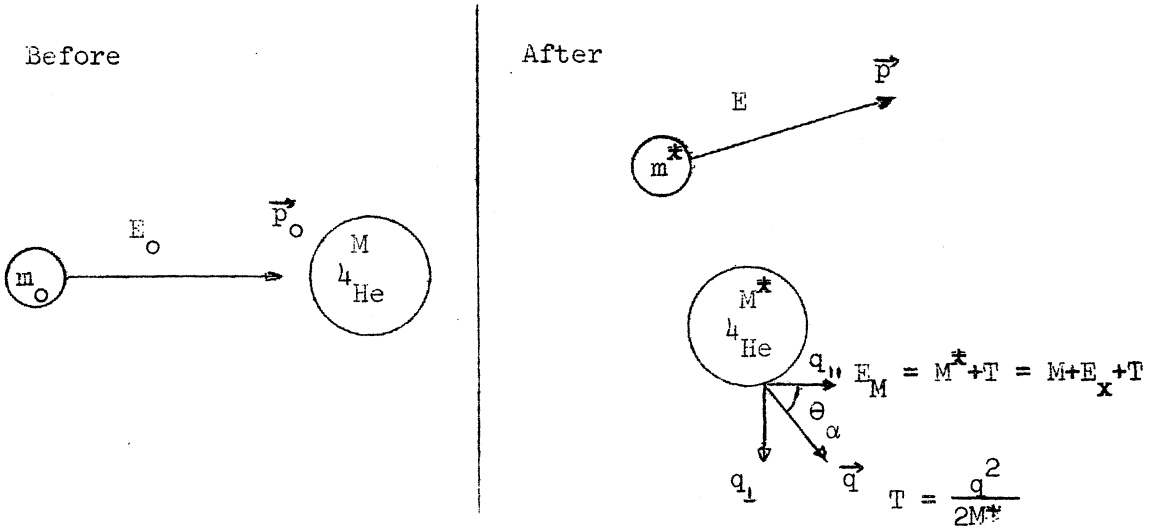

The helium recoil detector measures the recoil kinetic energy T and the scattering angle θ_α from which the missing mass m^* can be computed if the target nucleus is left unexcited ($M^* = M$, $E_x = 0$). We will first derive the formula for m^{*2} in the more general case when the target nucleus is excited as is discussed in sec. 2.1 in ref. 2. By setting $E_x = 0$ we will then get the missing mass formula in the coherent case.

The invariant m^{*2} is

$$m^{*2} = E^2 - p^2 =$$

$$= (E_o+M - E_{M*})^2 - (\vec{p}_o - \vec{q})^2 =$$

$$= E_o^2 + M^2 + E_{M*}^2 + 2E_oM - 2E_oE_{M*} - 2ME_{M*} - p_o^2 - q^2 - 2p_oq_{||} =$$

$$= m_o^2 + M^2 + (M+E_x)^2 + 2E_oM - 2(M+E_x+T)(E_o+M) + 2p_oq_{||} =$$

$$= m_o^2 + E_x(E_x-2E_o) - 2T(E_o+M) + 2p_oq_{||}$$

Supposing that $E_x << E_o$ gives the result

$$m^{*2} = m_o^2 + 2E_xE_o - 2T(E_o+M) + 2p_oq_{||}$$

a. Inserting $T = \frac{q^2}{2M^*} = \frac{q_\perp^2 + q_{\parallel}^2}{2M^*}$ and rearranging gives

$$q_{\parallel}\left[1 - \frac{E_o+M}{2p_oM^*}q_{\parallel}\right] = \frac{m^{*2} - m_o^2}{2p_o} + \frac{E_o + M}{2p_oM^*}q_\perp^2 + \frac{E_o}{p_o}E_x$$

which is the formula discussed in ref. 2.

b. Setting $E_x = 0$, $M^* = M$ and $q_{\parallel} = \sqrt{2MT}\,.\cos\theta_2$ gives

$$m^{*2} = m_o^2 - 2T(E_o+M) + 2p_o\sqrt{2MT}\,.\cos\theta_2$$

which is the coherent missing mass formula used for the investigation described in sec. 3.3.

References

1. T. Ekelöf, B. Höistad, A. Åsberg; C. Busi, S. Dahlgren, A.J. Herz, S. Kullander, G. Lee, D. Websdale; G. Landaud and J. Yonnet, Nucl. Phys. B35 (1971) 493.
2. S. Dahlgren, A.J. Herz, S. Kullander, R. Lorenzi; T. Ekelöf, B. Höistad and A. Åsberg, 'A helium-recoil spectrometer', CERN preprint, to appear in Nucl. Instr. and Meth.
3. T. Bunaciu, D. Evans, A.J. Herz, S. Kullander, A. Manz and Ph. Rosselet, Proposal to CERN Electronics Experiments Committee (CERN, Geneva, July 19, 1967).
4. J.K. Davies, B.G. Duff, R.C. Hanna, A.J. Herz, F.F. Heymann, D.C. Imrie, G.J. Lush, D.J. Miller, D.H. White and C. Wilkin, Proposal to CERN Electronics Experiments Committee (CERN, Geneva, October 6, 1971).
5. R.J. Glauber, 'High Energy Physics and Nuclear Structure', (S. Devons, Ed.) Plenum Press, New York, 1970, p. 207,and references therein. An extensive bibliography is given by H.H. Bingham in Proc. Topical Seminar on Interactions of Elementary Particles with Nuclei, Trieste, 15-17 September 1970 (INFN, Trieste, 1970).
6. O. Kofoed-Hansen and C. Wilkin, 'On the investigation of nucleon-nucleon correlations by means of high energy scattering'. Ref. TH. 1194 - CERN, Geneva, 1970.
7. J. Formanek and J. Trefil, Nucl. Phys. B3 (1967), 155.
   K.S. Kölbig and B. Margolis, Nucl. Phys. B6 (1968), 85.
8. P. Astbury, G. Finocchiaro, A. Michelini, D. Websdale, C.H. West; W. Beusch, B. Gobbi, M. Pepin, E. Polâr and M.A. Pouchon, Nucl. Instr. 46 (1967), 61.
   C. Bemporad, W. Beusch, A.C. Melissinos, E. Schuller; P. Astbury and J.G. Lee, Nucl. Instr. 80 (1970), 205.
9. B. Fagerström, A. Johansson, G. Tibell; G. Landaud, F. Lemeilleur, J. Yonnet; A. Cordaillat, S. Kullander and P.U. Renberg, Nucl. Instr. 91 (1971), 125.
   S. Kullander, G. Landaud, R. Lorenzi and J. Yonnet, Nucl. Instr. 92 (1971), 141.
10. S. Dahlgren, S. Kullander and R. Lorenzi, Nucl. Instr. 89 (1970), 29.
11. 'Studies in penetration of charged particles in matter', Publication 1133, Committee on Nuclear Science, National Academy of Sciences - National Research Council, Washington D.C., 1964.
12. S.K. Allison, Rev. Mod. Phys. 30 (1958), 1137.

13. J. Zoll, SUMX long write-up Y200, CERN computer program library, CERN, Geneva.

14. B. Höistad, J. Dorell and A. Åsberg, Gustaf Werner Institute, University of Uppsala, Internal Report GWI-PH 4/69, March 1969.

15. The χ^2 code that was used is named FITG, written by V. Chabaud, CERN, Geneva. The matematical principles used in this code are found in CERN Yellow Report 64-13 (1964),p. 81-85.

16. K. Gottfried, Annals of Physics 66 (1971), 868.

17. The Glauber code that was used is named ELSCAB, written by O. Kofoed-Hansen, CERN. It is the same code that was used for the calculations in ref. 6 for the case of no short range correlations.

18. W. Czyz and L. Lesniak, Phys. Lett. 24B (1967), 227.

19. E. Flaminio, J.D. Hansen,D.R.O. Morrison and N. Tovey. 'Compilation of cross sections VI- π^- induced reactions', CERN/HERA 70-7 (CERN, Geneva, 23 October 1970).

20. R.F. Frosch, J.S. McCarthy, R.E. Rand and M.R. Yearian, Phys.Rev. 160 (1967), 874.

21. S. Gartenhaus and C. Schwartz, Phys. Rev. 108 (1957), 482.

22. T.T. Chou, Phys. Rev. 168 (1967), 1594.

23. C. Tschalär and H.D. Maccabee, Phys. Rev. B1 (1970), 2863.

24. B. Rossi and K. Reisen, Rev. Mod. Phys. 13 (1941), 240.
L. Eyges, Phys. Rev. 74 (1948), 1534.

Figure captions

Fig. 1 Diagrammatic view of the recoil spectrometer.

Fig. 2. Range-energy relations for ^{4}He in (from the right) 1 atm helium gas, mylar and 1 atm spark chamber gas (86% He, 14% C_2H_5OH) used to calculate the energy losses suffered by the recoil in the helium recoil spectrometer. The figure illustrates a case where a 15 MeV α particle starts in the target, loses 2.84 MeV on its 2 cm long way in the 20 atm helium gas, enters the 70 μm thick target mylar foil in which it loses 5.05 MeV and then - starting with 7.11 MeV - traverses the 38 cm in 0.059 atm spark chamber gas losing 0.70 MeV and ends up at the scintillator with 6.41 MeV kinetic energy. This shows how fig. 10 in ref. 2 was obtained. In the evaluation of raw data the procedure was the inversed, going from T_3 to T_o.

Fig. 3. Flow diagram for the raw data evaluation code PIALPHA.

Fig. 4. 'Run identification and summing up' printed out by the PIALPHA code after the evaluations of all events in an experimental run. In this the 'CAEN TAPE' is the tape written on the IBM tape recorder, the 'CAEN CHAMBERS' are the spark chambers to measure the scattered pion and the 'UPPSALA CHAMBERS' are the recoil spark chambers.

Fig. 5. Distributions of four-momentum transfers squared, calculated from the measured pion scattering angles, for different combinations of the simple selection tests described in sec. 3.3.

Fig. 6. The distribution of χ^2 of the fitted data.

Fig. 7. Distributions of four-momentum transfers squared, given by the χ^2 fit, for different criteria on χ^2 (α = corresponding confidence level). The chosen value was $\chi^2 = 16.8$ ($\alpha = 1\%$) - the curves change shape for χ^2:s above this limit but not below.

Fig. 8. The differential cross section curves for elastic π^- ^{4}He scattering at 7.78 GeV/c as obtained from the Glauber theory together with the values resulting from the experiment. The theoretical curves are computed for different values of the ratio α of the real to imaginary part of the scattering amplitude.

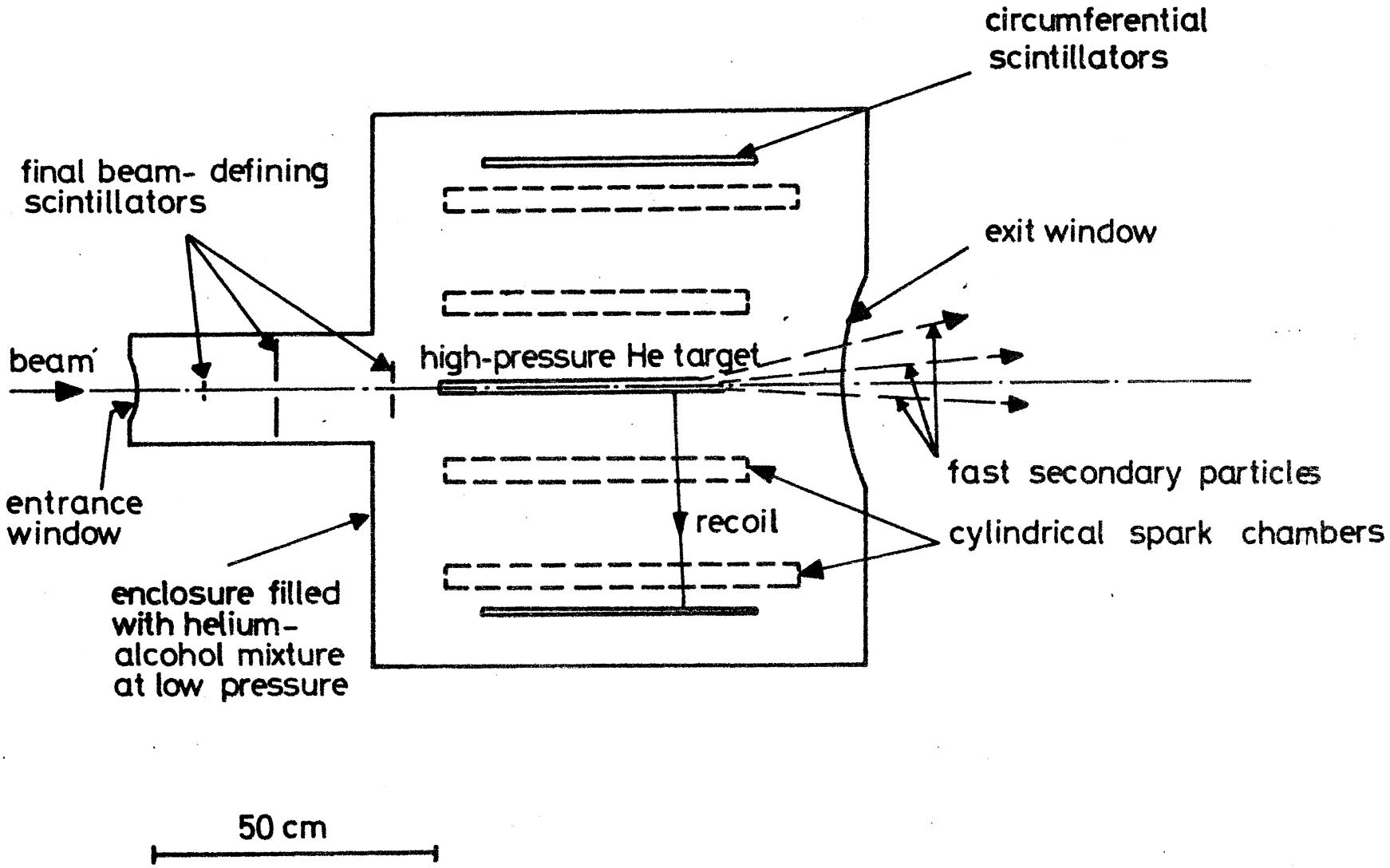
circumferential scintillators
final beam- defining scintillators
exit window
beam
high-pressure He target
fast secondary particles
entrance window
recoil
cylindrical spark chambers
enclosure filled with helium-alcohol mixture at low pressure
50 cm

Fig. 1

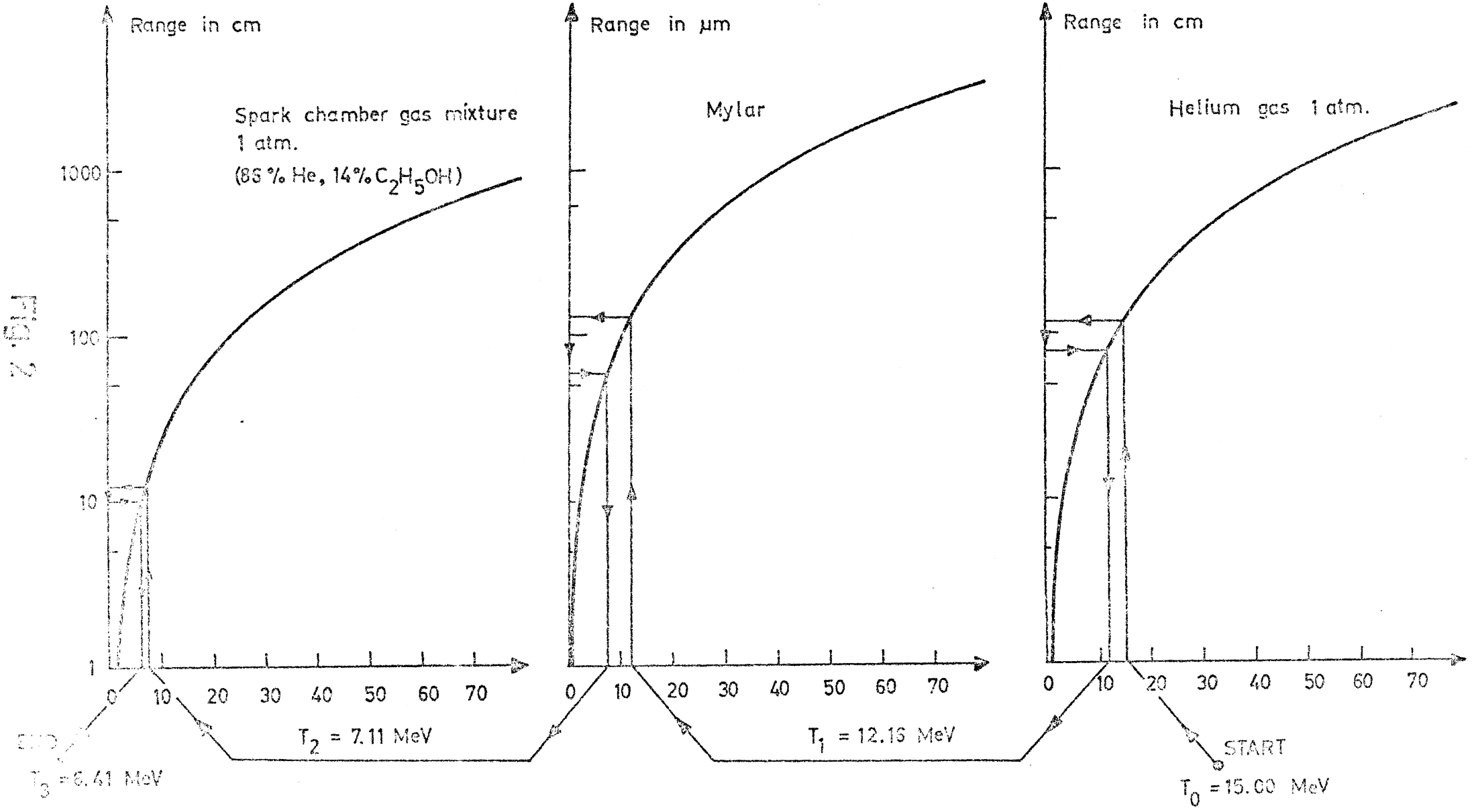
Range in cm
Spark chamber gas mixture
1 atm.
(86 % He, 14% C_2H_5OH)
1000
100
10
1
0
10
20
30
40
50
60
70
T_2 = 7.11 MeV
T_3 = 6.41 MeV
Range in μm
Mylar
T_1 = 12.16 MeV
Range in cm
Helium gas 1 atm.
START
T_0 = 15.00 MeV

Flow diagram for raw data evaluation code PIALPHA

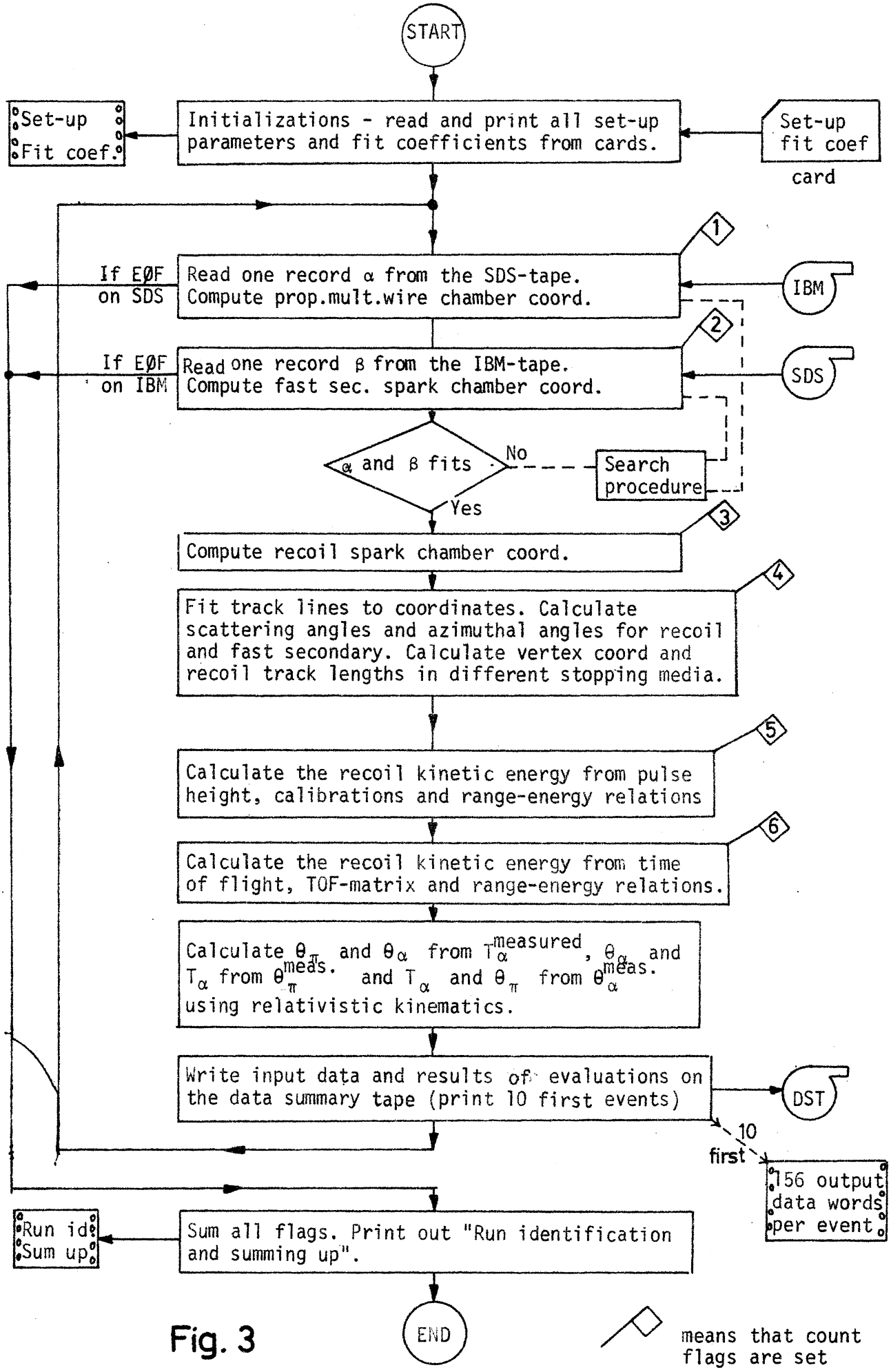

Fig. 3

RUN IDENTIFICATION
==========

NUMBER OF RUN 73
DATE OF RUN 10870
RUN END NOTED IN THE LOGBOOK AT PAGE 202

THE SDS RAW DATA TAPE
==========
TAPE LABEL 090894
FILE NUMBER = 13
LAST WORD(14) = 0796,0
LAST WORD(15) = 73,0

THE CAEN RAW DATA TAPE
==========
TAPE LABEL 012532L7902
FILE NUMBER = 14
LAST WORDCAN(29) = 9983,0
LAST WORDCAN(30) = 73,0

THE OUTPUT TAPE
==========
TAPE LABEL 026592L7244
FILE NUMBER = 1

SUMMING UP
==========

TOTAL NUMBER OF EVENTS FOUND IN THE SDS FILE = 9959
TOTAL NUMBER OF EVENTS FOUND IN THE CAEN FILE= 9601
TOTAL NUMBER OF RECORDS WITH FITTING SPCH-DATA = 9574

TOTAL NUMBER OF EVENTS LOST IN THE SDS FILE= 383 (I.E. NO EVENTS WITH FITTING SPCH-DATA ON THE CAEN TAPE COULD BE FOUND)
TOTAL NUMBER OF EVENTS LOST IN THE CAEN FILE = 26(I.E. NO EVENTS WITH FITTING SPCH-DATA ON THE SDS TAPE COULD BE FOUND

TOTAL NUMBER OF PARITY ERRORS ON THE SDS TAPE = 0 (EACH PARITY ERROR PROBABLY MEANING 13 EVENTS LOST)
TOTAL NUMBER OF PARITY ERRORS ON THE CAEN TAPE = 0 (EACH PARITY ERROR PROBABLY MEANING 32 EVENTS LOST)

NUMBER OF WHAT IS DEFINED AS GOOD EVENTS= 4251 (DEF.FOR A GOOD EVENT ALL MEASURED PARAMETERS COULD BE EVALUATED)
NUMBER OF WHAT IS DEFINED AS BAD EVENTS= 5323 (DEF.FOR A BAD EVENT AT LEAST ONE PARAMETER COULD NOT BE EVALUATED)

MEASUREMENTS EFFICIENCIES

CHARPAK CHAMBERS EFFICIENCY OF EACH CHAMBER

CHAMBER 1	CHAMBER 2	CHAMBER 3	CHAMBER 4	CHAMBER 5	CHAMBER 6	CHAMBER 7
81,58	81,94	73,96	81,23	80,72	83,43	85,08

PERCENTAGE OF RECONSTRUCTABLE INCOMING TRACKS =76,37

UPPSALA CHAMBERS EFFICIENCY IN PERCENT= 90,41

CAEN CHAMBERS EFFICIENCY OF EACH CHAMBER

CHAMBER 1X	CHAMBER 2X	CHAMBER 3X	CHAMBER 4X	CHAMBER 5X	CHAMBER 6X
87,78	87,83	79,57	82,86	86,43	82,85

CHAMBER 1Y	CHAMBER 2Y	CHAMBER 3Y	CHAMBER 4Y	CHAMBER 5Y	CHAMBER 6Y
0,00	89,52	82,99	89,09	81,78	80,29

PERCENTAGE OF RECONSTRUCTABLE OUTGOING TRACKS= 65,58

PULSEHEIGHT PARTIAL EFFICIENCIES

UPSTREAM	DOWNSTREAM	BOTH PH*S
95,67	99,96	95,64

PERCENT OF EVENTS WITH AT LEAST ONE PH = 100,00

TIME OF FLIGHT PARTIAL EFFICIENCIES

UPSTREAM	DOWNSTREAM	BOTH TOF*S
98,48	84,31	82,79

PERCENT OF EVENTS WITH AT LEAST ONE TOF= 100,00

NOTE THAT THE WORD *EFFICIENCY* HAS A SPECIAL MEANING INEACH CASE

Fig. 4

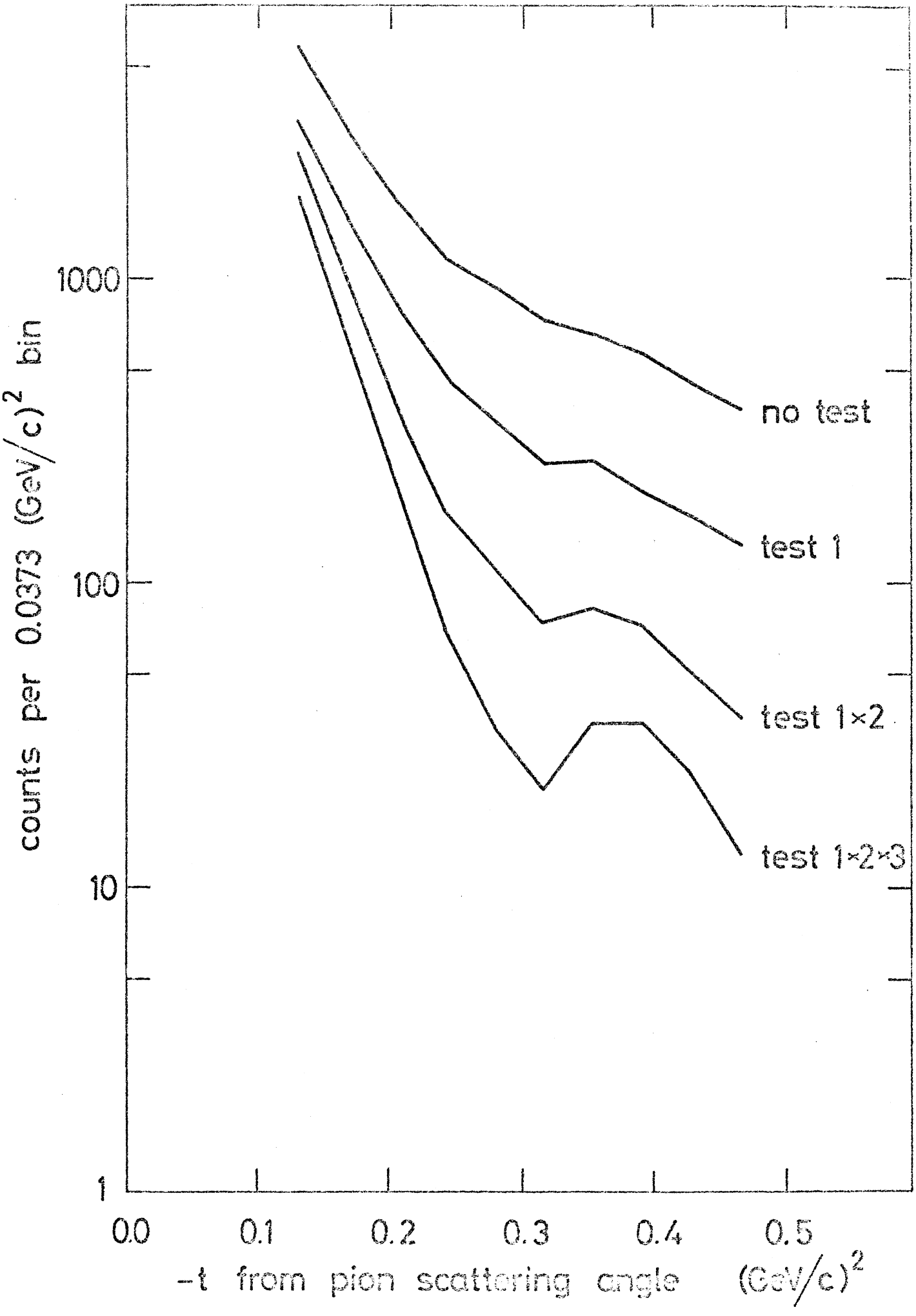
counts per 0.0373 (GeV/c)^2 bin
1000
100
10
1
no test
test 1
test 1×2
test 1×2×3
0.0
0.1
0.2
0.3
0.4
0.5
-t from pion scattering angle (GeV/c)^2

Fig. 5

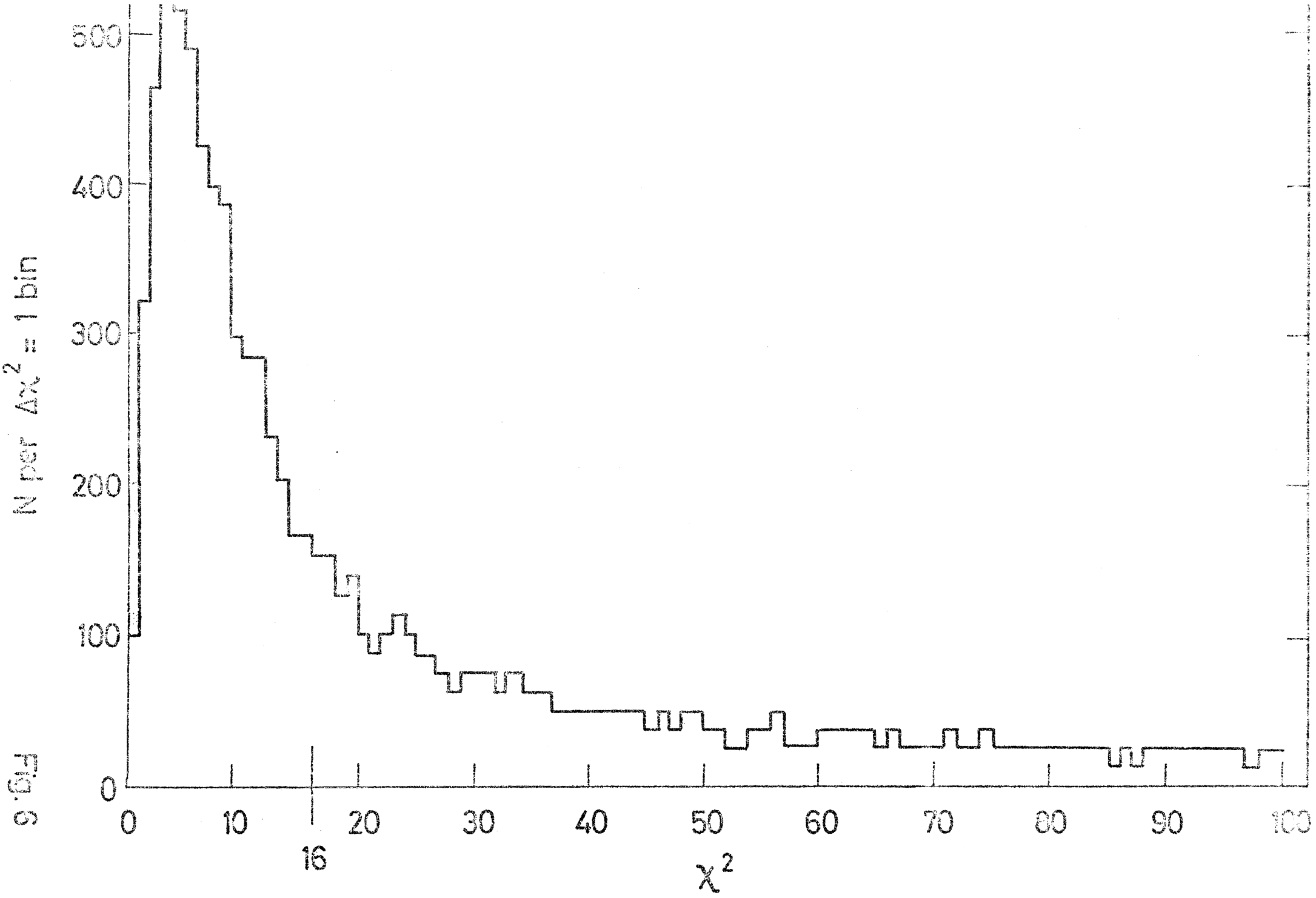
500
400
300
200
100
0
N per $\Delta\chi^2$ = 1 bin
0
10
16
20
30
40
50
60
70
80
90
100
χ^2

Fig. 6

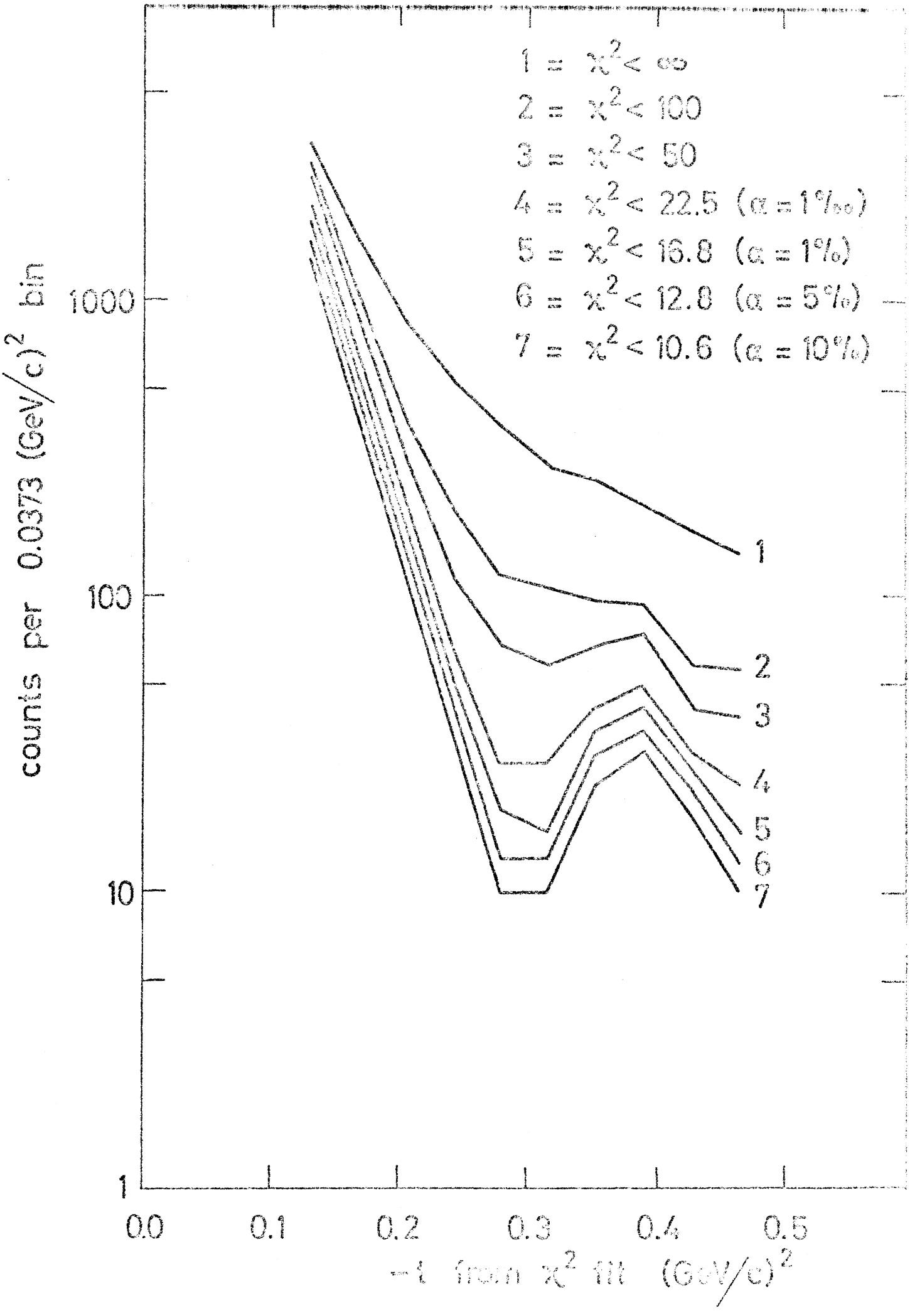
1 = $\chi^2 < \infty$
2 = $\chi^2 < 100$
3 = $\chi^2 < 50$
4 = $\chi^2 < 22.5$ ($\alpha = 1‰$)
5 = $\chi^2 < 16.8$ ($\alpha = 1\%$)
6 = $\chi^2 < 12.8$ ($\alpha = 5\%$)
7 = $\chi^2 < 10.6$ ($\alpha = 10\%$)
counts per 0.0373 $(GeV/c)^2$ bin
1000
100
10
1
0.0
0.1
0.2
0.3
0.4
0.5
$-t$ from χ^2 fit $(GeV/c)^2$

Fig. 7

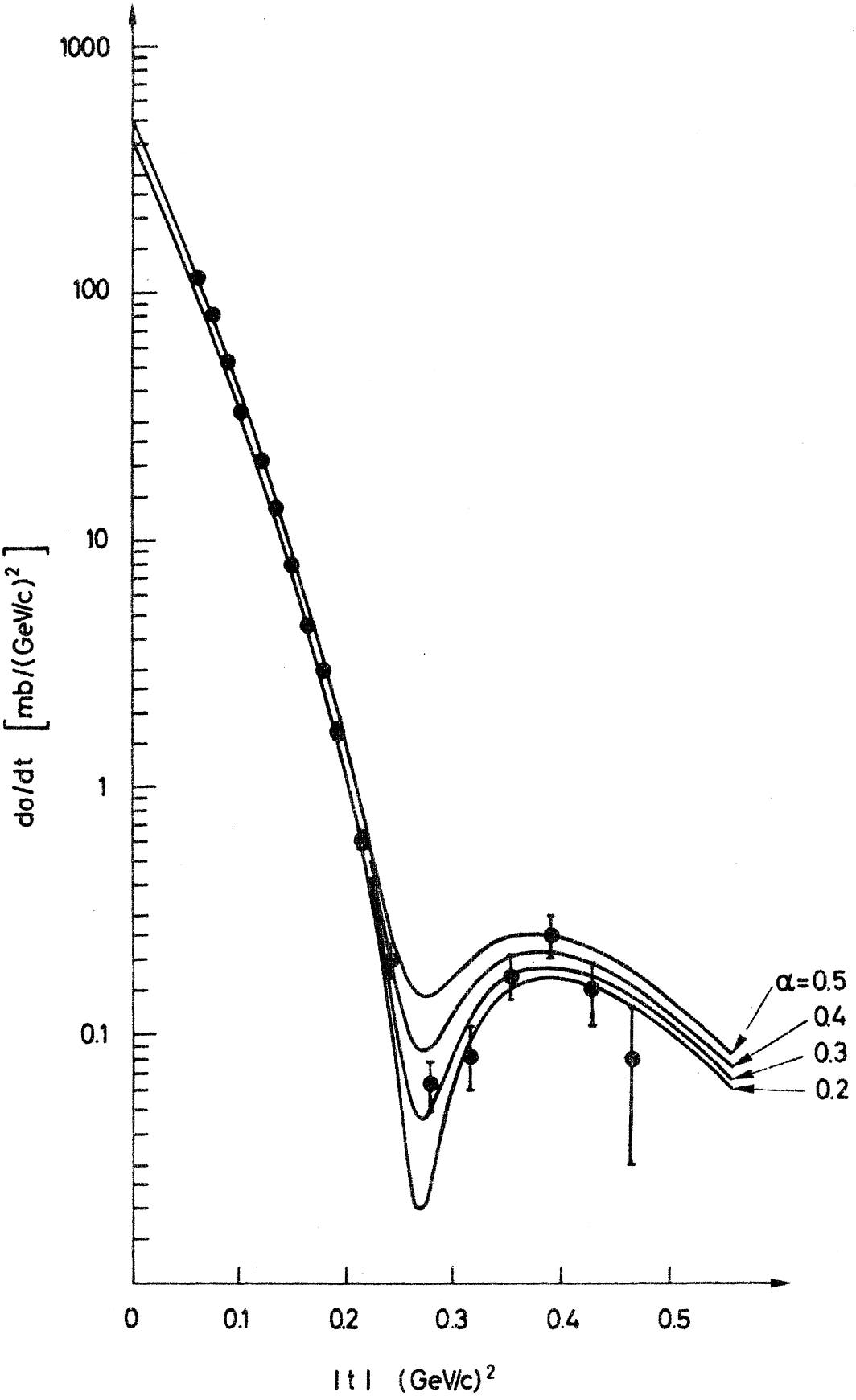

Fig. 8

UPPSALA UNIVERSITY, GUSTAF WERNER INSTITUTE

ON THE ρ MESON PRODUCTION IN π^4He INTERACTIONS

Tord Ekelöf
Gustaf Werner Institute, Uppsala, Sweden

ABSTRACT

Theoretical predictions about the coherent ρ meson production in π^4He interactions at multi-GeV energies are discussed. The Regge and Glauber theories are used for calculations of the production differential cross section at 6 GeV/c incident momentum. It is concluded that information on the ω trajectory, the ω exchange part of the amplitude for ρ hadroproduction on nucleons and the phase of the ρN scattering amplitude can be obtained from measurements of this reaction.

Uppsala - May 1972

Introduction

Hydrogen has been used as target in the great majority of elementary particle production reactions studied up till now. It is an old remark though that coherent production reactions on composite nuclei offer special advantages in that the selection rules for the production are more restrictive than in the proton target case. The experimental difficulty in measuring coherent reactions lies in separating the coherent events from the incoherent background.

To study total production cross sections it is sufficient to select the events in the forward diffraction peak (momentum transfers $\Delta < 1/R$ where R is the nuclear radius) which are nearly all due to coherent interactions. By making such measurements for a series of different nuclei, the interaction of the produced resonant state with the nucleons in the target nucleus can be studied as well. Results have recently been reported from such measurements [1]. The interaction between meson resonances and nucleons has also been the object of extensive studies of coherent photoproduction of vector mesons on composite nuclei over the last few years [2].

To obtain information on the amplitude for coherent production in hadron-nucleus interactions as function of momentum transfer the coherency of the reaction must be directly verified. At multi-GeV energies the only practical method for this is to observe the recoiling nucleus. The ^{4}He nucleus is especially suitable as target nucleus in this case because of its small size and high stability and in ref. 3 is described a device to measure ^{4}He recoils in high energy reactions. This ^{4}He recoil spectrometer has up till now been used to measure the differential cross section of π^- ^{4}He coherent elastic scattering [4] but new experiments with the recoil spectrometer concerning resonance production are now under preparation [5]. These new experiments concern baryon resonance production and since the helium nucleus has isospin zero the coherently produced resonances must have isospin one-half like the incident proton. Selection rules also apply to the exchanged particle and in meson resonance production on helium the exchanged boson must have both spin and parity either even or odd ($J^P = 0^+, 1^-, 2^+$ etc.) and isospin zero. Below are discussed the application of these ideas on coherent ρ meson hadroproduction on ^{4}He nuclei and what information that could be obtained from a measurement of the differential cross section for this reaction.

Isolation of the ω exchange ρ production

The total cross section for production of ρ mesons in πp reactions has been measured with good precision up to high energies and reliable data also excist for the differential cross section for this reaction. The theoretical interpretation of the experimental data is somewhat complicated by the fact that there are several exchange particles possible in the reaction. Among the established mesons the π, ω, A_1 and A_2 are allowed exchanges and among these the π and the ω are supposed to dominate.

In ref. 6 results from measurements on the reactions $\pi^{\pm} p \longrightarrow \rho^{\pm} p$ are interpreted in a model assuming only π and ω exchange. The contribution from the π exchange is predicted from other measurements and the only parameters that are varied in the fitting to the experimental data are those of the ω exchange amplitude. Good fits to the data are obtained but the conclusions about the ω exchange amplitude drawn from the fit cannot be very precize due to the mixing of exchanges.

Using isospin analysis and Regge pole exchange theory one can show [7] that the contribution to the ρ production from ω exchange can be obtained from $\pi^{\pm} p$ scattering data using the relation

$$X(s,t) = \frac{1}{2}\left[\frac{d\sigma}{dt}(\pi^- p \longrightarrow \rho^- p) + \frac{d\sigma}{dt}(\pi^+ p \longrightarrow \rho^+ p) - \frac{d\sigma}{dt}(\pi^- p \longrightarrow \rho^o n)\right] \qquad (1)$$

With this method the error will be rather great [7,8] though since the measurement error for each reaction add up.

An alternative method to isolate the ω exchange contribution to the ρ production is to study coherent π ^{4}He production reactions. The ground state of ^{4}He has $J^P I = 0^+ 0$ and only an exchange particle with $J^P I = 1^- 0$ can transform the π $(0^- 1)$ to a ρ $(1^- 1)$. π, A_1 $(1^+ 1)$ and A_2 $(2^+ 1)$ are thus forbidden as exchange particles whereas the ω $(1^- 0)$ is allowed. Also the Ø-meson would be allowed as exchange particle since it has $J^P I = 1^- 0$ like the ω-meson, but it is known to decouple from πN and πρ and can thus be disregarded. Any ρ production by π on ^{4}He is thus due to pure ω-exchange, provided that the reaction is coherent (i.e. that the ^{4}He is left in its ground state).

The Regge ω exchange amplitude for ρ hadroproduction on nucleons

The Regge theory amplitude in the s-chennel reaction $\pi^{\pm} p \longrightarrow \rho^{\pm} p$, assuming only ω trajectory exchange with helicity flip at the meson vertex and no helicity flip at the baryon vertex can be written [6]

$$f(s,t) = \sin\theta_t \cdot \beta(t) \cdot \frac{1+\eta e^{-i\pi\alpha(t)}}{\sin\pi\alpha(t)} \cdot \frac{\alpha(t)}{\Gamma(\alpha(t)+1)} \cdot \left(\frac{s}{s_o}\right)^{\alpha(t)-1} \qquad (2)$$

where

$$\sin\theta_t = 2\sqrt{t\cdot\phi(s,t)}/T_{ac}\cdot T_{bd} \quad \text{with}$$

$$\phi(s,t)=st(m_a^2+m_b^2+m_c^2+m_d^2-s-t) - s(m_b^2-m_d^2)(m_a^2-m_c^2) -$$

$$- t(m_a^2-m_b^2)(m_c^2-m_d^2) - (m_a^2m_d^2-m_c^2 m_b^2)(m_a^2+m_d^2-m_c^2-m_b^2)$$

$$T_{ac}= \sqrt{t^2+m_a^4+m_c^4-2(tm_a^2+tm_c^2+m_a^2 m_c^2)}$$

$$T_{bd}= \sqrt{t^2+m_b^4+m_d^4-2(tm_b^2+tm_d^2+m_b^2m_d^2)}$$

is the sine of the angle in the t-channel reaction corresponding to the s-channel reaction $m_a+m_b \longrightarrow m_c+m_d$ with total center of mass energy s and fourmomentum transfer squared t,

$\beta(t)$ is the ω pole residue function,
η is the ω trajectory signature parity,
s_o is a scaling constant and
$\alpha(t)$ is the exchange ω trajectory.

From this amplitude the corresponding differential cross section is obtained using the relation

$$d\sigma/dt(s,t) = |f(s,t)|^2/s\cdot p_{in}^{CM}\cdot p_{out}^{CM} \qquad (3)$$

Since the ω trajectory is an odd spin trajectory, its signature parity is negative. In fig. 1a and 1b are shown results from a calculation of $d\sigma/dt$ at incident momentum 6 GeV/c using as ω trajectory $\alpha(t) = 0.4+0.9t$ and with the residue function $\beta(t)$ constant and equal to 10.7. The trajectory parameters are estimated from the intercept value given in ref. 9, the pole and the A_2 and f poles, assuming the latter to have trajectories degenerated with the ω trajectory.

Integrating the relation (1) over t and inserting the measured $\pi^{\pm}p$ cross section values found in ref. 8 gives a value 70±30 μb for the ω exchange $\pi p \longrightarrow \rho p$ reaction. The β residue parameter was obtained from the condition that the differential cross section (3), integrated over t, should have the same value. The resulting $\beta=10.7\pm2.2$ is in fair accordance with the value $\beta=16.2$, obtained in the fit in ref. 6. - The s_o value used was 1.4 like in ref. 6.

The Regge parametrization (2) is the same as the one used in interpreting the experimental data in ref. 6 and the results of our calculations (fig. 1a) are in good agreement with what is obtained in the fit to the data in ref. 8 (see fig. 2 in this ref.) using a rather different parametrization. The main features of the differential cross section are the dips (zeros) in the forward direction and at $-t=0.45$ (GeV/c^2). The forward dip is required by angular momentum conservation in exchange of spin particles and it is due to the $\sin\theta_t$-factor vanishing for t=0. The dip at $-t=0.45$ $(GeV/c)^2$ is explained by the zero of the ω trajectory at this value.

The differential cross section for ρ hadroproduction on helium

In the impulse approximation the differential cross section for coherent hadroproduction on nuclei is related to the corresponding differential cross section on nucleons by the formula [10]

$$(d\sigma/dt)_{nucleus} = A^2 \cdot S^2(t) \cdot (d\sigma/dt)_{nucleon} \qquad (4)$$

where A = number of nucleons in the nucleus and

S(t) = nuclear density distribution form factor,

provided that the exchange mechanisms in the two processes are the same. Since ω exchange is the only exchange allowed in coherent hadroproduction of ρ on helium, the differential cross section (3), with (2) inserted, can be used in (4) to give dσ/dt for this reaction.

In figures 2a and 2b are shown results from a calculation of this differential cross section at incident momentum 6 GeV/c with A=4 and the form factor $S(t)=\exp(R^2t/4)$ where R=1.37 F. This form factor corresponds to a nuclear wave function of a harmonic oscillator, which is a good approximation for the ^{4}He ground state at low momentum transfers. The nuclear radius R used is taken from measurements on electron scattering from helium nuclei [11].

In the figures 2a and 2b are also inserted for comparison the form factor squared $S^2(t)$ and the differential cross sections for the ω exchange ρ production on nucleons. As is seen the differential

cross section on ^{4}He is enhanced by a factor growing from 1 to 16 when going from $-t=0.11$ (GeV/c)^2 to the forward direction. By integration the cross section on ^{4}He is found to be 140 μb which is a factor 2 greater than the given cross section for ω exchange ρ production on nucleons. On the other hand the depression of the differential cross section on ^{4}He at higher momentum transfers is dramatic. It should also be noted that for t values around -0.07 (GeV/c)^2, where the elementary cross section has a flat maximum, the slope of the ^{4}He differential cross section is entirely determined by the nuclear form factor.

The ω trajectory

Inserting formulae (2) and (3) in (4) gives:

$$(d\sigma/dt)_{He} = 16 \cdot S^2(t) \cdot R^2(t) \cdot \sin^2\theta_t(s,t) \cdot s^{2\alpha(t)-2} / s \cdot p_{in}^{CM} \cdot p_{out}^{CM} \qquad (5)$$

where the s independent factors in the Regge amplitude (2) have been summed up in R(t). At high energies p_{in}^{CM} is roughly equal to p_{out}^{CM} and proportional to $s^{1/2}$ and $\sin^2\theta_t$ is proportional to s^2 (see (2)!). The s dependence of the differential cross section is thus given by a factor $s^{2\alpha(t)-2}$.

By making measurements of $d\sigma/dt(\pi^4\text{He} \longrightarrow \rho^4\text{He})$ at different centre of mass energies s_1 and s_2 the ω trajectory can be directly determined from

$$\alpha(t) = \frac{1}{2} \ln \left[\frac{d\sigma/dt(s_1,t)}{d\sigma/dt(s_2,1)} \right] / \ln \frac{s_1}{s_2} + 1. \qquad (6)$$

To indicate the precision in such a determination the following numerical example is given:

Using incident laboratory momenta $p_1=4$ GeV/c and $p_2=8$ GeV/c the s_1/s_2 ratio will be 0.53 ($\approx p_1/p_2$). If the ratio of the differential cross sections for these two momenta at a certain t is measured to be 2.25 with error ± 0.25, then (6) gives the ω trajectory value 0.36 with error $\pm$ 0.09 for this t(= -0.04 (GeV/c^2 if $\alpha(t)=0.4+0.9\,t$). (Evaluating (4) at these two incident momenta and integrating over t gives cross section values for $\pi^4\text{He} \longrightarrow \rho^4\text{He}$ of 205 μb at 4 GeV/c and 104 μb at 8 GeV/c).

The differential cross section from multiple scattering at higher momentum transfers

For higher momentum transfers where multiple scattering becomes important the impulse approximation formula (4) is not relevant and use must be made of the Glauber multiple scattering formalism. In the case of double scattering the ρ production can be thought to proceed in two different ways:

1. Elastic scattering of the π in the first collision and production of the ρ in the second.
2. Production of the ρ in the first collision and scattering of the ρ in the second.

As can be seen both the πN and the ρN elastic scattering amplitudes as well as the $\pi N \longrightarrow \rho N$ production amplitude will enter the calculations.

For multiple scattering of higher order the basic processes will be the same as in double scattering and the only additional complication will be the counting of possible combinations. Using a Gaussian density function for ^{4}He, with a delta function to take the centre of mass motion into account:

$$\rho = R^{-12}\,\pi^{-6}\prod_{i=1}^{4}\exp(-r_i^2/R^2)\cdot\delta(1/4\sum_{i=1}^{4}\vec{r}_i) \tag{7a}$$

and amplitudes for the πN and ρN scattering and $\pi N \longrightarrow \rho N$ production that are exponential functions in t:

$$g_{\pi N}(\delta) = \frac{\sigma_{\pi N}\cdot p}{4\pi}\cdot(i+\alpha_{\pi N})\cdot\exp(a_{\pi N}\cdot\delta^2/2) \tag{7b}$$

$$g_{\rho N}(\delta) = \frac{\sigma_{\rho N}\cdot p}{4\pi}\cdot(i+\alpha_{\rho N})\cdot\exp(a_{\rho N}\cdot\delta^2/2) \tag{7c}$$

$$f(\delta) = \frac{G\cdot p}{4\pi}\cdot(i+\beta)\cdot\exp(b\cdot\delta^2/2) \quad \text{for } \pi N \longrightarrow \rho N \tag{7d}$$

the Glauber theory gives the following expression for the production amplitude in the $\pi\,^4$He $\longrightarrow$ $\rho\,^4$He reaction [11]:

$$F(t) = \frac{ip}{2}\cdot\exp(-\frac{R^2t}{16})\cdot\sum_{k=1}^{4}\sum_{n=1}^{k}\binom{4}{k}(-1)^{k+1}\cdot$$

$$\cdot\left[\frac{\sigma_{\pi N}(1-i\alpha_{\pi N})}{2\pi(R^2+2a_{\pi N})}\right]^{k-n}\cdot\left[\frac{G\,(1-i\beta)}{2\pi(R^2+2b)}\right]\cdot\left[\frac{\sigma_{\rho N}(1-i\alpha_{\rho N})}{2\pi(R^2+2a_{\rho N})}\right]^{n-1}\cdot\frac{1}{E}\cdot\exp(\frac{t}{4E}) \tag{8}$$

where $$E = \frac{k-n}{R^2+2a_{\pi N}} + \frac{1}{R^2+2b} + \frac{n-1}{R^2+2a_{\rho N}}$$

In this expression the first exponential factor comes from the δ function used in the nuclear wave function. The first summation adds up multiple scattering terms of different multiplicity k together with

the phase factor $(-1)^{k+1}$. Only first order effects are described with this formula, i.e. only processes with one transformation from π to ρ are taken into account. The second summation adds up terms of the same multiplicity k but different order number n of the producing collision. The three terms in brackets describe in sequence (k-n) elastic πN scatterings, one $\pi N \longrightarrow \rho N$ production reaction and (n - 1) ρN elastic scatterings. The exponential afterwards gives the exponential slope of each (k,n) term.

In fig. 3 are shown $d\sigma/dt$ curves for the reaction $\pi\,^4He \longrightarrow \rho\,^4He$ at incident momentum 6 GeV/c for different values of the ρN amplitude phase $\alpha_{\rho N}$. The $f_{\pi N}(\delta)$ parameters used are taken from ref. 4 and the $\sigma_{\rho N}$ is by now rather well established from ρ^o photoproduction measurements. According to isospin analysis the amplitude for $\rho^o N$ scattering is equal to the mean of the $\rho^+ N$ and $\rho^- N$ amplitudes and the value 27.5±1 mb from the measurements of the $\rho^o N$ elastic cross section [2] can be directly used. This cross section could be independently determined in a measurement of the differential cross section in fig. 3 from the position of the interference dip along the t scale [12] but the precision in this determination would not be as good as in the ρ photoproduction measurements.

From (6) it is clear that the phase β will not directly influence the $d\sigma/dt$ curve, only $|G(1-i\beta)|^2$ will enter the calculation. This quantity divided by 16π equals the value for $d\sigma/dt(\pi N \longrightarrow \rho N)$ for t=0 in our model where the amplitude $f(\delta)$ is an exponential slope in δ^2. As can be seen from fig. 1 this is a rather crude approximation.

In the region of the first diffraction minimum the single and double scattering terms are of equal importance. If the momentum transfer in the meson-nucleon collision in a single scattering at the minimum is δ_{min}, then the momentum transfer in each of the two meson-nucleon collisions in a double scattering in the same t region is on the average $\delta_{min}/2$. As a very crude estimate the tangent to the $f(\delta)$ curve inbetween δ^2_{min} and $\delta^2_{min}/4$ is taken to represent the elementary ρ production amplitude. In this way is obtained $|G(1-i\beta)|^2/16\pi \simeq 0.5$ mb$(GeV/c)^{-2}$ and $b \simeq 3.5 (GeV/c)^{-2}$ (see fig. 2b).

The value of b used is of rather little importance since the t dependance is masked by the very steep slope of the nuclear form factor. Furthermore the value of $|G(1-i\beta)|^2/16\pi$ enters linearly in the expression for $d\sigma/dt(\pi\,^4He \rightarrow \rho\,^4He)$ and will thus not influence the shape of the curve, only its absolute mag-

nitude. In these first-order calculations none of the ρ production amplitude parameters will thus influence the curve shape significantly and the only free parameter is $\alpha_{\rho N}$, the remaining parameters being well established in other measurements.

Conclusions

Information on the following quantities at non-zero momentum transfers can thus be obtained from a measurement of the differential cross section of the reaction $\pi^4He \longrightarrow \rho^4He$:

1. the ω trajectory in the s channel
2. the ω exchange part of the πN —> ρN amplitude
3. the phase of the ρN scattering amplitude.

For this measurement the helium recoil spectrometer mentioned in the introduction seems well suited. The ω trajectory could be determined at momentum transfer values up to the same values as for which double scattering becomes dominant, i.e. around $-t=0.2(GeV/c)^2$. The upper limit for the determination of the ω exchange amplitude is lower since the variation of this amplitude with t is masked by the nuclear form factor around $-t=0.07(GeV/c)^2$. The lower limit for the determination of these quantities is set by the recoil spectrometer. In the experiment in ref. 4 this lower limit was $-t=0.05\ (GeV/c)^2$. Using a target wall of 3μ thickness (mylar) and helium target gas of only 1 atm. would lower this figure to $-t=0.025\ (GeV/c)^2$. In spite of the low target gas pressure a reasonable event rate could be expected due to the high cross section at low momentum transfers and valuable information on the ω trajectory and the ω exchange amplitude would be obtainable.

The ρN amplitude phase value determined from the interference dip region at $t=t_{min}$ would be a mean taken over t values around t_{min} and $t_{min}/4$. Good possibilities for background elemination are needed for this measurement at 6 GeV/c incident momentum since the differential cross section at the interference dip is roughly a factor 10 less than in the elastic reaction measurement in ref. 1. With a good measurement of the direction and momentum of the secondary charged pion (from the ρ decay; $\rho^{\pm} \longrightarrow \pi^o\pi^{\pm}$), inclusion of the detection of two gamma rays (from $\pi^o \longrightarrow 2\gamma$) in the trigger and a sufficient number of beam particles the measurement seems quite possible though.

Acknowledgements

Many interesting and stimulating discussions with Sven Kullander, Göran Fäldt, Lars Gislén, Otto Kofoed-Hansen, Per Osland and Bengt E.Y. Svensson on the subjects in this paper and related topics are gratefully acknowledged. Lotten Borgman typed the manuscript.

References

1. C. Bemporad, W. Beusch, A.C. Melissinos, E. Polgár, D. Websdale, J.D. Wilson; J.P. Dufey, K. Freudenreich, R. Frosch, F.X. Gentit, P. Mühlemann; J. Codling, J.G. Lee, M. Letheren; G. Bellini, M. di Corato and G. Vegni, Nucl.Phys. B33 (1971), 397.
2. K. Gottfried, rapporteurs report at International Symposium on Electron and Photon Interactions at High Energies, Cornell Univ., Ithaca, N.Y., August 23-27, 1971 - CERN Ref. TH. 1407, 27 Sept. 1971.
3. S. Dahlgren, A.J. Herz, S. Kullander, R. Lorenzi;T. Ekelöf, B. Höistad and A. Åsberg: 'A helium-recoil spectrometer' - To appear in Nuclear Instruments and Methods.
4. T. Ekelöf, B. Höistad, A. Åsberg; C. Busi, S. Dahlgren, A.J. Herz, S. Kullander, G. Lee, D. Websdale; G. Landaud and J. Yonnet - Nucl.Phys. B35 (1971) 493.
5. J.K. Davies, B.G. Duff, R.C. Hanna, A.J. Herz, F.F. Heymann, D.C. Imrie, G.J. Lush, D.J. Miller, D.H. White and C. Wilkin. - Proposal to CERN Electronics Experiment Committee (CERN, Geneva, October 6, 1971).
6. D.J. Mellema and R. Henzi, Nucl.Phys. B19 (1970), 637.
7. A.P. Contogouris and J. Tran Thanh Van, Phys.Rev.Lett. 19 (1967), 1352.
8. D.J. Crennell, H.A. Gordon, M.L. Ioffredo, Kwan-Wu Lai and J.M. Scarr, Phys.Rev.Lett. 27 (1971), 1674.
9. M. Restignoli, L. Sertorio and M. Toller, Phys.Rev. 150 (1966), 1389.
10. L. Stodolsky, Phys.Rev. 144 (1966), 1145.
11. R.F. Frosch, J.S. McCarthy, R.E. Rand and M.R. Yearian, Phys.Rev. 160 (1967), 874.
12. J. Formanek and J.S. Trefil, Nucl.Phys. B3 (1967), 155.

Figure captions

Fig. 1a,b The ω exchange part of the amplitude for the reaction $\pi N \longrightarrow \rho N$ at 6 GeV/c, calculated using formulae (2) and (3) in the text. The ranges in -t are 0-1 $(GeV/c)^2$ (a) and 0-0.1 $(GeV/c)^2$ (b). Linear scales.

Fig. 2a,b The differential cross section of for coherent reaction $\pi + {}^4He \longrightarrow \rho + {}^4He$ at 6 GeV/c, calculated using formulae (2) and (3) in the text (full line). For comparison are also given the differential cross section for the ω exchange part of the reaction $\pi N \longrightarrow \rho N$ (dashed line) and, in fig. 2a, the nuclear form factor used (dot-dashed line). In fig.2b is shown the tangent to the $\pi N \longrightarrow \rho N$ ω-exchange cross section used for the approximate amplitude (7d). The ranges in -t are 0-0.8 $(GeV/c)^2$ (a) and 0-0.16 $(GeV/c)^2$ (b). Logarithmic $d\sigma/dt$ scales.

Fig. 3 The differential cross section of the coherent reaction $\pi + {}^4He \longrightarrow \rho + {}^4He$ at 6 GeV/c, calculated using formula (8) in the text for different values of the fraction $\alpha_{\rho N}$ of the real to the imaginary part of the ρN scattering amplitude.

Fig. 1a

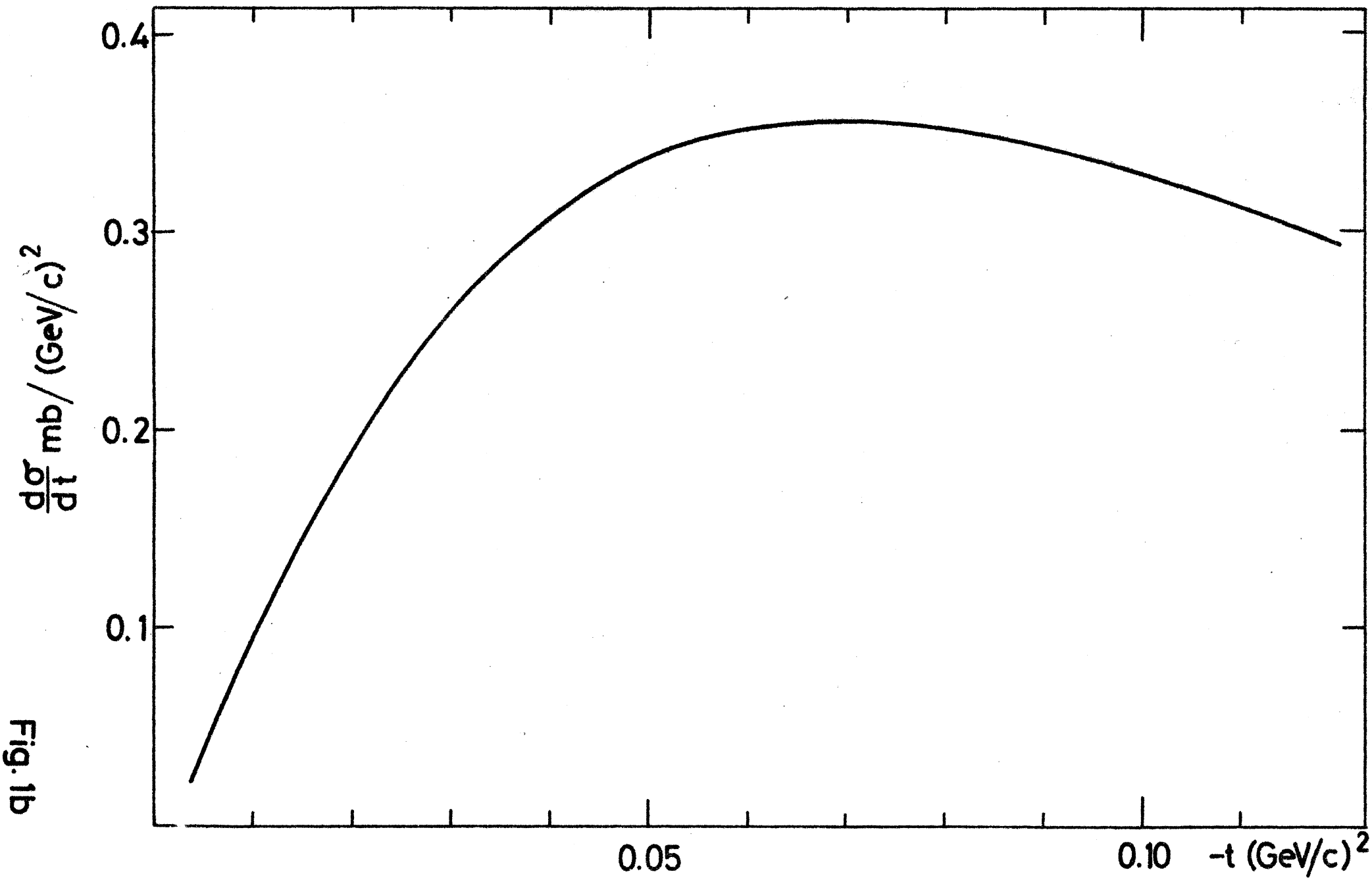

Fig. 1b

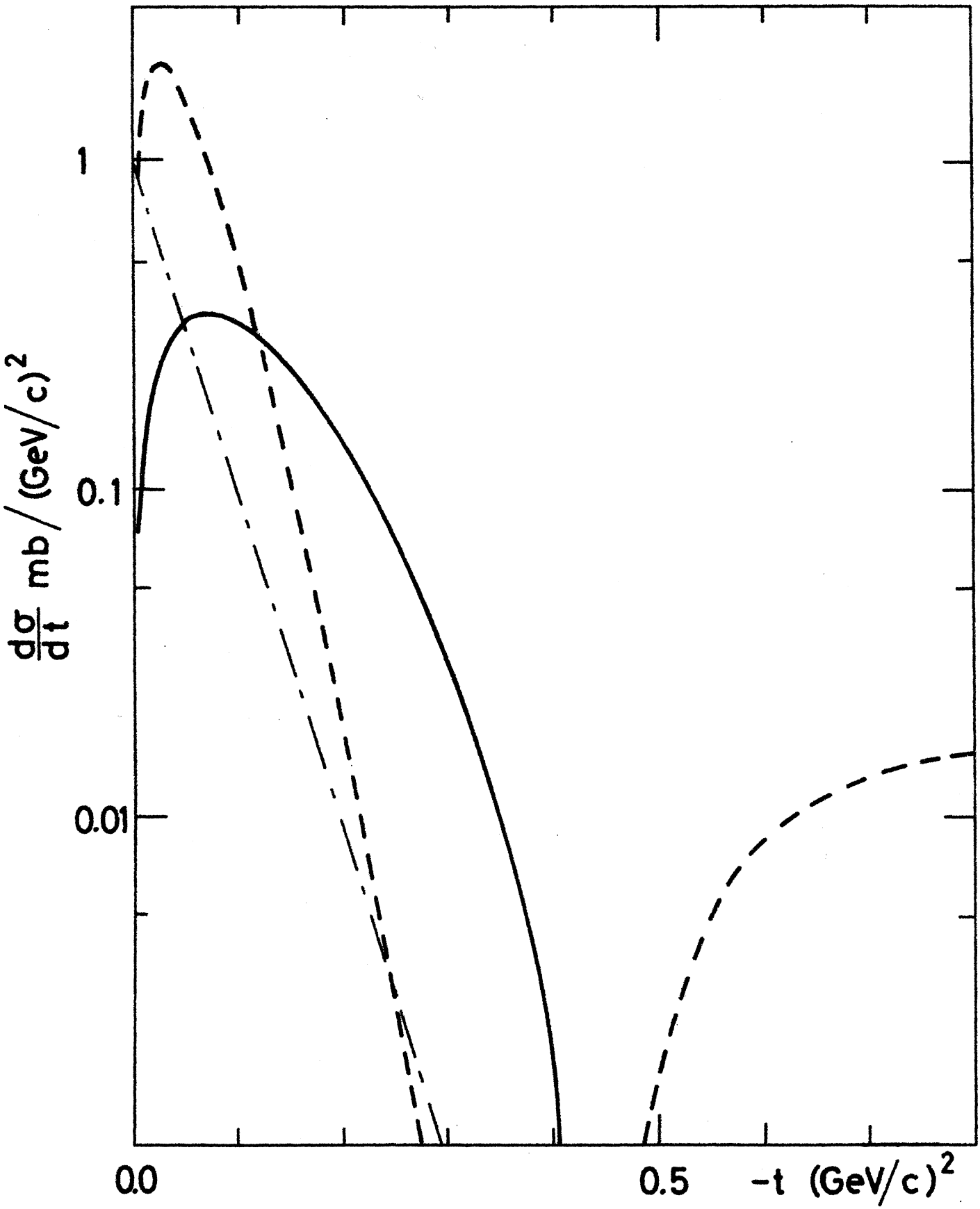

Fig. 2a

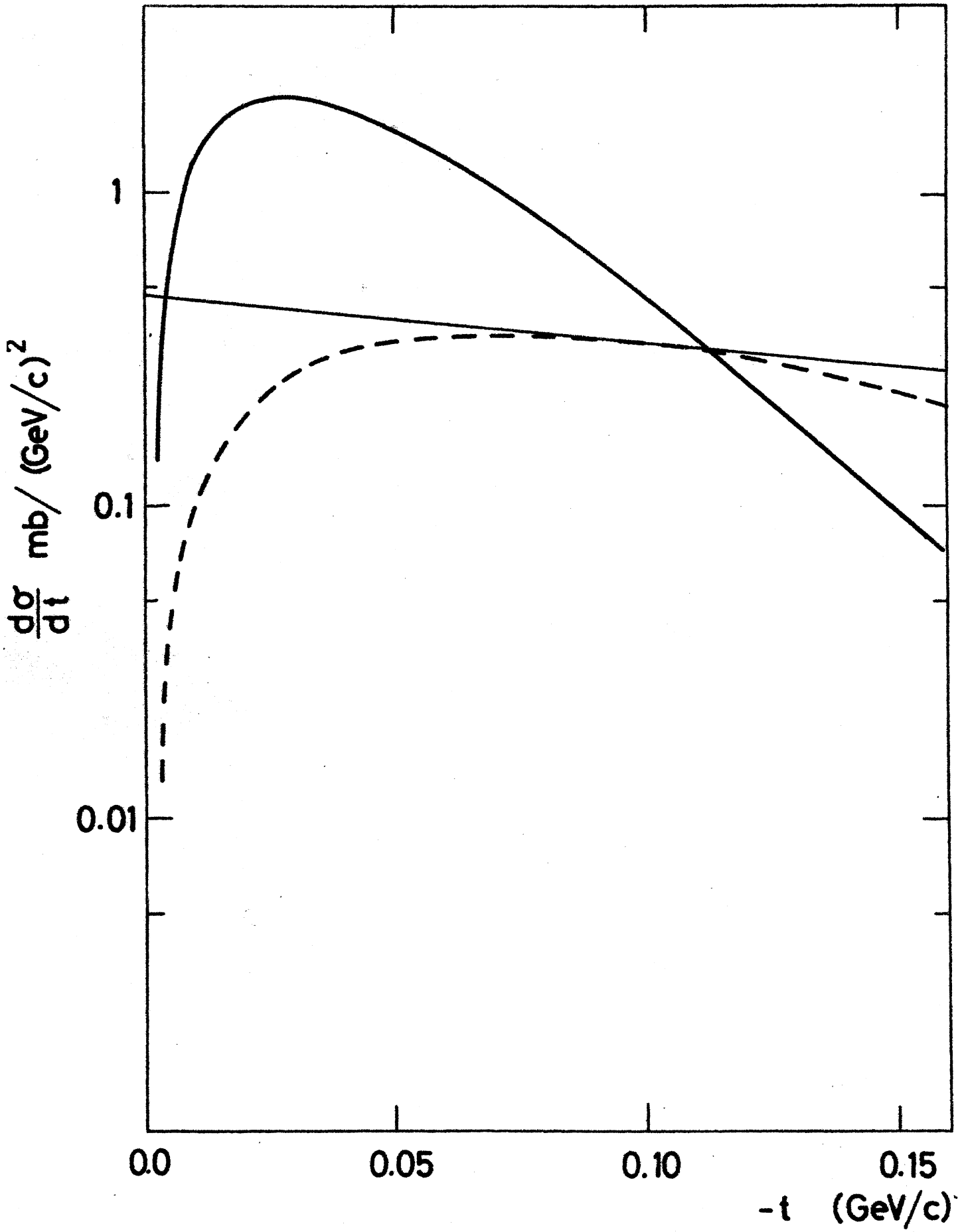

Fig. 2b

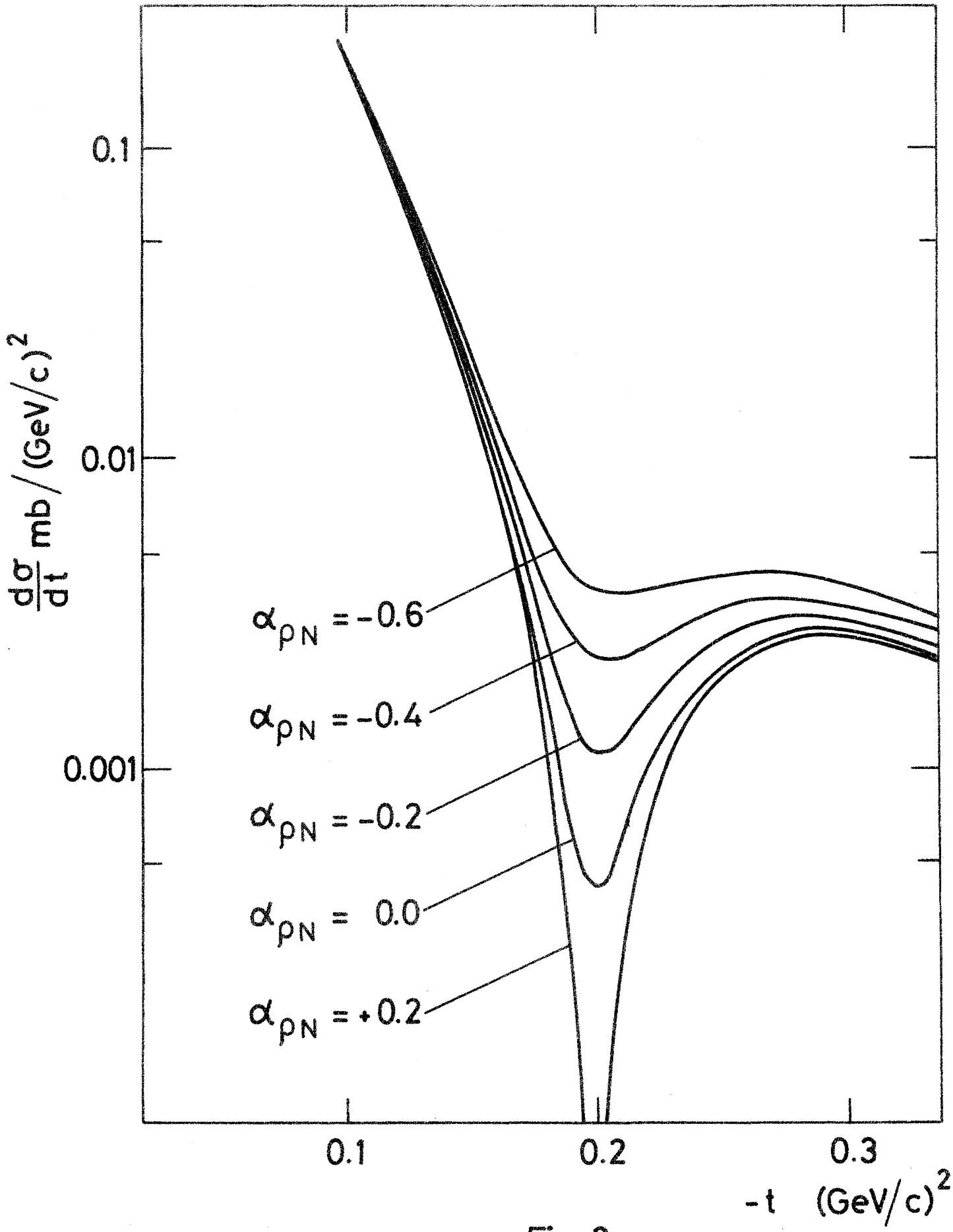
0.1
0.01
0.001
$\frac{d\sigma}{dt}$ mb/(GeV/c)^2
$\alpha_{\rho N} = -0.6$
$\alpha_{\rho N} = -0.4$
$\alpha_{\rho N} = -0.2$
$\alpha_{\rho N} = 0.0$
$\alpha_{\rho N} = +0.2$
0.1
0.2
0.3
$-t$ (GeV/c)^2

Fig. 3

E R R A T A

to

Coherent scattering of pi mesons from helium at high energies

Thesis by Tørd Ekelöf

Gustaf Werner Institute, Uppsala, Sweden

UPPSALA 1972

Errata

to

"A measurement of the differential cross section for elastic pion-helium scattering at 7.76 GeV/c",

T. Ekelöf, B. Höistad, A. Åsberg; C. Busi, S. Dahlgren, A.J. Herz, S. Kullander, G. Lee, D. Websdale; G. Landaud and J. Yonnet - CERN preprint 1971 (references in parenthesis refer to the published version, Nucl.Phys. B35 (1971), 493).

---

p.2, §3, line 5 (p.494, §6, line 5)

"-- pions as well as 0.8% --" should be "-- pions with a contamination of 0.8% --"

p2, §5, line 2 (p. 496, §2, line 2)

"-- (C_{1-4}), each chamber giving both the vertical and the horizontal coordinate --" should be "-- (C_{1-4}), of which three were giving both the vertical and the horizontal coordinate and one only the horizontal coordinate --"

p.4, §2, line 5 (p.497, §2, line 5)

"-- from 30 to 20 mr --" should be "-- from 30 to 10 mr --"

p.9, ref.5 (p.502, ref. 5)

"-- B4, 165 (1967)." should be "-- B3, 155 (1967)."

p.10, ref. 24

"-- and Practive of --" should be "-- and Practice of --"

p.11, figure caption 1 and also under the figure on the following page (p.495, caption of Fig. 1)

Add after last sentence: "In the beam, outside and to the left of the figure were placed to more scintillators, S_1 and S_2."

Errata

to

"A helium-recoil spectrometer"

S. Dahlgren, A.J. Herz, S. Kullander, R. Lorenzi;

T. Ekelöf, B. Höistad and A. Åsberg -

CERN preprint 1972

---

p.3, §2, line 4

"-- $E_x^2 << M^2$ --" should be "-- $E_x^2 << E_o^2$ --"

p.13, §2, line 4

"-- will be E_x MeV/c --" should be "-- will be around E_x MeV/c --"

p.13, §2, line 12

"-- Figs. 7 and --" should be "-- Figs. 6 and --"

p.16, §2, last line

"-- Fig. 7." should be "-- Fig. 6."

p.17, §2, line 6

"-- (Fig. 7) --" should be "-- (Fig. 6) --"

p.20, figure caption 6, last sentence

"-- The pressures were 5 atm and 15 atm respectively"

should be "-- In the case of 8 μm walls the target pressure was 5 atm and in the case of 70 μm walls 15 atm."

fig. 9

The word "(CALCULATED)" in the figure should be erased.

Errata

to

"The data analysis in a counter experiment at the CERN PS, using a helium-recoil spectrometer"

T. Ekelöf

Gustaf Werner Institute internal report 1/72 1972.

---

p.2, last line

The last word, "chambers", should be deleted.

p.7, §3, last line

"-- ref. 1." should be "-- ref. 2."

p.7, §4, line 14

"-- ref. 1.--" should be "-- ref. 2.--"

p.10, §2, last line

"-- are the inversed)." should be "-- are the inverse)."

p.10, §3, first and second lines

"-- between upstream downstream --" should be

"-- between upstream and downstream --"

p.10, §4, line 4

"-- consistancy --" should be "-- consistency --"

p.22, §1, line 4

"-- ref. 22 --" should be "-- ref. 23 --"

p.22, §4, line 5

"-- (see ref. 16) --" should be "-- (see ref. 23) --"

p.23, §1, line 2

"-- Greisen [23] --" should be "-- Greisen [24] --"

p.23, §1, line 4

"-- Eyges [23] --" should be "-- Eyges [24] --"

p.23, §3, first line
"-- between y^2 and θ^2 comes --" should be
"-- between σ_y^2 and σ_θ^2 comes --"

p.24, §1, line 4
"-- they occurs. --" should be "-- they occur. --"

p.24, §2, line 12
" $_i$ = density of medium i" should be
" ρ_i = density of medium i"

p.25, §2, line 4
"-- q^2-2p_oq = --" should be "-- q^2+2p_oq = --"

p.25, last line
"$m^{*2} = m_o^2+2E_xE_o$ --" should be "$m^{*2} = m_o^2-2E_xE_o$ --"

p.26, line 4
"-- cos θ_2 --" should be "-- cos θ_α --"

p.26, line 5
"-- cos θ_2 --" should be "--- cos θ_α --"

Figure captions (after p.28), Fig. 2, line 9
"-- losing --" should be "-- loosing --"

Errata

to

"On the ρ meson production in π^{4}He interactions"

T. Ekelöf

Gustaf Werner Institute internal report 2/72 1972.

---

p.2, §1, line 3

"-- excist --" should be "-- exist --"

p.2, §2, last line

"-- precize --" should be "-- precise --"

p.2, §4, line 3

"-- with $J^{P}I = 1^{-}0$ can --" should be

"-- with $J^{P}I = 1^{-}0, 2^{+}0, 3^{-}0$... etc can --"

p.2, §4, line 8

"-- be disregarded. Any ρ --" should be

"-- be disregarded. Pomeron exchange which also would be permitted according to the $J^{P}I$ quantum numbers is excluded by G parity conservation. Any ρ --"

p.3, last line but one

"-- ref. 9, the pole and --" should be

"-- ref. 9, the ω pole and --"

p.3, last line

"-- degenerated --" should be "-- degenerate --"

p.4, §2, line 6

The word in parenthesis is "zeros"

p.4, §2, line 7

"-- (GeV/c^{2}) --" should be "-- $(GeV/c)^{2}$ --"

p.5, §3, formula (6)

The denominator in the first logaritm should be

" $d\sigma/dt\ (s_{2},t)$", not "$d\sigma/dt\ (s_{2},1)$"

p.5, §3, line 10
"-- this t (= -0.04 (GeV/c^2 if $\alpha(t)$ --" should be
"-- this t (= -0.04 (GeV/c)^2 if $\alpha(t)$ --"

p.6, §2, line 13
"-- ρ^4He reaction [11]: --" should be "-- ρ^4He reaction [12]: --"

p.7, §2, line 3
"-- The $f_{\pi N}(\delta)$ parameters --" should be
"-- The $g_{\pi N}(\delta)$ parameters --"

p.7, §3, first line
"From (6) it --" should be "From (8) it --"

p.8, §4, line 3
"-- elemination --" should be "-- elimination --"

Figure captions, after p.10, Fig. 2a,b, first line
"-- section of for coherent --" should be
"-- section for the coherent --"

The same caption, line 2 and 3
"-- formulae (2) and (3) in --" should be
"-- formula (4) together with (2) and (3) in --"

Figure 2a
The full line curve should be dashed and the dashed curve to the left should be full line (the dashed curve to the right should remaine dashed?)